8-2008

STRATEGIES FOR EXPANDING THE HALOGEN BONDING PERIODIC TABLE AND DESIGINING COMPLEMENTARY HALOGEN/HYDROGEN BONDING SYNTHONS

Hadi Arman
Clemson University, hadia@clemson.edu

STRATEGIES FOR EXPANDING THE HALOGEN BONDING PERIODIC TABLE AND DESIGINING COMPLEMENTARY HALOGEN/HYDROGEN BONDING SYNTHONS

A Dissertation
Presented to
the Graduate School of
Clemson University

In Partial Fulfillment
of the Requirements for the Degree
Doctor of Philosophy
Chemistry

---

by
Hadi David Arman
August 2008

Accepted by:
William T. Pennington, Committee Chair
Steven J. Stuart
Jason McNeill
Donald G. Vanderveer

ABSTRACT

Halogen bonding is the donation of electron density from an electron donor, such as N, O, S, Se atoms, to an electron acceptor such as a dihalogen or organohalogen. This interaction plays an important role in biological systems, such as the thyroid gland and is useful in many other fields such as drug design, crystal engineering, synthetic chemistry, material science and bioinorganic chemistry. However, currently there is a lack of information for this interaction in systems involving organoiodines with sulfur and selenium electron donors.

A variety of sulfur and selenium Lewis base donors were investigated with various organoiodines. The main goal of this research was to better understand how different types of Lewis base donors affected the formation and strength of halogen bonds. This study investigated two classes of sulfur and selenium donors which included; thiones and selenones and tertiary phosphine sulfides and selenides. These donors were used with a variety of organoiodine acceptors which included 1,4-diiodotetrafluorobenzene, tetraiodoethylene, 1,2-diiodotetrafluorobenzene, and iodoform.

Single crystal X-ray diffraction analysis is by far the best method to study these interactions, however single crystals suitable for analysis cannot always be obtained. It has been shown that advanced algorithms such as Monte Carlo and the genetic algorithm can be used to elucidate crystal structures from X-ray powder diffraction data which would be advantageous in investigating halogen bonding. Our research focused on the application of a program, OCEANA (developed by Dr. C.W. Padgett), to elucidate

crystal structures from X-ray powder diffraction data. This program was tested against a variety of organic molecules in different space groups to determine the effectiveness of the program. In addition to this, the crystal structure of bis(5-quinoline) diacetylene was elucidated completely from X-ray powder diffraction data.

DEDICATION

I would like to dedicate this work to my parents for their sacrifices they made for me to obtain my degree. I would also like to dedicate this work to my brother Hassan Benjamin Arman (1981-2003) and my grandfather Albert Alfred Durkee (1925-2002).

ACKNOWLEDGMENTS

First and foremost I wish to thank my research advisor Dr. William T. Pennington, for his support and guidance in the completion of my degree. Subsequently, I would like to thank my committee members: Dr. Steven J. Stuart, Dr. Jason McNeill, and Dr. Donald G. Vanderveer for their help and guidance throughout this degree and in editing and refining this manuscript.

I would like to acknowledge my past undergraduate students who without their help I would not have been able to solve so many crystal structures. They include: Jonathan D. Buck, Sarah Dunaway, Sarah Hill, Josh Kimery, Christopher Louviere, Rebecca Glanville, and Joe Smoak. I would also like to thank Dr. Dorota Abramovitch for help in synthesizing the bis(diphenylphosphine chalcogenides) n-alkanes and her pertinent discussion on organic chemistry.

Finally, I would like to thank my parents Farshad and Sandra Arman, for the support throughout the years. Also like to thank Sawsan Zainal for her support and encouragement in helping me finish my dissertation.

TABLE OF CONTENTS

Table of Contents (Continued)

Page

Table of Contents (Continued)

Page

LIST OF TABLES

LIST OF FIGURES

List of Figures (Continued)

Figure Page

List of Figures (Continued)

Figure Page

CHAPTER ONE

INTRODUCTION

Halogen bonding

History

In the middle of the nineteenth century, Guthrie reported a molecular complex formed by addition of iodine to a saturated solution of ammonium chloride.[1] Thereafter, the primary focus on these systems was investigation of their behavior in solution. Attempts to describe this type of bonding from a theoretical standpoint using Lewis theories of valence were found to be inconsistent.[2,3] A variety of names were used to describe this interaction prior to MO theory: bumps–in–hollows, exaltation of valency, stray feeler lines of force, and electron clutching.[4] Eventually, Mulliken and others developed a classification process and conceptual framework for these "donor – acceptor" or "charge transfer" complexes.[2,5] These complexes are classified into two types: the outer type B•••XY which is weak and has little charge transfer, and the inner type $[BX]^{+}$•••Y^{-} which is strong and has substantial charge transfer.[5,6]

Structural characterization using X- ray crystallography, by Hassel and others, [2,7] showed that complex formation involved short intermolecular interactions, interactions shorter than the sum of the atoms' Van der Waals radii, between an electron pair donor and one or both atoms of the dihalogen. This was proven by the elucidation of the complex 1,4-dioxane and dibromine, which showed that there was a slight elongation in the Br-Br bond. However, the most impressive result was the short O•••Br contact distance (2.71 Å) which indicated a very strong interaction between oxygen and bromine

atoms.[7] It is now well understood that the halogen accepts electrons from the donor into a σ* antibonding orbital, which results in a strong, highly directional interaction.[8]

The term halogen bonding was first coined by Legon after his investigation of complexes involving dihalogens (XY) with Lewis bases (B). He noticed striking similarities between these B•••XY interactions and B•••HY hydrogen bonds. Since the hydrogen bond is accepted as being mainly electrostatic, it was logical to conclude that the characteristic that mainly defines the properties of B•••XY complexes is the electrostatic term. [2,6,9] Since Legon coined the term " halogen bond" there have been different views on which interactions constitute a halogen bond. The electron density around the halogen nucleus is highly anisotropic, therefore halogens can behave as both electron acceptors and as electron donors. Resnati suggests that the term halogen bonding be reserved for noncovalent interactions involving halogens that function as acceptors of electron density.[10] A conflicting viewpoint was reported by Glaser, who identifies an "interaction" as a "mutual or reciprocal action or influence" and stated that the influence is "attraction" or "affinity". Therefore, identifying bonding interactions can be achieved by naming the individual members involved in the interaction. This naming scheme is focused on the interacting species rather than the nature of the contact. An interaction involving two partners A and B, where A interacts with B, would be labeled as AB bonding. For example, the crystal structure of 4-chlorobenzaldazine has a chlorine atom situated in a pocket surrounded by various hydrogen atoms. Using Glaser's terminology, the intermolecular bonding, with numerous Ar-H "ligands", is labeled as Ar-Cl•$(H\text{-}Ar')_n$ halogen bonding, contrary to the definition suggested by Resnati. Resnati responded, that

interactions occurring in the structures involving halobenzald-azines have been correctly referred to as hydrogen bonding.[11] The definition provided by Resnati will be used in this dissertation.

Description

The basic scheme for a halogen bond interaction is D•••X-Y where D is an electron donor (such as N, O, S, etc), X is a halogen and Y is carbon, nitrogen, halogen, etc (figure 1.1).[10] A variety of bonding motifs are observed for this type of interaction, including adducts, chains, layers, and 3D networks. Adducts (figure 1.2) are finite and usually occur in a 1/1 or 2/1 molar ratio. Chains (figure 1.3) extend throughout the crystal lattice in one dimension, while layers (figure 1.4) and networks (figure 1.5) extend along two and three dimensions, respectively.

Previous Studies

Halogen bonding between nitrogen heterocycles with diiodine and organoiodines has been the primary concentration of our work and others.[12] A few examples of the N•••I interaction include the I_6 chain (figure 1.6). The prominent bonding motifs observed in this complex are 1/1 A/D adducts. These adducts are bridged to each other through the amphoteric behavior of the diiodine that is involved in the halogen bonding interaction with a nitrogen atom. The amphoteric diiodine accepts electron density from the nitrogen atom and donates electron density to the bridging diiodine, which behaves as a Lewis acid. Tetraiodoethylene (TIE) which displays robust stacking pattern (figure 1.7) complexes due to the formation of halogen bonded layers that are composed of extended halogen bonded chains linked together by I•••I halogen interactions.[14]

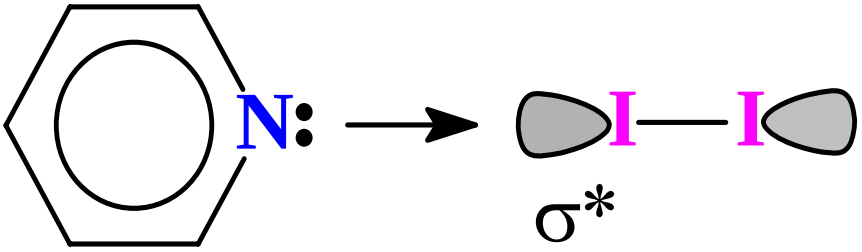

Figure 1.1. Schematic of a typical halogen bonding interaction.

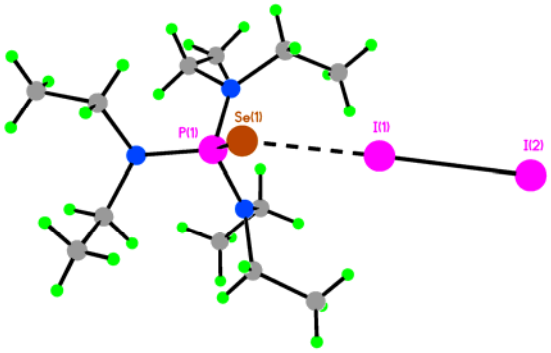

a)

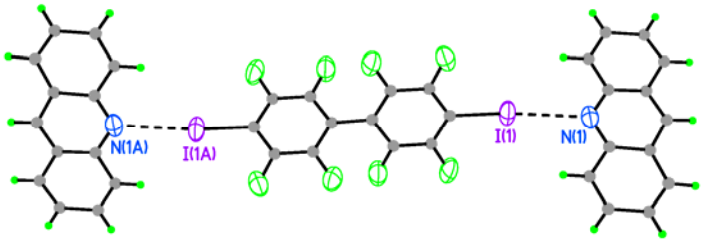

b)

Figure 1.2. Halogen bonded adducts: a) 1:1 complex, ((tris(diethylamino)phosphine)selenide • diiodide[15] b) 1:2 complex. (Acridine • diiodooctafluorobiphenyl).

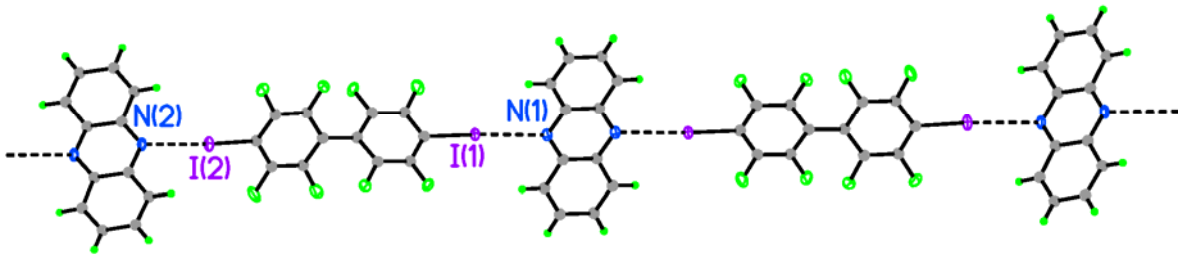

Figure 1.3. Extended chain complex of phenazine • diiodooctafluorobiphenyl.

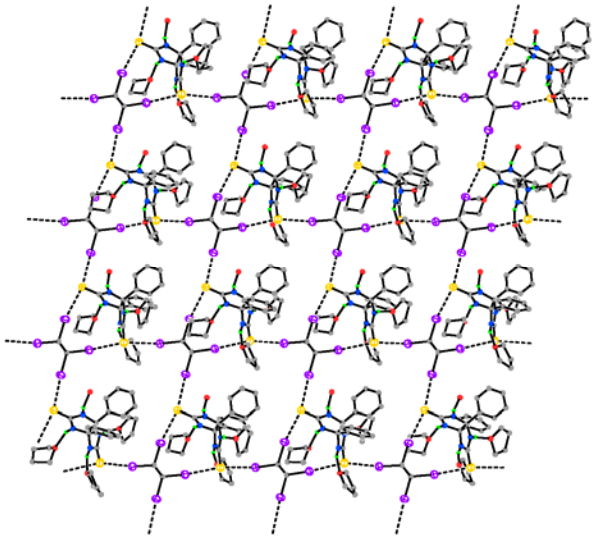

a)

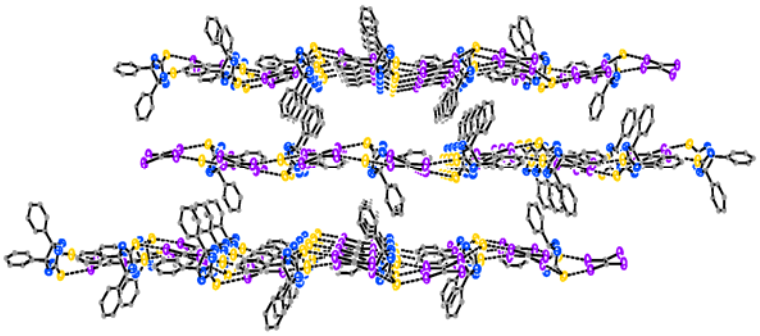

b)

Figure 1.4. Layered complex of diphenyldithioglycouril • tetraiodoethylene • THF: a) view normal to one layer, b) stacked layers, solvent is not displayed.

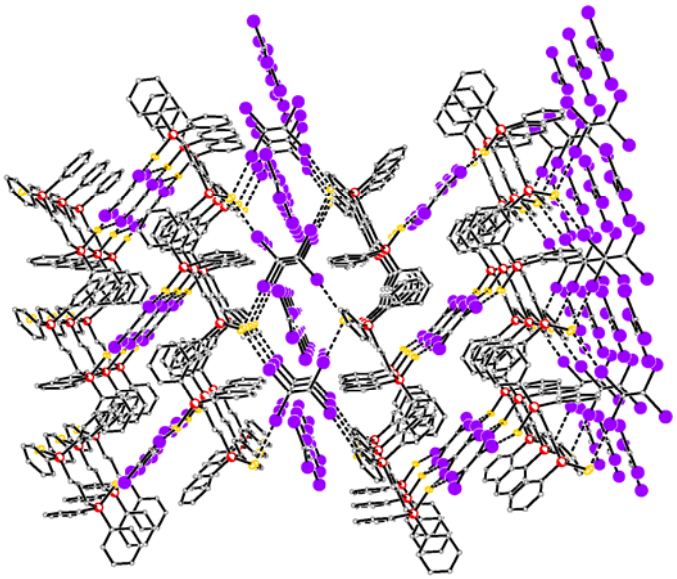

Figure 1.5. Network complex of bis(diphenylphosphine selenide) propane • tetraiodoethylene.

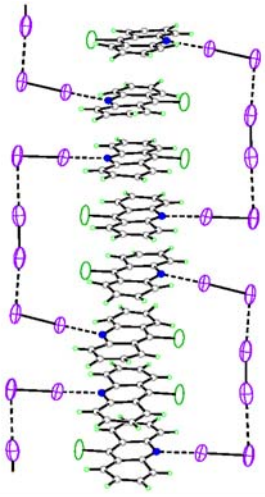

Figure 1.6. 9-Chloro-acridine • I_6

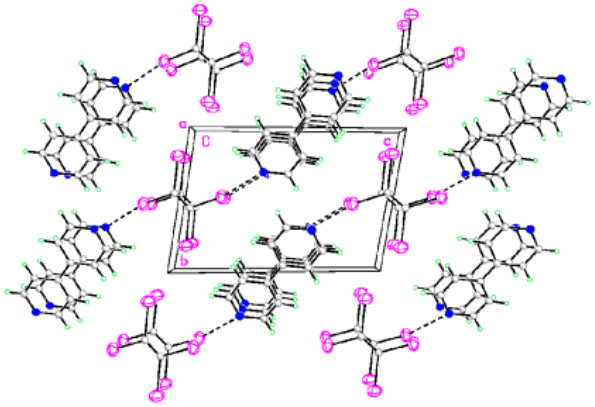

Figure 1.7. Packing of the 4,4'-bipyridine-TIE complex.

Investigation of halogen bonding synthons has led to discoveries that could prove useful in several fields such as drug design, crystal engineering, synthetic chemistry, material science and bioinorganic chemistry. One example is the control of polymorphism, a vital need in the pharmaceutical industry, through halogen bonding.[16] Such control is important because one polymorph of a drug may provide beneficial properties such as increased bioavailability, shelf life, crystal morphology, or processing properties, that others do not. However, control of polymorphism is often difficult to accomplish. Halogen bonding can be used to form a cocrystal of a drug in which the structure of the complex resembles that of the desirable polymorph of the drug. Solid-state decomposition involving removal of the halogen bonded guest, in many cases, yields the desirable form of the drug. Halogen bonding has also been used for the development of tetrathiofulvalene-based conductors,[17] novel liquid crystals[18] and crystals for optical second harmonic generation.[19] Halogen bonding plays a crucial role in biological systems, such as in the thyroid gland, that produces hormones whose main function is to regulate metabolism. Production of these hormones involves organosulfides, selenides and organoiodines.[20] The two main organoiodines are the thyroid hormone, 3,5,3′ - triiodothyronine (T3), and prohormone, 3,5,3′,5′-tetraiodothyronine (T4). Conversion of T4 to T3 is accomplished through the reductive cleavage of the aromatic C-I bond that is ortho to a phenolic or a diphenyl oxygen atom on the prohormone. Also, iodine in the form of iodide is utilized by the thyroid gland to assist in the iodination of tyrosine which is a precursor to the thyroid hormone (figure 1.8).[18] Selenocysteine, a residue on the iodothyronine deioidinase enzyme (ID-1), role is

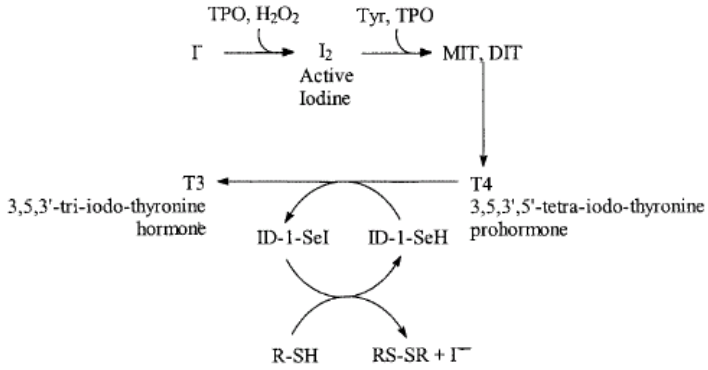

Scheme 1. Mechanism of TPO-catalyzed iodination reactions (MIT = 3-monoiodotyrosine and DIT = 3,5-diiodotyrosine)

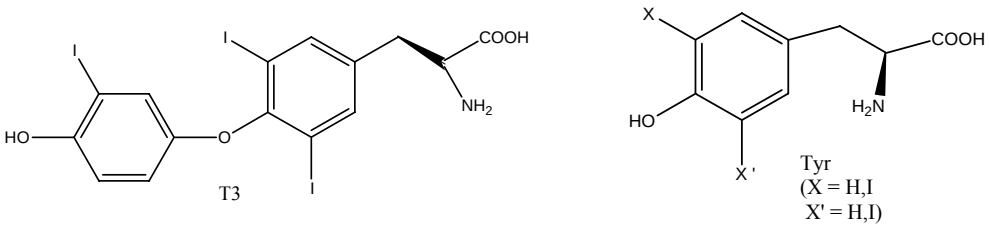

Figure 1.8. Mechanism for production of T3 hormone[21]

the monodeiodination of the T4 prohormone. Organosulfides (thiols) role is the deiodination of the selenocysteine residue on the ID-1 enzyme.[21]

One common disease associated with the thyroid is hyperthyroidism, overproduction of thyroid hormone, commonly known as Graves' disease. Thioamides (figure 1.9) have been used extensively in the treatment of this disease, as diiodine sponges.[18,22,23] Hypothyroidism, often resulting from a iodine deficient diet, is the underproduction of the T3 hormone and is usually treated by increasing the iodine content in the diet or with supplemental T4 prohormone to help facilitate production of thyroid hormone.[22b]

Given the limited scope of previous studies on complexes involving selenium and sulfur based donors with organoiodines, a larger library of structural data for these complexes are desirable. This will expand the knowledge of halogen bonding in general and may fuel new possibilities for treatment of a variety of diseases.

Most of the known complexes of sulfur and selenium involve dihalogens[24,25,26,27,28] and interhalogens.[12,29,30] There are only a few early investigations of organohalogens with sulfur[31,32] and selenium[31,33,34] based donors.[35] To the best of our knowledge, the only methodical study of an electron donor other than nitrogen or oxygen with organoiodines involves the investigation of mercaptomethylimidazole, an antithyroid drug, with various organoiodine molecules.[36]

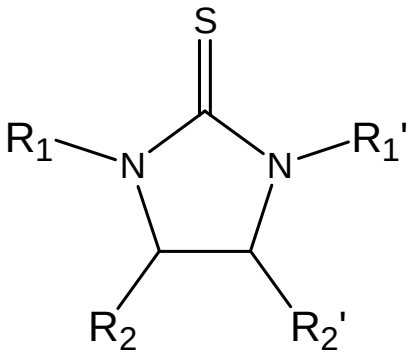

R_1/R_1'= H, CH_3 , etc.
R_2/R_2'= H, CH_3 , C_6H_4 , etc.

Figure 1.9. Generic structure of a thioamide.

Techniques for Elucidating Crystal Structures

Introduction

While single crystal X-ray diffraction is the preferred tool for investigating halogen bonded complexes. There are some limitations to using this technique, which requires that crystals be of good quality and size. This poses a problem since the investigation of halogen bonding involving organic compounds sometimes generate low quality crystals. These poor quality crystals make single crystal X-ray diffraction somewhat difficult, however a microcrystalline powder of these complexes is easily obtained. Powders of these materials can then be utilized to collect X-ray powder diffraction data.

The main focus of our research is organic molecular crystals. These types of crystals pose many obstacles, such as crystallizing in low symmetry space groups with rather large unit cells, and serve peak overlap of reflections. This makes it difficult to elucidate their crystal structures from X-ray powder analysis. Due to these drawbacks, powerful algorithms have recently been developed along with increasing computer processing speed which has made it practical to elucidate crystal structures via X-ray powder diffraction data.[37,38,39,40,41,42] There have been many software programs[43,44,45] developed to elucidate organic molecular crystal structures though the main disadvantage is that cell indexing is prerequisite. Our research focused on implementing and applying a program that did not require prior cell indexing and be able to utilize low quality X-ray powder diffraction data.

Methods

Three common methods are usually implemented for elucidating structures; direct space methods, reciprocal space methods and *ab initio*. All three methods require molecular connectivity of a sample. Direct space and reciprocal space methods also require X-ray diffraction data.

Direct-space methods utilize direct space (i.e real space) as opposed to reciprocal space. In this approach, the only variables of interest are position, orientation and the dihedral angles of a molecule. The complexity of this approach (i.e. number of dimensions) is related to the number of variables used to define the solution.[46] Mathematical algorithms are implemented to search a given solution space to generate realistic structures of best fit based on the chemical information specified. The algorithms encoded are global optimization techniques such as: Monte Carlo,[47,48] simulated annealing,[49] or genetic algorithms.[50] The best fit is determined by calculating X-ray powder patterns of feasible structures which are then evaluated against the experimental powder pattern using some type of cost function which is an equation used to determine how well a trial structure fits experimental data, such as R_{wp} (discussed later).

As stated above, most direct methods utilize some type of optimization technique. The three most common global optimization techniques are Monte Carlo (MC), simulated annealing (SA), and genetic algorithm (GA).

Monte Carlo, a random sampling technique, operates by randomly changing an initial configuration; governed by a set of rules, to generate a test configuration. The most

common way of evaluating the new configuration is by either energy or R_{wp}. Energy is defined as the potential packing energy and R_{wp} is defined as follows:

$$Rwp = 100 \times \sqrt{\frac{\sum_i w_i (Y_{Exp_i} - Y_{Cal_i})^2}{\sum_i w_i Y_{Exp_i}^2}} \quad (1)$$

This test configuration is accepted if its falls within these guidelines:

$E_{(i+1)} < E_{(i)}$ or $R_{wp(i+1)} < R_{wp(i)}$. The moves over the solution space are governed by: $x_i \rightarrow x_i \alpha_i \xi_i$. Where ξ is the direction of shift and is chosen between -1 and 1 and α parameter is the numerical shift. This is the best method to use when it comes to simplicity of coding the algorithm.[51]

Another optimization, simulated annealing, involves the cooling of a system by means of slow cooling or quenching (rapid cooling). The thermostat for cooling can be preset or be linked to a function whose value is based on fluctuations. The strategy here is to perform multiple runs to determine if the same result is found. One main concern of simulated annealing is the care taken in the way the system is cooled so that it avoids falling into a thermodynamically unfavorable configuration.[18] SA is the most popular optimization technique and is typically used in conjunction with MC algorithm.[8]

The genetic algorithm was first used in the field of biology around 50 years ago. Only in the last 15 years has the GA been used in the field of crystallography for the elucidation of crystal structures from X-ray powder diffraction data.[52,53] GAs are based on theories of natural selection such as Darwin[54]or Lamarckian[55] theories. In Darwin's theory the better adapted an individual is to its surroundings the higher probability for its survival. In Lamarckian theory the traits acquired by an individual during its lifetime are

passed down to its offspring. For example the long neck of a giraffe, Darwin's point of view propose that the giraffes obtained longer necks because the ones with longer necks were better able to survive in their environment therefore the longer neck giraffe were able to reproduce and over time their necks eventually got longer. In contrast to Darwin, Lamarckian's view point suggested a giraffe that stretched its neck throughout its lifetime and developed a long neck would pass this trait to its offspring. GAs use genes to store information of a solution for a problem at hand. In the case of elucidating crystal structures these genes contain information about a trial structure of the solution space. The genetic algorithm is composed of many steps which will be discussed in a later chapter. The advantage of GAs, is that they generate a population of trial structures, not just one structure that is sequentially generated from the previous one as in MC and SA.[8]

The procedure for using direct space methods for elucidating crystal structures involves three stages. The first stage is obtaining unit cell parameters. Most structure determining programs use algorithms for indexing powder patterns such as Ito[56] and Treor90.[57] These programs have little trouble determining unit cell parameters from high quality X-ray data, for all but low symmetry space groups or large unit cells with significant peak overlap. The second stage involves a global optimization technique which is used to elucidate structures in optimal agreement with the experimental powder diffraction pattern. The final stage is structure refinement, which further refines unit cell dimensions, atomic coordinates, and thermal displacement parameters. The method most commonly used is the Rietveld refinement technique.[58,59]

Reciprocal space techniques are generally used for single crystal analysis which involves the measurement of intensity for each single reflection. From the intensities structure factors are derived and assigned phases, and then Fourier techniques are used to determine atomic positions. This approaches works well for powders of materials crystallizing in high symmetry space groups with strongly diffracting atoms (i.e. inorganic compounds).

Ab initio techniques require only molecular connectivity. Structures are generated based on a selected space group, and are evaluated based on the calculated energy (i.e. the lowest energy structure corresponds to correct structure). The solution space is then searched using global optimization techniques. A disadvantage of *ab initio* methods is that the lowest energy structure found may not always correspond to the correct crystal structure.[60] This is due to polymorphism which is a phenomenon where a compound crystallize in more than one state.

Conclusion

At present, single crystal x-ray diffraction data is the best technique to investigate halogen bonding interactions. However, with advances in computational speed and better algorithms, that can handle the larger atoms involved in halogen bonding, elucidation of crystal structures by x-ray powder diffraction data may become a more plausible route. This would be a great advancement in the investigation of halogen bonding since many of these complexes crystallize in low symmetry space groups and sometimes generate crystals unsuitable for single crystal analysis.

References

1. Guthrie, F. *J. Chem. Soc*. **1863**, *16*, 239.

2. Pennington, W.T.; Hanks, T.W.; Arman, H.D, "Halogen Bonding with Dihalogens and Interhalogens," in *Structure and Bonding Series: Halogen Bonding, Fundamentals and Applications*, (Eds. G. Resnati, P. Metrangolo), Springer, London, **2007**, chapter 3.

3. Lewis, G.N. *J. Franklin Inst.* **1938**, 226.

4. Mulliken, R.S. *J. Phys.Chem.* **1952**, 56. (b) Mulliken , R.S.; Person, W.B. *Molecular complexes* Wiley-Interscience, New York, **1969**, 498.

5. Legon, A. C. *Angew. Chem. Int. Ed*. **1999**, *38*, 2686.

6. Hassel, O.; Hvoslef, J. *Acta Chem. Scand.* **1954**, *8*, 873.

7. Bent, H.A. *Chem. Rev.* **1968**, *68*, 587.

8. This is a somewhat simplified description, since the C-I sigma bonding orbital also mixes in also. (a) Landrum, G.A.; Goldberg, N.; Hoffmann, R.J. *J. Chem. Soc., Dalton Trans.* **1997**, 3605. (b) Hanks, T.W.; Pennington, W.T.; Bailey, R.D. *Anisotropic Organic Materials Approaches to Polar Order, ACS Symp. Ser.* Vol. 798, Glaser, R.; Kaszynski, P. Eds. **2001**.

9. (a) Legon, A.C. *Chem. Eur. J.* **1998**, *4*, 1890. (b) Dumas, J.M.; Gomel, L.; Guerin, M. in *The Chemistry of Functional Groups, Supplement D*, S. Patai, Z. Rappoport, Eds. Wiley, New York, **1983**, 985.

10. (a) Metrangolo, P.; Resnati, G. *Chem. Eur. J.* **2001**, *7*, 2511. (b) Metrangolo, P.; Pilati, T.; Resnati, G. *Cryst. Eng. Comm.* **2006**, *8*, 946.

11. Glaser R.; Murphy, R.F. *Cryst. Eng. Comm*. **2006**, *8*, 948.

12. Pennington, W.T.; Bailey, R.D.; Holmes, B.T.; Hook, L.L.; Watson, R.P.; Warmoth, M.; Hanks, T.W. *Trans. Am. Cryst. Assoc.; Cryst. Eng. Symp.* **1998**, *33*, 145.

13. Hanks, T. W.; Metrangolo, P.; Resnati, G.; Walsh, R. B.; Pennington, W. T. *Cryst. Growth & Des.* **2001**, *1*, 165.

14. Bailey, R.D.; Hook, L.L.; Watson, R.P.; Hanks, T. W.; Pennington, W. T. *Cryst. Eng.* **2000**, *3*, 155.

15. (a) Bailey, R. D.; Grabarczyk, M.; Hanks, T. W.; Pennington, W. T. *J. Chem. Soc., Perkin Trans. II* **1997**, 2773. (b) Bailey, R. D.; Grabarczyk, M.; Hanks, T. W.; Pennington, W. T. *J. Chem. Soc., Perkin Trans. II* **1997**, 2781.

16. Padgett, C.W.; Pennington, W.T.; Hanks, T.W. *Cryst. Growth & Des.* **2005**, *5*, 737.

17. Nguyen, H. L.; Horton, P. N.; Hursthouse, M. B.; Legon, A. C.; Bruce, D. W. *J. Am. Chem. Soc.* **2004**, *126*, 16.

18. Kohrle, J.; Jakob, F.; Contempre, B.; Dumont, J.E. *Endocrine Reviews* **2005**, *26*, 944.

19. (a) Darma, J.A.R.P.; Allen, F.H.; Hoy, V.J.; Howard, J.A.K.; Thaimattam, R.; Biradha, K.; Desiraju, G.R. *Chem. Commun.* 1997, 101. (b) Norman, J.; Politz, D. " Hypothyroidism Too little thyroid hormone", http://www.endocrineweb.com/hypo1.html (04/22/07)

20. Godfrey, S.M.; Jackson, S.L.; McAuliffe, C.A.; Pritchard, R.G. *J. Chem. Soc., Dalton Trans.* **1997**, 4499.

21. Antoniadis, C. D.; Corban, G. J.; Hadjikakou, S. K.; Hadjiliadis, N.; Kubicki, M.; Warner, S.; Butler, I.S. *Eur. J. Inorg. Chem.* **2003**, 1635.

22. Daga, V.; Hadjikakou, S. K.; Hadjiliadis, N.; Kubicki, M.; dos Santos, J H. Z.; Butler, I. S. *Eur. J. Inorg. Chem.* **2002**, 1718.

23. Corban, G. J.; Hadjikakou, S.K.; Hadjiliadis, N.; Kubicki, M.; Tiekink, E.R.T.; Butler, I.S.; Drougas, E., Kosmas, A.M. *Inorganic Chem.* **2005**, *44*, 8617.

24. F. Cristiani, F. A. Devillanova, F. Isaia, V. Lippolls, G. Verani,F. Demartin, *Polyhedron* **1995**, *14*, 2937.

25. Chao, G.Y.; McCullough, J.D. *Acta Cryst.* **1960**, *13*, 727.

26. (a) Esseffar, M.; Bouab, W.; Lamsabhi, A.; Abboud, J. L. M.; Notario, R.; Yanez, M. *J. Am. Chem. Soc.* **2000**, *122*, 2300. (b) Boyle, P. D.; Christie, J.; Dyer, T.; Godfrey, S. M.; Howson, I. R.; McArthur, C.; Omar, B.; Pritchard, R. G.; Williams, G.R. *J. Chem. Soc., Dalton Trans.* **2000**, 3106.

27. (a) Bigoli, F.; Deplano, P.; Ienco, A.; Mealli, C.; Mercuri, M.L.; Pellinghelli, M.A.; Pintus, G.; Saba, G.; Trogu, E. F. *Inorg. Chem.* **1999**, *38*, 4626. (b) Boyle, P. D.; Godfrey, S. M. *Coord. Chem. Re*v. **2001**, *223*, 265.

28. (a) Deplano, P.; Ferraro, J. R.; Mercuri, M. L.; Trogu, E. F. *Coord. Chem. Re*v. **1999**, *188*, 71. (b) Aragoni, M. C.; Arca, M.; Devillanova, F. A.; Garau, A.; Isaia, F.; Lippolis, V.; Verani, G. *Coord.Chem. Re*v. **1999**, *184*, 271.

29. Daga, V.; Hadjikakou, S. K.; Hadjiliadis, N.; Kubicki, M.; dos Santos, J H. Z.; Butler, I. S. *Eur. J. Inorg. Chem.* **2002**, 1718.

30. (a) Kubiniok, S.; du Mont, W.W.; Pohl, S.; Saak, W. *Angew.Chem.,Int.Ed.* **1988***, 27***,** 431. (b) du Mont, W.W.; Martens, A. ; Pohl, S.; Saak, W *Inorg.Chem.* **1990**, *29***,** 4847. (c) Knobler, C.; McCullough, J.D. *Inorg.Chem.* **1968**, *7*, 365. (d) Maddox, H.; McCullough, J.D. *Inorg.Chem.* **1966**, *5*, 522. (e) Godfrey, S.M.; McAuliffe, C.A.; Pritchard, R.G.; Sarwar, S. *J.Chem.Soc.,Dalton Trans.* **1997**, 3501. (f) Chao, G.Y.; McCullough, J.D. *Acta Crystallogr.* **1961**, *14***,** 940. (g) Godfrey, S.M.; McAuliffe, C.A.; Pritchard, R.G.; Sarwar, S. *J.Chem.Soc.,Dalton Trans.* **1997**, 1031.

31. (a) Jeske, J. ; du Mont, W.W.; Jones, P.G. *Chem. Eur. J.* **1999**, *5***,** 385. (b) Demartin, F.; Devillanova, F.A.; Garau, A.; Isaia, F.; Lippolis, V.; Verani, G. *Polyhedron* **1999**, *18***,** 3107. (c) Boyle, P. D.; Cross, W.I.; Godfrey, S.M.; McAuliffe, C.A.; Pritchard, R.G.; Teat, S. *J.Chem.Soc.,Dalton Trans.* **1999**, 2219. (d) Cristiani, F. ; Demartin, F. ; Devillanova, F.A. ; Isaia, F. ; Saba, G. ; Verani, G. *J.Chem.Soc.,Dalton Trans.* **1992**, 3553. (e) Cristiani, F. ; Demartin, F. ; Devillanova, F.A. ; Isaia, F. ; Lippolis, V. ; Verani, G. *Inorg.Chem.* **1994**, *33*, 6315. (f) Bigoli, F. ; Pellinghelli, A.M. ; Deplano, P. ; Devillanova, F.A. ; Lippolis, V. ; Mercuri, L.M. ; Trogu, E.F. *Gazz.Chim.Ital.* **1994**, *124***,** 445.

32. Homesland, O.; Romming, C. *Acta Chem. Scand.* **1966**, *20*, 2601.

33. Bjorvatten, T.; Hassel, O. *Acta Chem. Scand.* **1961**, *15*, 1429.

34. Dahl, T.; Hassel, O. *Acta Chem. Scand.* **1965**, *19***,** 2000.

35. Bjorvatten, T. *Acta Chem. Scand.* **1963**, *17*, 2292.

36. Hassel, O. *Science* **1970**, *170*, 497, and references therein.

37. Jay, J.I.; Padgett, C.W.; Walsh, R.D.B.; Hanks, T.W.; Pennington, W.T. *Cryst. Growth & Des.* **2001**, *1*, 501.

38. Cheetham, A.K.; Wilkinson, A. P. *Angew. Chem. Int. Ed. Engl.* **1992**, *31*, 1557.

39. Harris, K. D. M.; Tremayne, M. *Chem. Mater.* **1996**, *8*, 2554.

40. Langford, J. I.; Louer, D. *Rep. Prog. Phys.* **1996**, *59*, 131.

41. Poojay, D.M.; Clearfield, A. *Acc. Chem. Res.* **1997**, *30*, 414.

42. Meden, A. *Croat. Chem. Acta.* **1998**, *71*, 615.

43. Harris, K. D. M.; Tremayne, M.; Kariuki, B. M. *Angnew. Chem. Soc.* **1994**, *40*, 1626.

44. Tsue, H.; Horiguchi, M.; Tamura R.; Fujii K.;Uekusa, H. *J. of Synthetic Organic Chemistry, Japan* **2007**, *65,* 1203.

45. Hanson, A.J.; Cheung, E.Y.; Harris, K.D.M. *J. Phys. Chem. B* **2007,** *111,* 6349.

46. Altomare, A.; Caliandro, R.; Cuocci, C.; Giacovazzo, C.; Moliterni, A.G.G.; Rizzia, R.; Platteaua, C. *J. Appl. Cryst.* **2008**, *41*, 56.

47. Treymayne, M. *Phil. Trans. R. Soc. Lond.* A. **2004**, 362, 2961.

48. Harris, K. D. M.; Tremayne, M.; Lightfoot, P.; Bruce, P. G.; *J. Am. Chem. Soc.* **1994**, *116*, 3543.

49. Brodski, R. P. and Schenk, H. *J. Appl. Cryst.* **2003**, *36*, 239.

50. Engel, G. E.; Wilke, S.; König, O.; Harris, K. M. D.; Leusen, F. J. J.; *J. Appl. Crystallogr.* **1999**, *32*, 1169.

51. David, W.I.F.; Shankland, K.; McCusker, L.B.; Baerlocher, C. *Structure Determination from Powder Diffraction Data* Oxford University Press, New York, **2002**, 308.

52. Harris, K.D.M.; Kariuki, B.M.; Treymayne, M.; Johnston, R.L. *Mol. Cryst. Liq. Cryst.* **1998**, *1*, 313.

53. Bazterra, V.E.; Ferraro, M.B.; Facelli, J.C. *J. Chem. Phys.* **2002**, *116*, 5984.

54. Lawerence D., ed. *Handbook of Genetic Algorithms* Van Nostrand, New York, **1991**.

55. Solomon, E.P.; Berg, L.R.; Martin, D.W. *Biology* Saunders College Publishing, New York, 5th ed., **1999**, 371.

56. Visser, J. W., *J Appl. Crystallogr.* **1969,** *2*, 89.

57. Werner, P. E.; Eriksson, L.; Westdahl, M. *J. Appl. Crystallogr*. **1985**, *18*, 367.

58. Rietveld, H.M. *J. Appl. Crystallogr.* **1969**, *2*, 65.

59. Larson, A.C.; Von Dreele, R.B. Los Alamos Lab. Report No. LA-UR-86-748, **1987**.

60. Brodski, V.; Peschar, R.; Schenk, H. *J. Appl. Cryst.* **2005**, *38*, 688.

CHAPTER 2

HALOGEN BONDED COMPLEXES OF TRIPHENYLPHOSPHINE SELENIDE

Introduction

Halogen bonding is a highly directional and relatively strong, noncovalent interaction comparable to hydrogen bonding.[1] It involves the donation of a lone pair of electrons from a donor, such as N, O, S, Se atoms, to a σ* orbital of an acceptor, such as dihalogens or organohalogens.

The most widely studied halogen bonded complexes involve Lewis acid acceptors such as dihalogens, interhalogens and organohalogens with nitrogen, oxygen, and sulfur Lewis base donors. The investigation of Lewis base donors containing a selenium atom; for example selenoethers, [10] selenones, [11] and phosphorus selenides,[12] with Lewis acid acceptors; such as dihalogens and interhalogens, are well studied and documented. However, studies of these electron donors with organohalogens are far less common, and are limited to diselenane with various organoiodines [13,14,15] and a complex of 1,6,12,17,23,28-hexaselenacyclotritriaconta-2,4,13,15,24,26-hexayne 4-bromoanisole clathrate.[16]

Selenium based donors have mainly been studied to determine their effectiveness as antithyroid agents. A search of reported structures involving Se•••X interactions reveals that the majority of these structures are with diiodine and dibromine. The prominent bonding motif observed for dihalogen complexes are simple adducts. Other

bonding motifs such as bridging adducts, extended adducts, and bridging amphoteric adducts are observed in a few examples (these motifs will be discussed later).

In addition to halogen contacts, phenyl embraces have been observed in complexes involving $Ph_3P{=}Se$ and can display a variety of conformations.[18] These interactions have recently been acknowledged as a potential contributor in the formation of solid state structures.[19]

This chapter describes the structural and thermal characterization of halogen bonding complexes involving $Ph_3P{=}Se$ (figure 2.1) with tetraiodoethylene (TIE), 1,4-diiodotetrafluorobenzene (1,4-F_4DIB) and 1,2-diiodotetrafluorobenzene (1,2- F_4DIB).

Halogen Bonded Complexes

Selected distances and angles for the three complexes are given in Table 2.1. Crystal packing of these complexes is controlled by noncovalent interactions between donor and acceptor molecules. These noncovalent interactions include Se•••I contacts and phenyl embraces, and for the 1,2-F_4DIB complex, I•••π interactions are also observed.

Crystal Structure of $(Ph_3P{=}Se)_4 \bullet (TIE)_3$

Two molecules of $Ph_3P{=}Se$, situated on general positions, and four half molecules of TIE (each located on an inversion center) form the asymmetric unit. There are four unique Se•••I contacts with an average distance of 3.49(6) Å. The average observed P=Se•••I and C-I•••Se angles are 110(4)° and 169(4)°, respectively. Halogen bond distances and angles are similar to those of the other complexes reported here. The geometry, observed at the selenium atom, resembles tetrahedral rather than the predicted geometry of trigonal planar and linear geometry is observed for the iodine atom. This is commonly

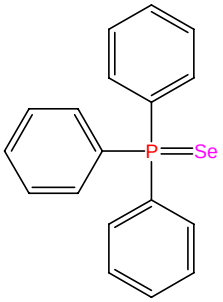

$Ph_3P{=}Se$

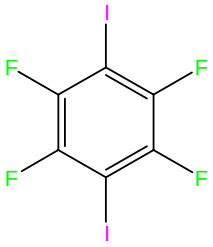

1,4-F_4DIB

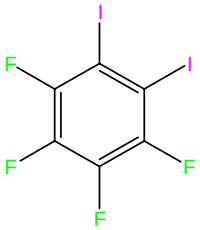

1,2-F_4DIB

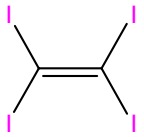

TIE

Figure 2.1. Structures of Donor and acceptors

Table 2.1. Selected Distances (Å) and Angles (º) for Ph_3P=Se complexes.

TIE		1,4-F_4DIB		1,2-F_4DIB	
Distances					
P=Se	2.125(3), 2.126(3)	P=Se	2.107(2), 2.127(2)	P=Se	2.1152(19)
Se•••I	3.4510(15), 3.4519(14), 3.5573(15), 3.6483(15)	Se•••I	3.4224(13), 3.4944(11), 3.6841(12)	Se•••I	3.4354(10)
C-I	2.09(3)(b), 2.105(12), 2.107(15), 2.115(16), 2.119(14)	C-I	2.078(8), 2.082(8), 2.092(8)	C-I	2.095(7)
Angles					
TIE		1,4-F_4DIB		1,2-F_4DIB	
P- Se•••I	104.99(9), 108.60(9), 113.17(9), 113.73(9)	P- Se•••I	88.90(6), 112.60(7), 113.01(7)	P- Se•••I	100.10(6)
C-I•••Se	163.1(9), 169.9(4), 170.0(5), 171.3(3), 172.6(4)	C-I•••Se	154.9(3), 166.5(2), 171.4(2)	C-I•••Se	170.92(19)

observed in halogen bonded complexes involving a selenium atom. Extended halogen bonded chains involve two molecules of $Ph_3P{=}Se$ and three molecules of TIE, while the fourth TIE molecule is uncomplexed. Infinite chains run parallel to *a* and *c*, resulting in fused halogen bonded rings (figure 2.2). A schematic of a layer (figure 2.3) shows that the corners or junctions of these rings are formed by TIE molecules that halogen bond to selenium atoms through all four iodine atoms, and that the size of the rings is expanded by TIE molecules that link the junctions through halogen bonding involving only two of the four iodine atoms. For a given layer, with the four-coordinate TIE at (½ , ½, ½) and the two-coordinate TIE's at (½, ½, 0) and (0, ½, ½) running along the *a* and *c* axes, respectively, there is an empty space at the center of the fused ring at (0, ½, 0), where an uncomplexed partial occupancy TIE sits. Although the uncomplexed TIE diffuses out of the crystal rather easily (in the data crystal, the cavities were only about 20% occupied), crystalline order was well maintained, opening the possibility of diffusing π-stacking ligands, such as dinitrotoluene, into the empty cavities. Layers stack with phenyl embraces being the dominant stacking interaction (which will be discussed later) to complete the structure. Stacked layers are generated by an *n*-glide operation (figure 2.4) which places the four-coordinate junction TIE over the center of a fused ring, i.e. above the site of the uncomplexed TIE. The packing of this complex reveals that the crystal lattice is segregated into regions of donor and acceptor molecules (figure 2.5).

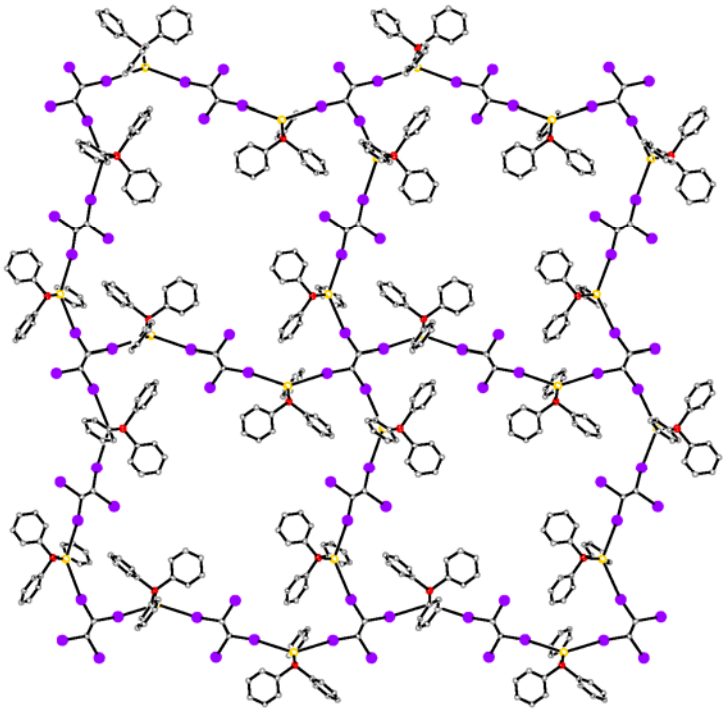

Figure 2.2. Fused octameric rings in the $Ph_3P{=}Se \bullet TIE$ complex.

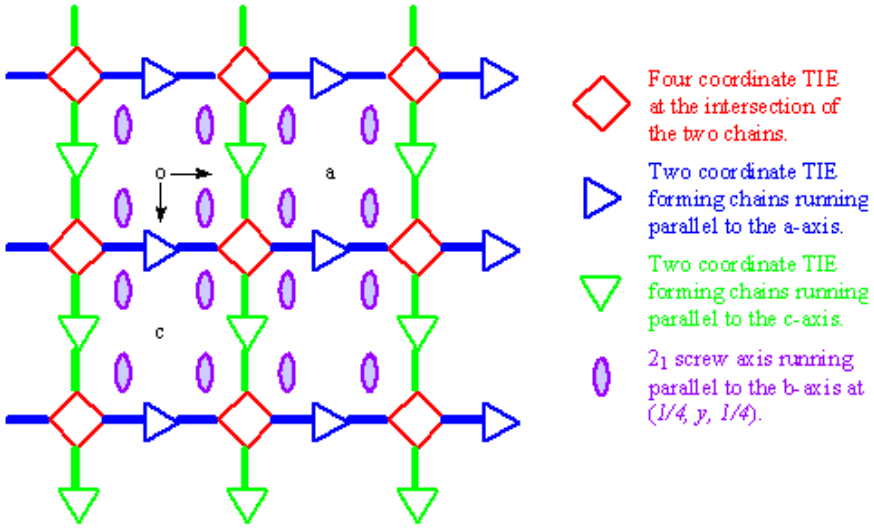

Figure 2.3. A schematic of a layer of $Ph_3P{=}Se$ • TIE

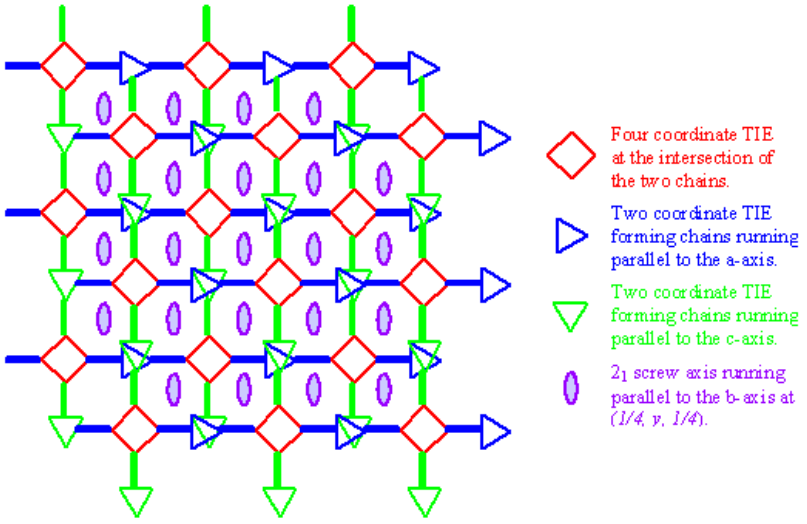

Figure 2.4. A schematic of the stacking of $Ph_3P{=}Se$ • TIE.

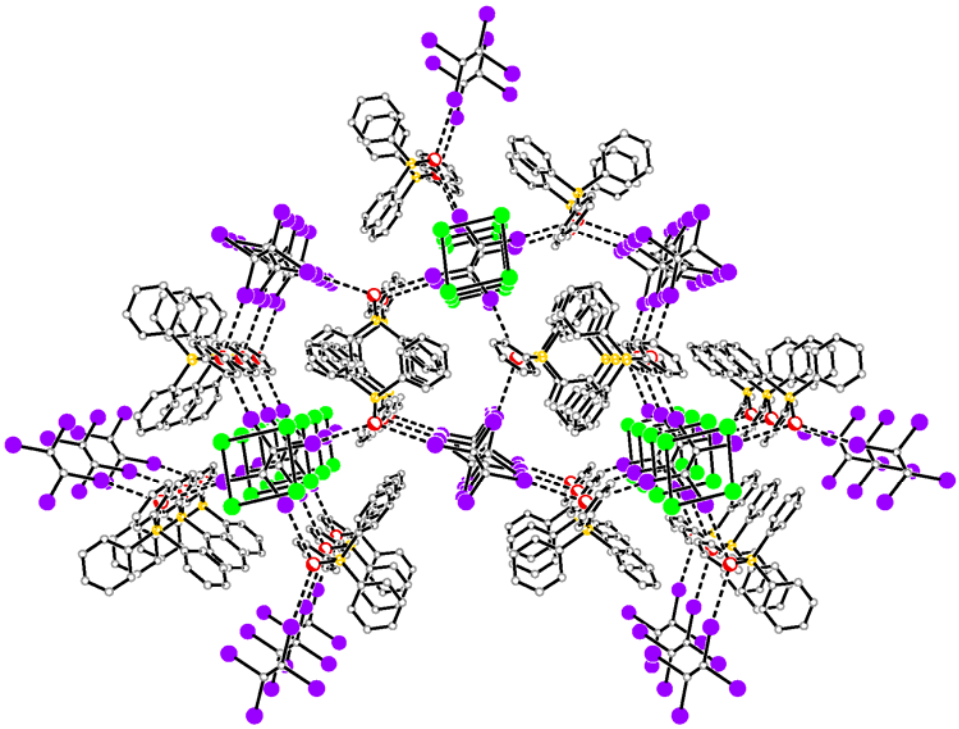

Figure 2.5. Stacking of layers of $Ph_3P{=}Se$ • TIE complex where the bright green atoms are from the uncomplexed TIE.

Crystal Structure of $Ph_3P{=}Se \bullet 1,4\text{-}F_4DIB$

The asymmetric unit consists of two unique donor molecules and four acceptor half molecules, each situated about an inversion center at (0,0,0), (1, 0, ½), (-½, ½ , 0), or (½, 0, 0). There are three unique Se•••I contacts with an average distance of 3.5(1) Å. Similar to the TIE complex, the selenium atom with two unique Se•••I contacts, two different P=Se•••I angles are reported (88.90(6) and 113.01(7)°), either displays orthogonal or tetrahedral geometry. The selenium atom involved in the ½ adduct displays tetrahedral geometry (P=Se•••I angle of 112.60(7) °). Linear geometry is maintained at the iodine atom with an average C-I•••Se angle of 164(8)°. One $Ph_3P{=}Se$ molecule and two molecules of 1,4-F_4DIB form extended halogen bonded chains, while another acceptor bridges two donor molecules into a 1:2 adduct (figure 2.6). The fourth molecule of 1,4-F_4DIB is uncomplexed. Similar to the TIE complex, layers segregated into separate regions of donor and acceptor molecules and phenyl embraces play a dominant role in the stacking of layers (figure 2.7).

Crystal Structure of $Ph_3P{=}Se \bullet 1,2\text{-}F_4DIB$

In this complex, the asymmetric unit consists of one donor and one acceptor molecule situated on general positions. Unlike the previous two complexes where multiple halogen contacts were observed at the selenium atom, there is only one Se•••I contact (3.4354(10) Å) present. Similar to TIE and 1,4-F_4DIB complexes, the P=Se•••I angle (100.10(6)°) confirms that tetrahedral geometry is observed at the selenium atom and the C-I•••Se angle (170.92(19)°) shows that linear geometry is present at the iodine

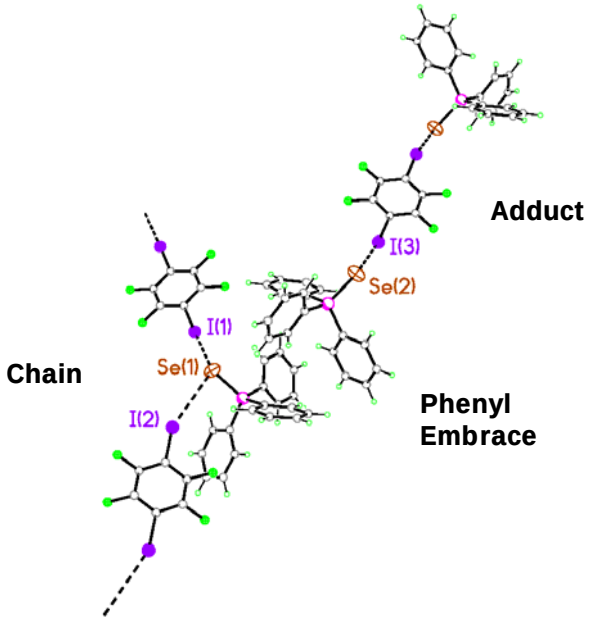

Figure 2.6. $Ph_3P{=}Se$ • 1,4-DITFB infinite halogen bonding chain and 1:2(A/D) adduct.

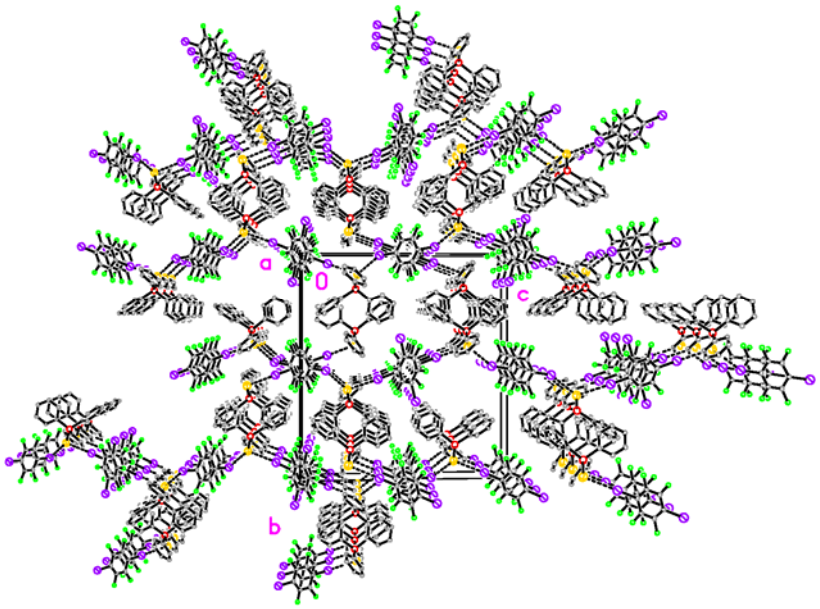

Figure 2.7. Stacking of the $Ph_3P{=}Se$ • 1,4-F_4DIB complex.

atom. The motif observed in the crystal lattice is a 1:1 adduct. However, interactions involving the other iodine atom on the acceptor with the π- cloud of a phenyl ring of the donor, with I•••Ar contacts of approximately 3.7-3.8Å, are also present (figure 2.8). Phenyl embraces are also present in the crystal lattice.

Comparison to known halogen bonding complexes

The prominent bonding motif for dihalogen complexes are adducts. However, there are various types of adducts observed for dihalogen complexes, these include simple adducts, bridging adducts, extended adducts, and bridging amphoteric adducts. A simple adduct (A) is formed when an electron donor interacts at only one end of a dihalogen. When D•••X interactions occur at both ends of a dihalogen, this is referred to as a bridging adduct (B). For robust electron donors, polarization of a dihalogen may be sufficient that the halogen atom not complexed to the donor molecule behaves as an electron donor to a second dihalogen molecule. The dihalogen molecule that serves as both an electron donor and electron acceptor is referred to as amphoteric. An extended adduct (AA) is formed when a 1:1 $D•••X_2:X_2$ ratio is present. However, if a second dihalogen molecule behaves as a Lewis acid acceptor at both ends of the molecule then a bridged amphoteric adduct is formed (BA).[21] For organohalogens, other structural motifs are observed besides adducts these include extended chains (EC), layers (LY) and 3-D networks (3N). Bonding motifs observed in the complexes reported here involved not only adducts but also extended chains and layers. Tables 2.2 – 2.6 shows the D•••X distances (D = N,O,S, and Se; X = Cl, Br, I) and D•••X-Y (Y = C, X, etc.) and Y-D•••X

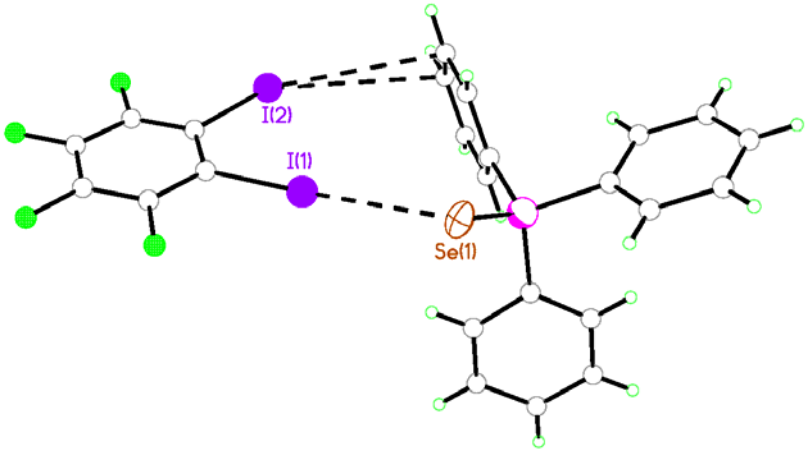

Figure 2.8. Unique interactions for the $Ph_3P{=}Se \bullet 1,2\text{-}F_4DIB$ complex.

Table 2.2. Selected distances (Å) and angles (º) for known organoselenium complexes of dihalogens.[21]

Se···I-I REFCODE	Compound Name	Se•••I	Y-Se•••I	Se•••I-I	Mode
DSEIOD	1.4-Diselenane bis(iodine)	2.830	100.80, 101.40	178.67	A
EZOXUM	Bis(tri-*t*-butylphosphine)-bis(diiodo)-diselenium m2-iodo)-bis(tri-*t*-butylphosphine)-diselenium triiodide	2.760	113.33	171.69	A
GIHZIG	Diphenyldiselenide iodine	2.992	83.92	174.21	A
HECMOR	Di-t-butyliodophosphane selenidediiodine	2.782	105.38	175.84	A
KUWDUB	5,5-Dimethyl-2-selenoimidazolidine-4-one diiodine	2.699	100.10	170.73	A
OXSELI	1,4-Oxaselenane iodine	2.755		174.77	A
PAQKAT	Triphenylphosphineselenido-diiodine	2.802	105.95	173.67	A
PAQKEX	(Tris(dimethylamino)phosphine)selenide-diiodide	2.721 2.711	101.35, 99.62	176.78 177.35	A
PAQKIB	(Tris(diethylamino)phosphine)selenido-diiodide	2.715	106.37	178.05	A
PELHUK	6-Propyl-2-(diiodoseleno)uracil	2.781	96.91	176.75	A
REBNER	Bis(*N*,*N*_-dimethylimidazolidin-2-yl)-di-selenone bis(triiodide) *N*,*N*-dimethylimidazolidine-2-selone iodine	2.683	92.34	175.52	A
RIZMES	Dimethyl-selenium diiodin	2.768	97.75, 94.73	174.31	A
RUQPOI	1,3,5-Triselenacyclohexane diiodine	2.734	100.76, 96.73	179.31	A
THSEL01	Tetrahydroselenophene iodine	2.765	96.95, 108.06	179.06	A
YEYFEN	(*N*-Methyl-1,3-thiazolidine-2(3*H*)-selenone)-diiodine	2.725	98.81	177.48	A
ZOBDOJ	1,1_-Bis(3-methyl-4-imidazolin-2-selenone)methane bis(diiodine)	2.716 2.776	96.89, 92.96	175.63 176.86	A
KIGFEL	Bis(2,4,6-triisopropylphenyl) diselenide diiodide	3.483	101.15	169.18	B

Se···Br-Br REFCODE	Compound Name	Se•••Br	Y-Se•••Br	Se•••Br-Br	Mode
IRABEI	5 : 5_-Tribromo-5, 10_-dibromo-5,10-bromo-bis(5,10-selenanthrene) bis(5,5-dibromoselenanthrene)	2.645	91.99, 91.24	174.19	A

Table 2.3. Selected distances (Å) and angles (º) for known organosulfur complexes of dihalogens.[21]

S···I-I REFCODE	Compound Name	S•••I	Y-S•••I	S•••I-I	Mode
BENZSI	Benzyl sulfide-iodine	2.779	100.59	178.93	A
BIMMEP	4,4-Bis(methylsulfanyl)-1,3-dithiole-2-thione-diiodine	2.716	101.92	177.45	A
DAXXOQ	*N*-Methylbenzothiazole-2-thione-diiodine	2.808	104.4	176.95	A
DAYBOU	1,3-Dithiacyclohexane-2-thione-diiodine	2.755	110.82	175.41	A
DITHINI	1,4-Dithiane bis(iodine)	2.870	100.94, 96.21	177.89	A
FAJPUB	Dithia(3.3.1)propellane bis(iodine)	2.825, 2.806	102.58,106.95 107.20,101.67	176.71, 176.08	A
FAJRAJ	Dithia(3.3.2)propellane bis(iodine)	2.803, 2.901	102.73, 97.79 107.51, 114.67	173.00, 176.97	A
GEGNUB	1,3-Dimethyl-2-thioimidazolium diiodine	2.616	97.65	175.08	A
HAFLAC	(6-Propylthiouracil)-diiodine	2.780	96.06	175.85	A
HEMDIM	Bis((μ2-diiodosulfido-*S*,*S*)-(η5-cyclopentadienyl)-*t*-butylimino-molybdenum)	2.720	126.13, 112.53	175.24	A
LOPQIQ	1,3-Bis(thiourea)triiodonium thiourea-diiodine diiodine triiodide	2.437	105.87	171.59	A
TOTWUU	1,1_-Methylenebis(*S*-iodine-3-methyl-4-imidazoline-2-thione)	2.683	96.79	175.71	A
VARCIA10	1,3,6,7-Tetrathiapentalene-2,5-dione iodine	2.711	99.50	176.63	A
LINHEV	1,4,7,10-Tetrathiacyclododecane diiodide	3.220	89.24	170.54	B
MSNROD	5-(2-Methylmercapto-4-methyl-4,5-dihydro-1' ,3',4'-thiadiazol-5-ylidene)-3-ethyl-rhodanine-iodine	3.099	99.55	178.46	B
PELXUZ	Tetrakis(μ-diiodo)-bis(1,4,7-trithiacyclononane)	3.055, 3.239	99.09, 93.79 87.90, 101.41		B
RUQPIC	*catena*((μ^2-Diiodo)-1,3,5-trithiacyclohexane)	3.169	95.11, 120.42	169.03	B
CEWMIA	2-Imidazolidinethione bis(diiodine)	2.487	102.68	177.90	AA
ZEBQOM	2-(3*H*)-(Diiodothio)benzoxazole diiodine	2.873, 3.298	101.48, 110.21	178.44, 169.79	AA
BAQTOC	Triphenylphosphine sulfide tris(diiodine)	2.591	105.45	178.11	BA
CEWMOG	Bis(2-imidazolidinethione) tris(diiodine)	2.580	102.70	177.57	BA
S···Br-Br REFCODE	Compound Name	S•••Br	Y-S•••Br	S•••Br-Br	Mode
RORNIV	Dimethylsulfide-dibromide	2.299	99.26, 100.01	175.05	A
RORNIV01	Dibromo-dimethyl sulfide	2.328	97.21, 95.67	176.05	A
TEBKIU	1,2,4,5-Tetrakis(ethylthio)benzene bis(dibromine)	3.239	96.97, 89.61	164.45	B

Table 2.4. Selected distances (Å) and angles (º) for known nitrogen heterocycles complexes of dihalogens.[21]

N···I-I REFCODE	Compound Name	N•••I	Y-N•••I	N•••I-I	Mode
GAWXEH	N-Iodine-2,3-diazabicyclo(2.2.2)oct-2-ene	2.431	122.17	175.49	A
TMEAMI	Trimethylamine-diiodine	2.271	107.05,114.47	178.33	A
WEKGIC	(Triphenylphosphonio(trimethylsilyl)iminio)diiodine	2.432	114.70,113.02	178.93	A
CHXADI10	9-Cyclohexyladenine diiodine	2.520	116.16,120.76	177.14	A
HMCPZI	Hexamethylcyclotriphosphazene diiodine	2.418	118.51,117.29	177.80	A
HXMIOD	Hexamethylenetetramine bis(diiodine)	2.497	103.89,113.84	173.92	A
		2.498	108.4, 115.01	173.85	
NULBEB	2,3-bis(2'-Pyridyl)quinoxaline diiodine	2.530	125.56,116.09	173.80	A
NULBIF	4-Cyanopyridine diiodine	2.543	116.27,127,71	175.47	A
		2.554	115.92,126.01	175.50	
VUKDIO	Pyrazine diiodine	2.817	121.64	175.18	*B*
QARGUL	bis(9-Chloroacridine) diiodine	2.981	121.29,118.74	178.75	*B*
PHNAZI01	Phenazine diiodine	2.986	121.20,	180.00	*B*
		3.099	119.76	180.00	
NULBUR	Quinoxaline diiodine	2.949	120.73,116.51	178.77	*B*
		2.918	120.89,123.09	175.77	
HXMTDI	Hexamethylenetetramine diiodine	2.439	112.11,106.67	173.07	*B*
		3.482	84.36, 121.80	179.75	
HMTNTI	Hexamethylenetetramine tri-iodo-nitrogen diiodine	2.475	109.19,113.27	175.41	*B*
		3.247	89.13,118.54	178.10	
CECZAL	2,2'-Bipyridine tris(diiodide)	2.604	134.37,111.99	179.41	BA
DARZAY	2,3,5,6-tetrakis(2-Pyridyl)pyrazine hexakis(diiodine)	2.498	123.95,115.08	174.46	BA
		2.568	110.22,132.69	168.30	
QARGIZ	bis(Acridine) tris(diiodine)	2.440	118.88,119.98	175.08	BA
QARGOF	bis(9-Chloroacridine) tris(diiodine)	2.613	118.88,119.98	179.21	BA
		2.619	120.62,118.25	176.94	
N···Br-Br REFCODE	Compound Name	N•••Br	Y-N•••Br	N•••Br-Br	Mode
ICUGES	N-Bromo-N-(bromine)-triphenylphosphineimine	2.245	110.17	177.24	A
TEYPES	1,3-bis(Dibromo)-s-triazine	2.515	114.83,130.36	174.94	A
ACTNBM	bis(Acetonitrile)-dibromine	2.837	171.81	179.40	B

Table 2.5. Selected distances (Å) and angles (º) for known organooxides complexes of dihalogens.[21]

O···I-I REFCODE	Compound Name	O•••I	Y-O•••I	O•••I-I	Mode
ATICEL	catena-(dodecakis(m3-Formato-O,O,O')-hexa-manganese di-iodine clathrate)	2.827	108.93	174.49 174.58	A
QOJKEF	1,4-Dioxane diiodine	2.808	115.58	178.74	B
VAMDOD	catena-(bis(μ_2-isonitcotinato)-copper di-iodide)	2.947	139.80	174.23	B
CDEXTI10	Cyclohexa-amylose-iodine tetrahydrate	3.070 3.315	108.04, 149.02	167.21 167.46	B
O···Br-Br REFCODE	Compound Name	O•••Br	Y-O•••Br	O•••Br-Br	Mode
ACETBR	Acetone-dibromine	2.818	124.98	178.36	B
DOXABR	1,4-Dioxane-dibromine	2.723	114.45	178.34	B
METHOB	bis(Methanol)-bromine complex	2.705 2.907 2.676 2.826	105.00, 102.21, 107.92, 119.50,	179.10 175.09 178.06 173.75	B
O···Cl-Cl REFCODE	Compound Name	O•••Cl	Y-O•••Cl	O•••Cl-Cl	Mode
ULISAJ	1,4-Dioxane dichlorine	2.647	116.82	178.08	B

Table 2.6. Selected distances (Å) and angles (º) for known nitrogen heterocycles and organosulfides complexes of organohalogens.

N···I-C Compound Name	N•••I	C-N•••I	N•••I-C	Mode
Tetramethylpyrazine 1,4-difluoro-tetraiodobenzene	3.007	116.80,117.50	175.19	EC
4,4'-Dipyridyl diiodo-octafluorobiphenyl	2.734, 2.760	120.29,122.53 121.85,120.59	179.69, 178.04	EC
Phenazine diiodo-octafluorobiphenyl	2.999 2.931	122.27,121.42 117.72,118.52	176.20, 175.39	EC
Phenazine 1,4-difluoro-tetraiodobenzene	2.983	119.96,121.98	169.08	EC
Phenazine 1,4-diiodo-tetrafluorobenzene	3.103	121.23,121.39	173.78	EC
1,4-Diazabicyclo[2.2.2]octane 1,4-difluoro-tetraiodobenzene	2.823, 2.805	97.30,116.07 104.69,119.51	171.26, 169.21	EC
1,4-Diazabicyclo[2.2.2]octane diiodo-octafluorobiphenyl	2.677, 2.691	108.62,111.91 109.62,111.33	177.04, 176.32	EC
Dimethylquinoxaline 1,4-diiodo-tetrafluorobenzene	3.121	119.10,122.42	169.72	EC

N···Br-C Compound Name	N•••Br	C-N•••Br	N•••Br-C	Mode
1,4-Diazabicyclo[2.2.2]octane dibromo-octafluorobiphenyl	2.769	106.97,110.67	174.89	EC
4,4'-Dipyridyl dibromo-octafluorobiphenyl	2.853, 2.823	121.07,122.42 119.14,122.32	178.28, 178.97	EC

S···I-C Compound Name	S•••I	C-S•••I	S•••I-C	Mode
1,4-Dithiane tetraiodoethylene	3.305	111.79,91.36	179.47	EC
1,4-Dithiane 1,4-diiodo-tetrafluorobenzene	3.426, 3.432	89.97,88.46 101.94,103.03	164.64, 175.73	EC
1,4,7-Trithiacyclononane 1,4-diiodo-tetrafluorobenzene	3.264, 3.305	99.55,98.69 85.38,109.02	178.54, 166.86	EC
Thiourea 1,4-diiodo-tetrafluorobenzene	3.281, 3.348, 3.404	86.66, 91.30, 84.56	179.19, 176.73, 171.01	EC
Triphenylphosphine sulfide 1,4-diiodo-tetrafluorobenzene	3.309, 3.419	115.30, 114.83	166.91, 172.48	
2-Mercapto-1-t-butylimidazole 1,4-diiodo-tetrafluorobenzene	3.235, 3.304	91.78, 92.76	175.23, 167.38	
Ethylene thiourea tetraiodoethylene	3.374, 3.498	93.96, 92.76	169.04, 172.31	
2-Mercaptopyrimidine 1,4-diiodo-tetrafluorobenzene	3.222	91.49	170.79	B

angles for dihalogen and organohalogen complexes. D•••X distances for dihalogen complexes are significantly shorter than organoiodine complexes reported here, due to the greater Lewis acid behavior compared to organohalogens. The D•••X-Y angles for the dihalogen and organohalogens, listed in the tables, show that there is little deviation from linear geometry at the halogen atom. Also for our complexes linear geometry is observed at the iodine atom. However, trigonal planar geometry was not observed for the listed dihalogen and organohalogen complexes of O, S, and Se donors because the Y-D•••X angle deviated greatly from 120º. Tetrahedral geometry (109.5°), orthogonal geometry (90°) or a variation between the two was observed for these complexes unlike complexes of nitrogen heterocycles where trigonal planar geometry was observed. Similar to the dihalogen and organohalogen complexes of O, S, and Se donors, the complexes reported here do not display trigonal planar geometry but display tetrahedral geometry because the Y-D•••X angle reported for these complexes is closer to 109.5º than 120º

Phenyl Embraces

Phenyl embraces are motifs that are formed through C–H•••π interactions involving multiple aryl groups. These motifs are classified as two types: edge-to-face (EF) and offset-face-to-face (OFF), figure 2.9.[22] The phenyl rings on triphenylphosphines can exhibit three different conformations based on the X-P-C-C (where X is a metal or chalcogen) torsional angles (*T*) for each phenyl group. These three different conformations are orthogonal ($0 \leq |T| < 20º$), parallel ($70 < |T| \leq 90º$) and staggered ($20 \leq |T| \leq 70º$). A ligand can assume three different conformations based on

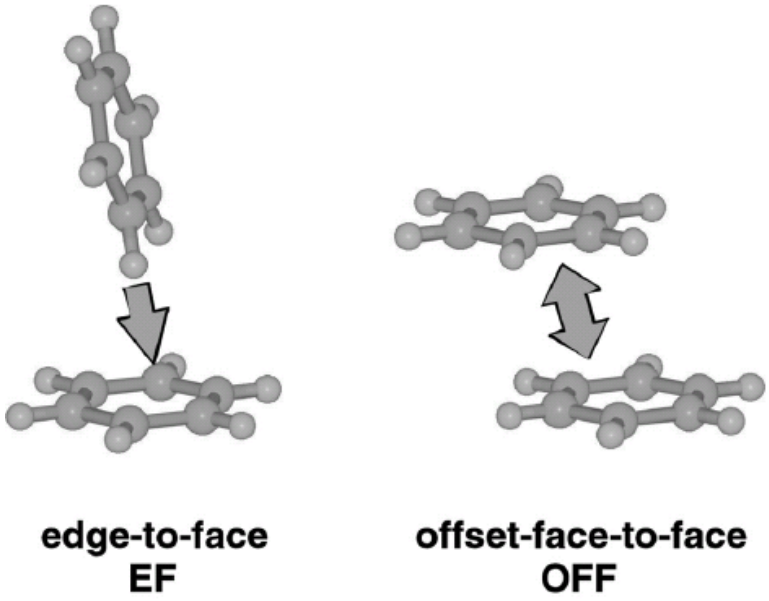

Figure 2.9. Phenyl embrace motifs.[22]

the individual conformations of the phenyl groups. These conformations include the *rotor* conformation which exists if all three phenyl groups exhibit staggered conformation and is the most favorable conformation for the triphenylphosphine ligand. *Orthogonal flipper* conformation occurs when one phenyl ring shows orthogonal conformation and the other two rings have torsional angles of similar magnitude, within +/- 20º, but opposite signs. *Irregular* conformation is defined as all three phenyl rings displaying a different conformation or when two of the rings show the same conformation and the third displays a different one. The most common phenyl embraces for the triphenylphosphine ligand are four-fold phenyl embrace (4PE), which is classified as orthogonal (O4PE) or parallel (P4PE) where the latter is more common, or a six-fold phenyl embrace (6PE). Six-fold phenyl embraces are identified by meeting three criteria: the ligand must display rotor conformation, distance of P•••P is less than 7.5 Å, and X-P•••P angle between 160-180º.[18,19,20]

$(Ph_3P=Se)_4 \bullet (TIE)_3$

In the TIE complex, donor molecules are involved in 4PE, the donor with one halogen bonding contact with a disordered TIE molecule exhibits *orthogonal flipper* conformation. *Irregular* conformation is observed on the donor molecule with both Se•••I contacts to the ordered TIE molecule, two of the phenyl rings are staggered and one is orthogonal. In these phenyl embraces, the selenium atoms are all symmetrically equivalent by 2_1/b and there are two unique columns.

$Ph_3P{=}Se$ • 1,4-F_4DIB

In addition to extended chains and adducts present in the 1,4-F_4DIB complex, extensive 4PE are also observed which link donors, related by translation along cell side *a*, into columns with centroid···centroid distances of ~4.8 Å (figure 2.10). The donor molecule involved in the formation of extended chains exhibits *rotor* conformation. The donor molecule involved in the formation of the adduct exhibit *irregular* conformations, two phenyl groups are staggered and one is orthogonal. While almost identical to the phenyl embraces in the TIE complex, there are two unique selenium atoms in each column which are related by pseudo 2_1 operation, though there is only one unique column observed.

$Ph_3P{=}Se$ • 1,2-F_4DIB

Unlike the previous two complexes, this complex involves 6PE. *Rotor* conformation is observed for the donor molecule, a P•••P distance of ~6.6 Å and X-P•••P angle of ~179° was measured.

Thermal Analysis

Thermal analysis methods have been reported as useful devices for inspecting the stability of halogen bonded complexes.[8] Table 2.7 shows the melting points, vaporization onset temperatures and mass changes for the acceptors, donor and the three complexes reported here. Pure acceptors and donor are thermally stable and evaporate completely in a single event.

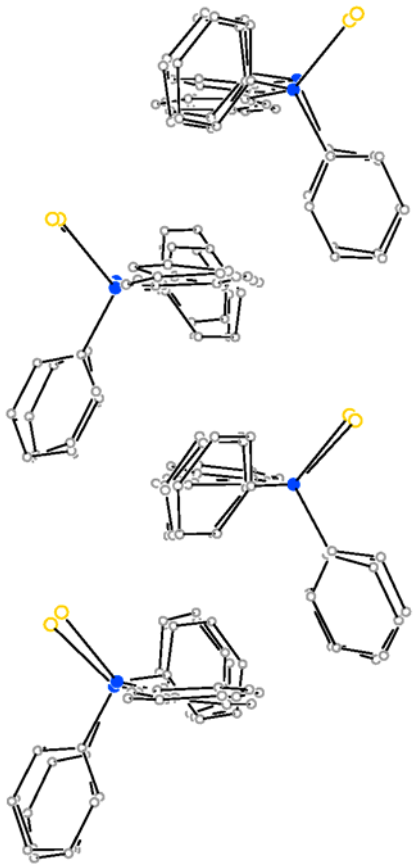

Figure 2.10. A diagram of phenyl embraces linking donor molecules in the $Ph_3P{=}Se$ • 1,4-F_4DIB complex.

$(Ph_3P{=}Se)_4 \bullet (TIE)_3$

This complex melts at 122ºC and decomposes in two thermal events; unfortunately these events were not well defined. This discrepancy is probably due to the similarities of the melting points of pure donor and acceptor. In all likelihood, the first thermal event relates to the loss of acceptor, while the second event corresponds to loss of the donor. This is confirmed by the presence of an endotherm at 363ºC that coincides with the boiling point of $Ph_3P{=}Se$. Also present is an exotherm with an onset at 150ºC, this exotherm has been observed in other TIE complexes involving thiones.[8]

$Ph_3P{=}Se \bullet 1,4\text{-}F_4DIB$

Two thermal events are observed for this complex and it decomposes cleanly into two thermal events and the complex melts at 123ºC. The first thermal event corresponds to the loss of the acceptor and the onset occurs at 105ºC. The second thermal event is the loss of donor at the onset of 275ºC. This is supported by an endotherm that occurs at 366ºC.

$Ph_3P{=}Se \bullet 1,2\text{-}F_4DIB$

Similar to the $Ph_3P{=}Se \bullet 1,4\text{-}F_4DIB$ complex, this complex melts at 128ºC, and decomposes cleanly in two thermal events. Complete loss of the acceptor occurs at the first thermal event with an onset at 98ºC, while the second thermal event has an onset at 255ºC which corresponds to the loss of the donor. This is confirmed by the endotherm at 355ºC which is near the boiling point for $Ph_3P{=}Se$ (363ºC).

Table 2.7. Thermal Behavior of Organoiodine acceptors, $Ph_3P{=}Se$ and their complexes

compound	melting point (ºC)	thermal onset (ºC)	mass loss (%)
TIE	191- 193[a]		
1,4-F_4DIB	108- 110[a]		
1,2-F_4DIB	49- 50[a]		
$Ph_3P{=}Se$	186-190[a]		
$(Ph_3P{=}Se)_4 \bullet (TIE)_3$	122[b]	N/A	N/A
		N/A	N/A
$Ph_3P{=}Se \bullet$ 1,4-F_4DIB	123[b]	105	50 (54)
		275	49 (46)
$Ph_3P{=}Se \bullet$ 1,2-F_4DIB	128[b]	98	52 (54)
		255	45 (46)

[a] Vendor- supplied data. [b] Onset of melting by DSC. Mass loss is given as experimental (theoretical)

Conclusion

Halogen bonding involving triphenylphosphine selenide with an assortment of organoiodides generates a variety of structures. Similar to complexes involving sulfur or nitrogen donors with organoiodines, the complexes of TIE and 1,4-F_4DIB pack such that donor and acceptor molecules are segregated. However, for the 1,2-F_4DIB complex the donor and acceptor molecules did not pack into segregated regions. The complexes reported here have significantly longer bond distances than complexes of seleones and I_2. Complexes of seleone and I_2 mainly result in terminal structures. The acceptors involved in the complexes presented here, act as bridging ligands between donors. In the case of TIE and 1,4-F_4DIB complexes, the bridging between donors leads to the formation of extended chain structures.

References

1. Crihfield, A.; Hartwell, J.; Phelps, D.; Walsh, R. B.; Harris, J.L.; Payne, J.F.; Pennington, W.T.; Hanks, T.W. *Cryst. Growth & Des.* **2003**, *3*, 313.

2. (a) Blake, A. J.; Gould, R. O.; Radek, C.; Schroder, M. *J. Chem. Soc., Chem. Commun.* **1993**, 1191. (b) Blake, A. J.; Devillanova, F. A.; Garau, A.; Isaia, F.; Lippolis, V.; Parsons, S.; Schroder, M. *J. Chem. Soc., Dalton Trans.* **1999**, 525. (c) Blake, A. J.; Devillanova, F. A.; Garau, A.; Gilby, LM.; Gould, R. O.; Isaia, F.; Lippolis, V.; Parsons, S.; Radek, C.;Schroder, M. *J. Chem. Soc., Dalton Trans.* **1998**, 2037. (d) Blake, A. J.; Cristiani, F.; Devillanova, F. A.; Garau, A.; Gilby, LM.; Gould, R. O.; Isaia, F.; Lippolis, V.; Parsons, S.; Radek, C.; Schroder, M. *J. Chem. Soc., Dalton Trans.* **1997**, 1337.

3. (a) Ahlsen, E. L.; Stromme, K. O. *Acta Chem. Scand.* **1974**, *A28*, 175. (b) Herbstein, F. H.; Schwotzer, W. *Angew. Chem., Int. Ed. Engl.* **1982**, *21*, 219. (c) Herbstein, F. H.; Schwotzer, W. *J. Am. Chem. Soc.* **1984**, *106*, 2367. (d) Bricklebank, N.; Skabara, P. J.; Hibbs, D. E.; Hursthouse, M. B.; Malik, K. M. A. *J. Chem. Soc., Dalton Trans.* **1999**, 3007.

4. Schweikert, W. W.; Meyers, E. A. *J. Phys. Chem.* **1968**, *72*, 1561.

5. Arca, M.; Demartin, F.; Devillanova, F. A.; Garau, A.; Isaia, F.; Lippolis, V.; Verani, G. *J. Chem. Soc., Dalton Trans.* **1999**, 3069.

6. Bjorvatten, T.; Hassel, O. *Acta Chem. Scand.* **1961**, *15*, 1429.

7. Homesland, O.; Romming, C. *Acta Chem. Scand.* **1966**, *20*, 2601.

8. Jay, J. I.; Padgett, C. W.; Walsh, R. D. B.; Hanks, T. W.; Pennington, W. T. *Cryst. Growth & Des.* **2001**, *1*, 501.

9. (a)Hartl, H.; Steidl, S. *Acta Crystallogr.* **1980**, *B36*, 65. (b) Nassimbeni, L. R.; Niven, M. L.; Suckling, A. P. *Inorg. Chim. Acta* **1989**, *159*, 209. (c) Bjorvatten, T. *Acta Chem. Scand.* **1962**, *16*, 749. (d) Imakubo, T.; Sawa, H.; Kato, R. *J. Chem. Soc. Chem. Commun.* **1995**, 1097.

10. (a) Kubiniok, S.; du Mont, W.W.; Pohl, S.; Saak, W. *Angew. Chem., Int. Ed.* **1988**, *27*, 431. (b) du Mont, W.W.; Martens, A. ; Pohl, S.; Saak, W *Inorg. Chem.* **1990**, *29*, 4847. (c) Knobler, C.; McCullough, J.D. *Inorg. Chem.* **1968**, *7*, 365. (d) Maddox, H.; McCullough, J.D. *Inorg. Chem.* **1966**, *5*, 522. (e) Godfrey, S.M.; McAuliffe, C.A.; Pritchard, R.G.; Sarwar, S. *J. Chem. Soc. Dalton Trans.* **1997**, 3501. (f) Chao, G.Y.; McCullough, J.D. *Acta Crystallogr.* **1961**, *14*, 940. (g) Godfrey, S.M.; McAuliffe, C.A.; Pritchard, R.G.; Sarwar, S. *J. Chem. Soc. Dalton Trans.* **1997**, 1031.

11. (a) Jeske, J.; du Mont, W.W.; Jones, P.G. *Chem. Eur. J.* **1999**, *5*, 385. (b) Demartin, F.; Devillanova, F.A.; Garau, A.; Isaia, F.; Lippolis, V.; Verani, G. *Polyhedron* **1999**, *18*, 3107. (c) Boyle, P. D.; Cross, W.I.; Godfrey, S.M.; McAuliffe, C.A.; Pritchard, R.G.; Teat, S. *J. Chem. Soc.,Dalton Trans.* **1999**, 2219. (d) Cristiani, F.; Demartin, F.; Devillanova, F.A.; Isaia, F.; Saba, G.; Verani, G. *J. Chem. Soc. Dalton Trans.* **1992**, 3553. (e) Cristiani, F.; Demartin, F.; Devillanova, F.A.; Isaia, F.; Lippolis, V.; Verani, G. *Inorg. Chem.* **1994**, *33*, 6315. (f) Bigoli, F.; Pellinghelli, A.M.; Deplano, P.; Devillanova, F.A.; Lippolis, V.; Mercuri, L.M.; Trogu, E.F. *Gazz. Chim. Ital.* **1994**, *124*, 445.

12. Godfrey, S.M.; Jackson, S.L.; McAuliffe, C.A.; Pritchard, R.G. *J. Chem. Soc., Dalton Trans.* **1997**, 4499.

13. Dahl, T. ; Hassel, O. *Acta Chem. Scand.* **1965**, 19, 2000.

14. Holmesland, O.; Romming, C. *Acta Chem. Scand.* **1966**, *20*, 2601.

15. Bjorvatten, T. *Acta Chem. Scand.* **1963**, *17*, 2292.

16. Werz, D.B.; Gleiter, R.; Rominger, F. *J.Org.Chem.* **2004**, *69*, 2945.

17. Kohrle, J.; Jakob, F.; Contempre, B.; Dumont, J.E. *Endocrine Reviews* **2005**, *26*, 944.

18. Dance, I.; Scudder, M. *Chem. Eur. J.* **1996**, *2*, 481.

19. Dance, I.; Scudder, M. *J. Chem. Soc., Dalton Trans.* **2000**, 1579.

20. Burrows, A.D. *Cryst. Eng. Comm.* **2001**, *46*, 1.

21. Pennington, W.T.; Hanks, T.W.; Arman, H.D, "Halogen Bonding with Dihalogens and Interhalogens," in *Structure and Bonding Series: Halogen Bonding, Fundamentals and Applications*, (Eds. G. Resnati, P. Metrangolo), Springer, London, **2007**, chapter 3.

22. (a) Dance, I. *Mol. Cryst. Liq. Cryst.* **2005**, *440*, 265. (b) Burrows, A.D. *Cryst. Eng. Comm.* **2001**, *46*, 1.

CHAPTER THREE

HALOGEN BONDED COMPLEXES OF BENZIMIDAZOLES

Introduction

Hyperthyroidism, commonly known as Graves' disease, is the overproduction of the thyroid hormones: 3,5,3′-triiodothyronine (T3) and 3,5,3′,5′-tetraiodothyronine (T4).[1] Most anti-thyroid drugs focus on the removal of diiodine through the introduction of thioamides to form stable charge-transfer complexes with the diiodine.[1,2 3] Anti-thyroid drugs, containing thioamides, are classified into two categories: ionic salts and weak charge-transfer complexes. The first class inhibits the production of T4 hormone by the disruption of the iodination mechanism.[4,5 ,6 ,7] The other class prevents either the production of thyroid peroxide (TPO) – iodonium complex[5,6 ,7] or iodothyronine deiodinase, an enzyme used for the monodeiodination of the T4 prohormone to the T3 hormone.[4,6 ,7] Mercaptothiazoline (TZTDH), 2-Mercapto-1-methylimidazole (MMI), and 6-n-propyl-2-thiouracil (PTU) are some of the most widely prescribed drugs for hyperthyroidism. TZTDH and MMI belong to the class forming ionic salts while PTU belongs to the class of antithyroid drugs which form weak charge-transfer complexes.

Many investigations have been conducted to understand the interaction between thioamides and diiodine,[1,2,3,8,9,10,11,12] however relatively little is known about the interactions of these compounds with organoiodines. The only recent report involves halogen bonding of MMI with tetraiodoethylene, 1,4-diiodotetrafluorobenzene, and 1,2-diiodotetrafluorobenzene.[13] The investigation of thioamides, including ones that may not be effective as anti-thyroid drugs through the two routes stated above, could provide

another route to the treatment of hyperthyroidism by inhibiting the organoiodines involved in the production of the T3 hormone.

Herein we report the structural and thermal characterization of halogen bonding complexes (table 3.1) involving 2- mercapto-benzimidazole (MBZIM), 2-mercapto-5-methyl-benzimidazole (MMBZIM), 2-mercapto-benzoxaole (MBZOX), and 2-mercapto-benzothiazole (MBZTH) with 1,4-diiodotetrafluorobenzene (1,4-F_4DIB), 1,2-diiodotetrafluorobenzene (1,2-F_4DIB), tetraiodoethylene (TIE), and iodoform (CH_3I).

Halogen Bonded Complexes

Selected distances and angles for these complexes are given in Tables 3.2, 3.3, 3.4, and 3.5. Crystal packing of all complexes is controlled by noncovalent interactions between the donor and acceptor which include S•••I, N-H•••S and I•••I interactions.

Crystal Structure of MBZIM • 1,4-F_4DIB

One acceptor and one donor situated on general positions make up the asymmetric unit (figure 3.1). The acceptor is linked to the donor through one S•••I contact (3.301(2) Å) and another interacts with the π cloud of the phenyl ring on the donor. The C=S•••I angle is 131.0(3)°, which deviates from the predicted geometry of trigonal planar. It also diverges from tetrahedral geometry observed in many halogen bonded complexes involving thiones. The C-I•••S angle of 168.0(2)° indicates that linear geometry is present at the iodine atom. Halogen bonding interactions generate extended chains and adjacent chains are related through an inversion operation. MBZIM molecules of two inversion

Table 3.1. Benzimidazole complexes to be discussed.

Donors \ **Acceptors**	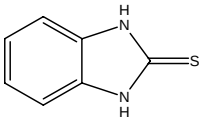 MBZIM	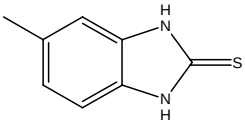 MMBZIM	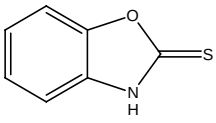 MBZOX	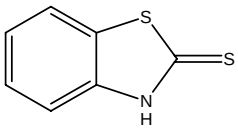 MBZTH
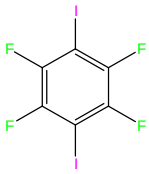 1,4-F_4DIB	MBZIM • 1,4-F_4DIB	($MMBZIM)_2$ • 1,4-F_4DIB • $(H_2O)_2$	$(MBZOX)_2$ • 1,4-F_4DIB	$(MBZTH)_2$ • 1,4-F_4DIB
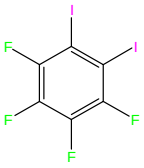 1,2-F_4DIB	MBZIM • 1,2-F_4DIB		MBZOX • 1,2-F_4DIB	
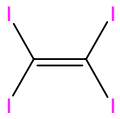 TIE	MBZIM • TIE			MBZTH • TIE
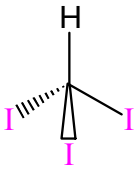 CH_3I				MBZTH • CHI_3

Table 3.2. Selected Distances (Å) and Angles (º) for 1,4-F_4DIB complexes.

Distances

MBZIM		MMBZIM		MBZOX		MBZTH	
C-S	1.689(8)	C-S	1.703(3)	C-S	1.666(10)	C-S	1.670(7)
C-I	2.080(8), 2.084(7)	C-I	2.095(3)	C-I	2.069(8)	C-I	2.092(6)
S•••I	3.301(2)	S•••I	3.2696(9)	S•••I	3.241(2)	S•••I	3.3086(18)
S•••N	3.372(6)[a], 3.331(6)[b]	S•••N	3.434(2)[a]	S•••N	3.325(7)[a]	S•••N	3.375(6)[a]
I•••C	3.532(9)[c], 3.712(10)[c]	S•••O	3.457(2)[b]				
		N•••O	2.897(3)				
		O•••O	2.765(5)[c], 2.781(5)[b]				

Angles

MBZIM		MMBZIM		MBZOX		MBZTH	
C=S•••I	131.0(3),	C=S•••I	95.98(9)	C=S•••I	110.4(3)	C=S•••I	104.4(2)
C-I•••S	168.0(2)	C-I•••S	169.31(7)	C-I•••S	173.8(2)	C-I•••S	178.26(18)
C-N•••S	123.9(4)[a], 125.2(5)[a], 127.4(5)[b], 120.8(4)[b]	C-N•••S	116.99(15)[a], 130.36(17)[a]	C-N•••S	122.5(6)[a], 128.2(5)[a]	C-N•••S	118.0(4)[a], 124.0(4)[a]
C=S•••N	104.8(3)[b], 108.2(3)[a]	C=S•••N	101.42(10)[a]	C=S•••N	108.8(3)[a]	C=S•••N	108.1(2)[a]
C-I•••C	71.7(5)[d], 86.3(6)[d], 92.5(5)[d], 98.0(6)[d], 145.9(3)[c], 154.6(3)[c]	C-N•••O	124.71(18), 124.98(17)				
		C=S•••O	104.55(10)[b]				
		O•••O•••S	83.55(10)[b]				
		O•••O•••N	78.48(10)[c], 93.21(11)[b]				

[a] Atoms listed with a lower case letter were generated by the following symmetry operators: For mbzim: (a) 1-x, 1-y, 1-z, (b) 1-x, 1-y, -z, (c) 1-x, y-0.5, 0.5-z, (d) 1-x, y+0.5, 0.5-z. For mmbzim: (a) -1-x, -y, -z , (b) -1-x, 1-y, -z, (c) –x, 1-y, -z. For mbzox a: (a) 1-x, -y, 1-z. For mbzth: (a) -1-x, 1-y, 2-z

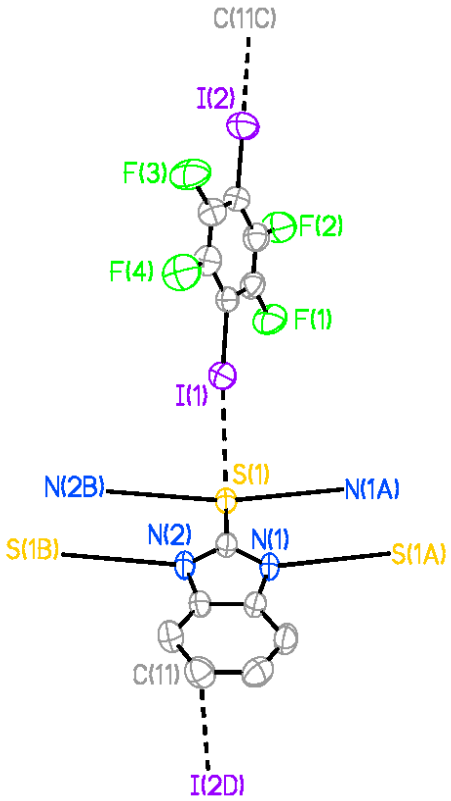

Figure 3.1. Thermal ellipsoid plot of MBZIM • 1,4-F_4DIB (50% probability); hydrogen atoms are omitted for clarity. The atoms with letter suffixes were generated by symmetry operations in table 3.1

related chains form centrosymmetric dimers (center at ½ , ½ , ½) through N-H•••S contacts. An infinite array of these chains linked through hydrogen bonding generates infinite 1-D N-H•••S ribbons (figure 3.2).Layers are generated by translation and stack along the *a* axis which show that acceptors are interdigitated (figure 3.3). A view down *a* axis, shows that extended halogen bonded chains lie perpendicular to infinite hydrogen bonded ribbons. Molecules of donor stack in a step wise head to head manner and the π cloud of a phenyl ring on a donor molecule interacts with an acceptor with a C-I•••$C_{(phenyl)}$ distance of 3.532(9) Å.

Crystal Structure of $(MMBZIM)_2$ • 1,4-F_4DIB• $(H_2O)_2$

Unlike the crystal structure of MBZIM • 1,4-F_4DIB, the asymmetric unit contains one donor and one water molecule situated on general positions and one acceptor molecule that lies on an inversion center at ½ , ½ , ½ (figure 3.4). An acceptor molecule is linked to a donor molecule through one S•••I contact (3.2696(9) Å) which leads to the formation of 1/2 (A/D) halogen bonded adducts. This was the shortest halogen contact reported in this study for 1,4-F_4DIB complexes. The C=S•••I angle was reported as 95.98(9)° which suggests that the geometry at the sulfur atom is more characteristic of orthogonal geometry rather than trigonal planar. The C-I•••S angle (169.31(7)°) is similar in magnitude to the MBZIM complex and not surprising the iodine atom displays linear geometry. Halogen bonded adducts are linked together by the formation of N-H•••S dimers between donor molecules. Centrosymmetric dimers of donors (centered at -½ , 0 , 0) are generated by a pair inversion related chains. These dimers in combination with water molecules from extended hydrogen bonded ribbons composed of N-H•••S, O-H•••S

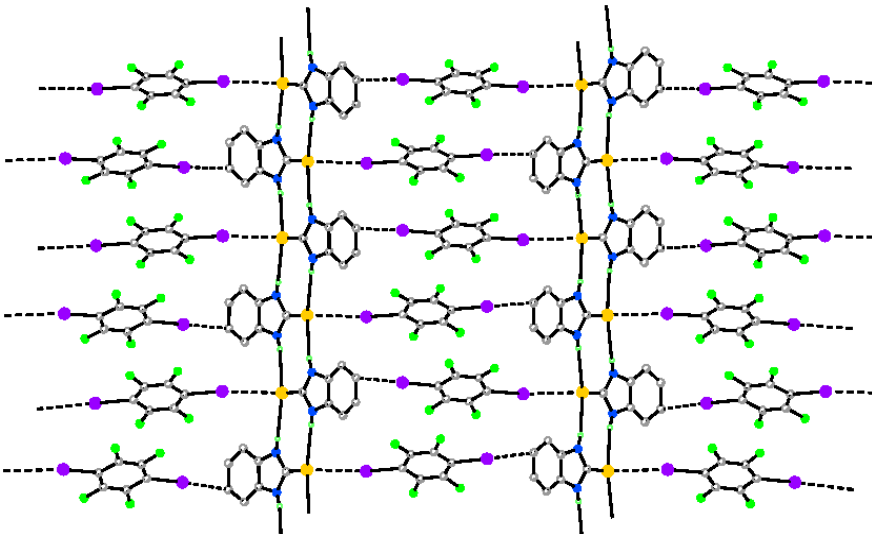

Figure 3.2. View of a layer of the crystal down the *a*- axis.

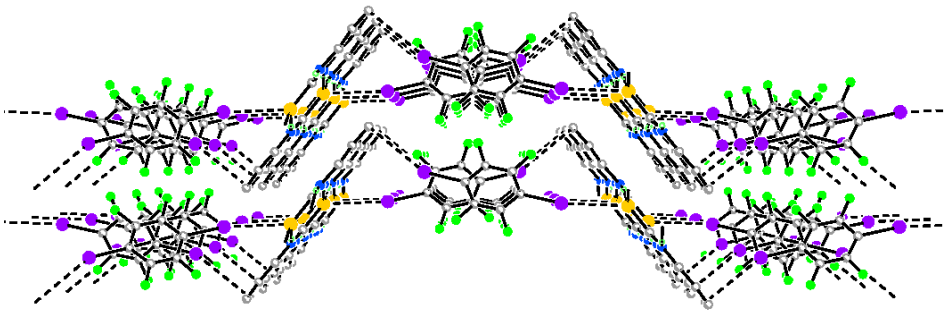

Figure 3.3. Packing diagram of MBZIM • 1,4-F_4DIB.

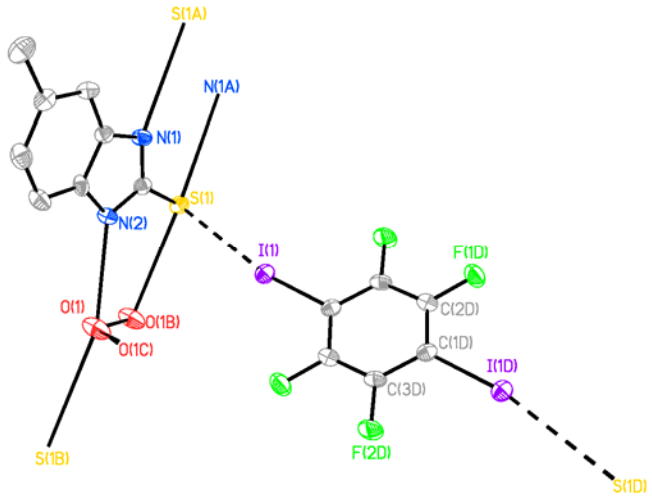

Figure 3.4. Thermal ellipsoid plot of MMBZIM • 1,4-F_4DIB • $(H_2O)_2$ (50% probability). The atoms with letter suffixes were generated by symmetry operations in table 2 except for the suffix 'd' which was generated by the symmetry operation: 1-x, 1-y, 1-z.

and N-H•••O interactions (figure 3.5). A pair of water molecules, containing disordered hydrogen atoms (centered at 0 , ½ , 0), form extended chains of water molecules which are out of the plane of the hydrogen bonded ribbons between donor molecules. The combination of interactions between the water and donor molecules with the halogen bonding interactions leads to the formation of layers. These layers are linked through a water backbone (figure 3.6).

Crystal Structures of $(MBZOX)_2$ • 1,4-F_4DIB and $(MBZTH)_2$ • 1,4-F_4DIB

Both complexes contain one donor molecule which is situated on a general position and one acceptor molecule that lies on an inversion center at ¾ , ¾ , ½ , for MBZOX • 1,4-F_4DIB, and ½ , ½ , ½ , for MBZTH • 1,4-F_4DIB (figures 3.7 and 3.8) in the asymmetric unit. One unique S•••I contact is observed in both complexes (3.241(2) for MBZOX and 3.3086(18) Å for MBZTH) which allows for the formation of 1/2 (A/D) halogen bonded adducts. The shorter halogen bonded contact distance reported for MBZOX complex may be due to the size of the oxygen atom. The C=S•••I angles (110.4(3) and 104.4(2)° for MBZOX and MBZTH, respectively) suggest that tetrahedral geometry is observed at the sulfur atom. The C-I•••S angles (173.8(2) and 178.26(18)° for MBZOX and MBZTH, respectively) confirm that linear geometry is maintained at the iodine atom. In both complexes, the donors form the common N-H•••S hydrogen bonded dimers. Unlike the 1,4-F_4DIB complexes of MBZIM and MMBZIM, these complexes lack infinite hydrogen bonded ribbons due to the replacement of the amide proton with either an oxygen or sulfur atom. These hydrogen bonded dimers link the halogen bonded

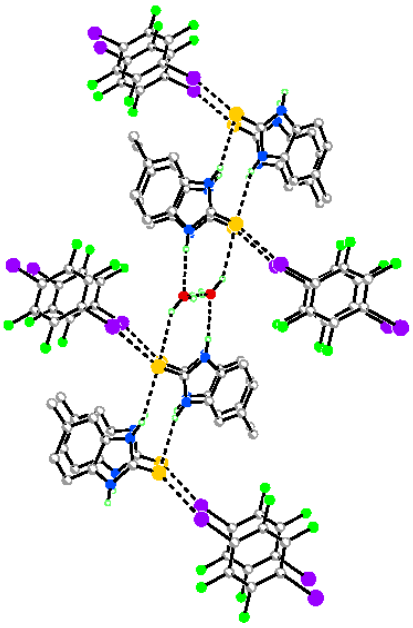

Figure 3.5. View down the *a* axis, showing the linking of the infinite hydrogen bonded ribbons.

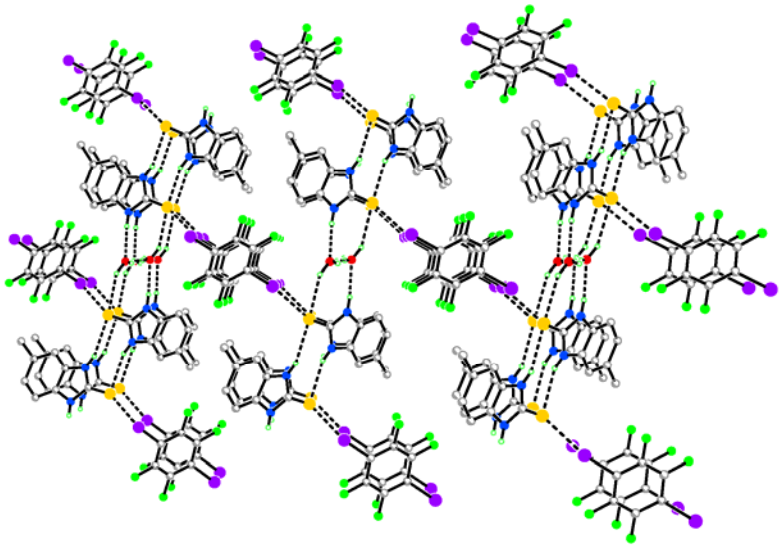

Figure 3.6. Packing diagram of MMBZIM • 1,4-F_4DIB complex, View down the *a* axis

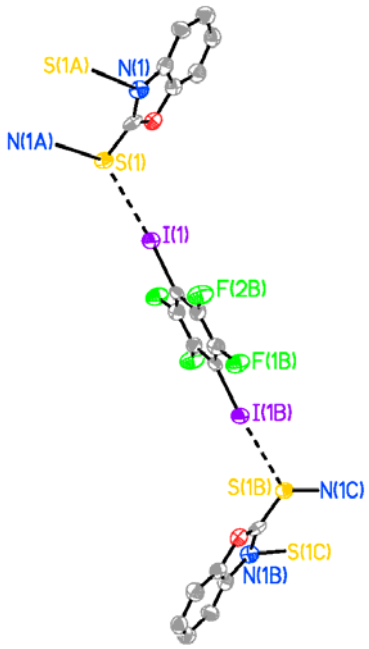

Figure 3.7. Thermal ellipsoid plot of MBZOX • 1,4-F_4DIB (50% probability). The atoms with letter suffixes 'a' were generated by symmetry operations in table 3.1 except for suffixes 'b' and 'c' which were generated by the symmetry operations 1.5 –x, 1.5-y, 1-z and 0.5+x, 1.5+y, z, respectively.

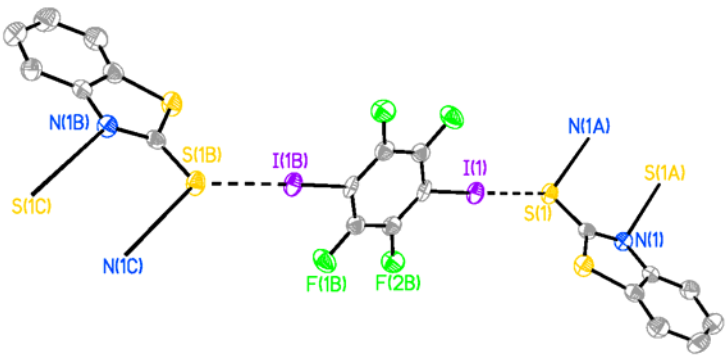

Figure 3.8. Thermal ellipsoid plot of MBZTH • 1,4-F_4DIB (50% probability). The atoms with letter suffixes 'a' were generated by symmetry operations in table 3.1 except for suffixes 'b' and 'c' which were generated by the symmetry operations 1–x, 1-y, 1-z and 2+x, y, z-1, respectively.

adducts together. The packing diagram of MBZOX • 1,4-F_4DIB reveals that these infinite chains pack in a crisscross fashion (figure 3.9),while the packing MBZTH • 1,4-F_4DIB, shows that infinite chains stack parallel to each other (figure 3.10).

Crystal Structures of MBZIM • 1,2-F_4DIB

The asymmetric units of MBZIM • 1,2-F_4DIB (figure 3.11) contains one donor and one acceptor molecule situated on general positions. There is only one unique halogen bond contact (3.309(2) Å) which leads to the formation of a 1/1 adduct between a donor and acceptor molecule. Similar to what is observed in other MBZIM complexes, the common N-H•••S ribbons are present. These ribbons link two halogen bonded adducts together form a 2/2 adduct. Packing of the MBZIM complex shows infinite N-H•••S ribbons are linked through S•••I interactions and π stacking, 3.520(6) Å, of the interdigitated acceptors (figure 3.12). π stacking is a strong interaction formed between two porphyrins that are parallel to one another with an interplanar separation of 3.4-3.6 Å.[14] The packing diagram of MBZIM • 1,2-F_4DIB is similar to MBZIM • 1,4-F_4DIB except N-H•••S ribbons are not linked directly to one another through halogen bonding.

Crystal Structures of MBZOX • 1,2-F_4DIB

This crystal structure contains one donor and one acceptor molecule situated on general positions (figure 3.13). Similar to MBZIM • 1,2-F_4DIB, there is only one unique S•••I contact which forms 1/1 adduct. Analogous to other MBZTH complexes, the common N-H•••S dimers are present. These dimers link two adducts which generate a 2/2 adduct. These 2/2 adducts are linked together by weak I•••I interactions, between

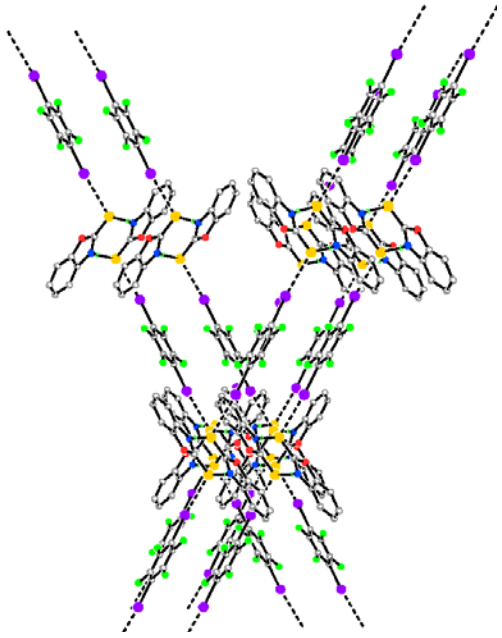

Figure 3.9. View down the *c* axis of MBZOX • 1,4-F_4DIB complex.

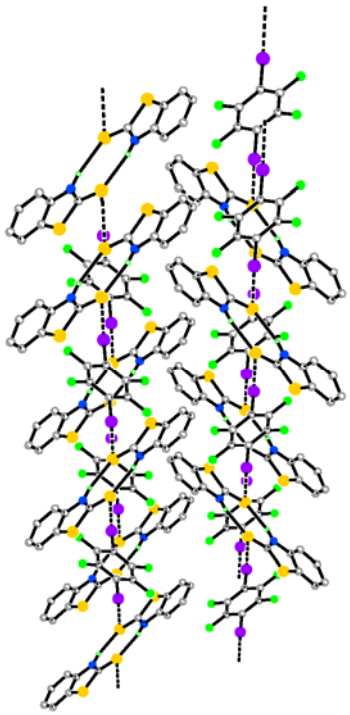

a. View down *c* axis

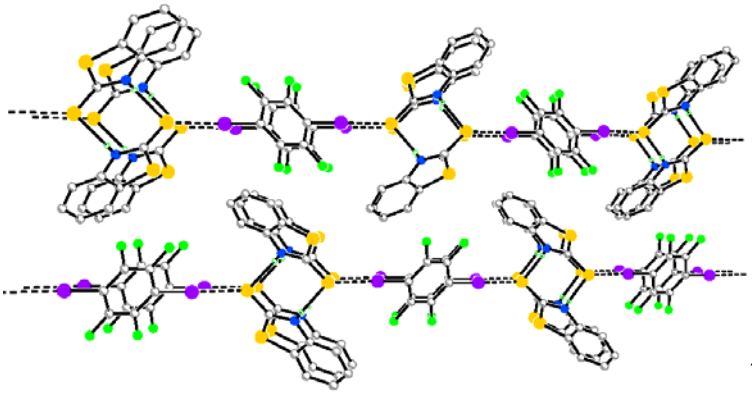

b. View down the *a* axis

Figure 3.10. Packing diagrams of MBZTH • 1,4-F_4DIB complex.

Table 3.3. Selected Distances (Å) and Angles (º) for 1,2-F_4DIB complexes.

Distances

MBZIM		MBZOX	
C=S	1.703(8)	C=S	1.655(11)
C-I	2.074(8), 2.107(8)	C-I	2.062(13), 2.081(12)
S•••I	3.309(2)	S•••I	3.294(3)
S•••N	3.317(6)[b], 3.320(7)[a]	S•••N	3.350(10)[a]
		I•••I	4.0702(14)[b]

Angles

MBZIM		MBZOX	
C-I•••S	173.5(2)	C-I•••S	166.5(3)
C=S•••I	119.2(3)	C=S•••I	104.74(4)
C-N•••S	121.5(5)[b], 122.4(4)[a], 127.8(5)[a], 128.4(5)[b]	C-N•••S	118.8(7)[a], 130.5(7)[a]
C=S•••N	104.6(3)[b], 105.9(3)[a]	C=S•••N	111.8(4)[a]
		C-I•••I	128.4(3)[b], 165.8(4)[c]

[a] Atoms listed with a lower case letter were generated by the following symmetry operators: For mbzim: (a) 1-x, 1-y, -z, (b) 1-x, -y, -z. For mbzox: (a) 1-x, 1-y, -z, (b) 1.5-x, -0.5+y, 0.5-z (c) 1.5 –x, y+0.5, 0.5-z.

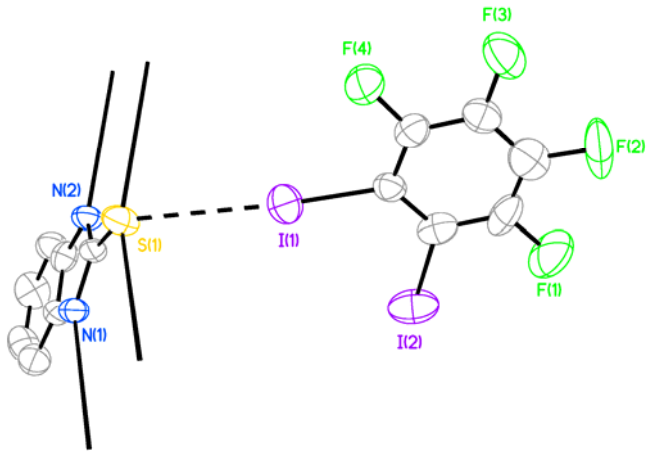

Figure 3.11. Thermal ellipsoid plot of MBZIM • 1,2-F_4DIB (50% probability).

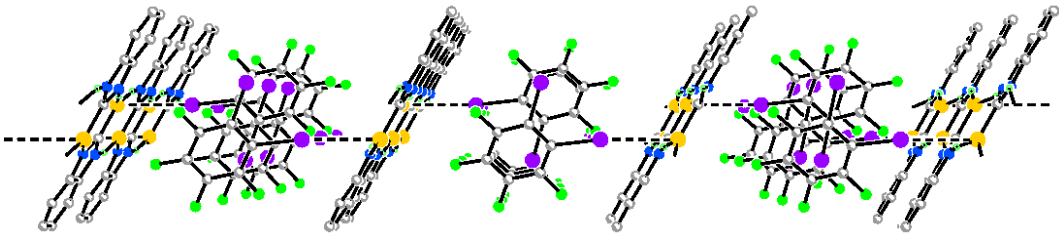

Figure 3.12. View down *b* axis for the packing of MBZIM • 1,2-F_4DIB complex.

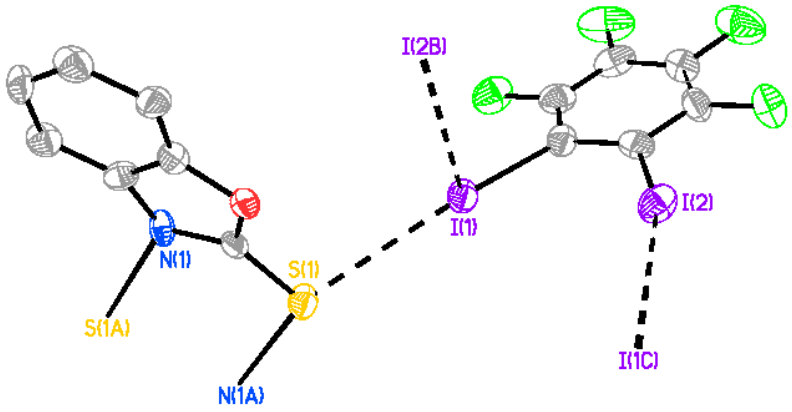

Figure 3.13. Thermal ellipsoid plot of MBZOX • 1,2-F_4DIB (50% probability). The atoms with letter suffixes were generated by symmetry operations in table 3.2.

acceptor molecules. An interesting note, one of the iodine atoms on the acceptor has amphoteric behavior, it acts as a Lewis acid toward the thione while acting as a Lewis base toward an iodine atom on another acceptor. The packing of MBZOX • 1,2-F_4DIB reveals that the crystal lattice is segregated into hydrophobic and hydrophilic regions.

Crystal Structure of MBZIM • TIE complex

One donor molecule and one acceptor molecule occupy the asymmetric unit situated on general positions (figure 3.16). The donor molecule interacts with the acceptor through three S•••I interactions (3.5(2) Å). The geometry at the sulfur atom is orthogonal, trigonal planar, or a mixture of the two. There were great differences in the C=S•••I angles at each sulfur atom (72.3(3), 117.6(3), 144.3(3)º), though the iodine atom displays linear geometry (average C-I•••S angle of 168(12)º). In addition to S•••I interactions, I•••$C_{(phenyl)}$ interactions are present. This was confirmed by calculating the contact distance for this interaction which is 3.708(10) Å. This distance is less than the sum of the van der Waals radius of iodine (1.98 Å) and half the distance of two phenyl rings interacting (1.8 Å). This interaction along with the three S•••I contacts form a 3-D network. As in the benzimidazole complexes already discussed, the infinite N-H•••S ribbons are present. A unique characteristic of this complex is the five interactions occurring at the sulfur atom, involving two hydrogen bonding and three halogen bonding contacts. The packing diagram reveals that infinite N-H•••S ribbons are intersected by layers of TIE (figure 3.15).

Table 3.4. Selected Distances (Å) and Angles (º) for TIE complexes.

Distances

MBZIM		MBZTH	
C-I	2.079(12), 2.110(10), 2.117(11), 2.124(12)	C-I	2.093(16)[aa], 2.093(8) 2.103(14), 2.107(8) 2.133(5) 3.000(16)[aa]
C=S	1.694(9)	C=S	1.685(8)
S•••I	3.296(3)[d], 3.528(3)[c], 3.599(3)	S•••I	3.295(3)
S•••N	3.368(8)[b], 3.371(8)[a]	S•••N	3.281(7)[a]
		I•••I	3.9541(13)[d], 3.9848(18)

Angles

MBZIM		MBZTH	
C=S•••I	72.3(3), 117.6(3)[d], 144.3(3)[c]	C=S•••I	122.4(3)
C-I•••S	172.6(3), 177.5(3)[e], 153.8(3)[f]	C-I•••S	162.4(4), 165.5(3)[aa]
C=S•••N	110.3(3)[a], 110.8(3)[b]	C=S•••N	104.8(3)[a]
C-N•••S	121.7(6)[a], 122.0(6)[b], 127.2(6)[a], 127.4(6)[b]	C-N•••S	116.1(5)[a], 128.0(5)[a]
		C-I•••I	69.0(3)[d], 70.9(4)[d], 97.4(4)[aa], 110.4(4), 169.0(2), 171.1(2)[d]

[a] Atoms listed with a lower case letter were generated by the following symmetry operators: For mbzim: (a) 2-x, -y, 4-z, (b) 1-x, -y, 4-z, (c) x, 0.5-y, z+0.5, (d) x, y, 1+z, (e) x, y, 1-z, (f) x, 0.5-y, z-0.5. For mbzth: (aa) disorder atom, (a) 2-x, -y, 1-z, (d) 1-x, 1-y, -z,

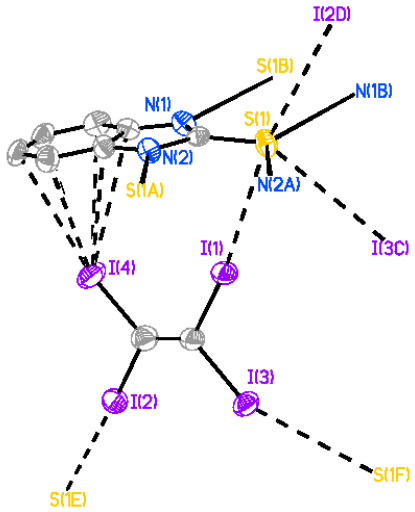

Figure 3.14. Thermal ellipsoid plot of MBZIM • TIE (50% probability). The atoms with letter suffixes were generated by symmetry operations defined in Table 3.3.

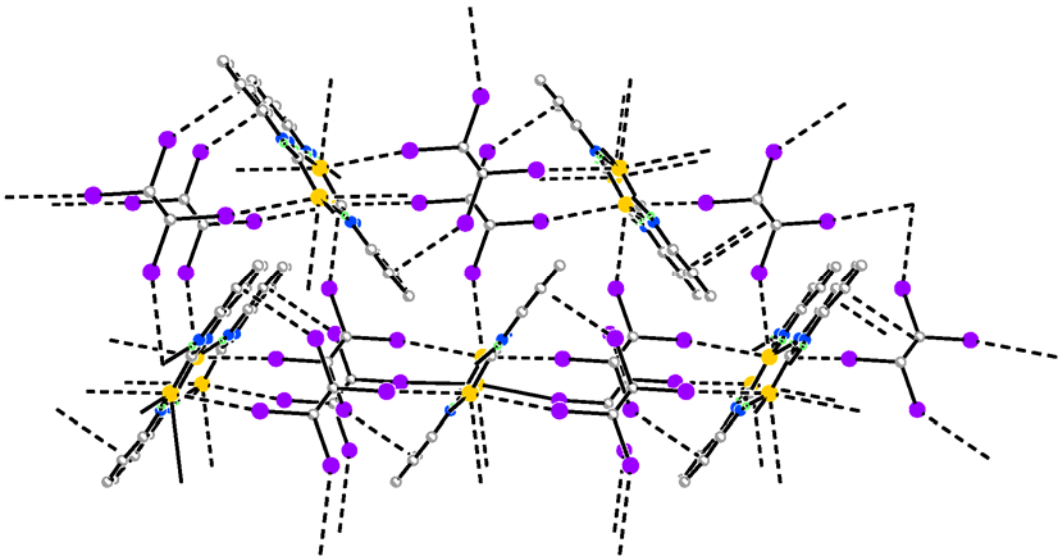

Figure 3.15. Crystal packing of MBZIM • TIE, view down the *a* axis.

Crystal Structure of MBZTH • TIE complex

The asymmetric unit contains one donor molecule situated on a general position and two TIE molecules which lie on inversion centers at 0, ½ , ½ and 1, ½ , 0 (figure 3.16). Donor molecules are linked to acceptor molecules by one halogen bonded contact (3.295(3) Å) which form 1/2 (A/D) adducts. In contrast to other MBZTH complexes discussed, the sulfur atom displays trigonal planar geometry. Linear geometry is observed at the iodine atom. Similar to other MBZTH complexes, the common N-H•••S dimer is links the halogen bond adducts together forming extended chains. The unbound TIE are linked to the bound TIE by two weak I•••I interactions (average I•••I distance is 3.97(2) Å). Packing diagram of MBZTH • TIE (figure 3.17) reveals that the extended chains, composed of adducts and hydrogen bonded dimers, are linked together through I•••I interactions between the bound and unbound TIE (which sits orthogonal to the bound TIE) forming layers.

Crystal Structure of MBZTH • CH_3I complex

The asymmetric unit contains one donor and one acceptor situated on general positions (figure 3.18). Two unique S•••I contacts (average S•••I distance of 3.39(8) Å) are observed in this complex generating 1/2 (A/D) halogen bonded adducts. Tetrahedral geometry is observed at the sulfur atom (average C=S•••I angle is 105(8)º). The iodine atoms involved with halogen bonding display linear geometry (average C-I•••S angle is 170(1)º). These adducts are linked to one another through N-H•••S dimers formed

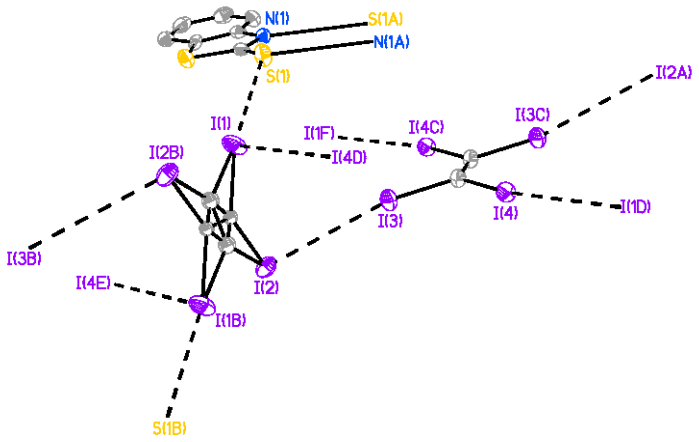

Figure 3.16. Thermal ellipsoid plot of MBZTH • TIE (50% probability). The atoms with letter suffixes were generated by symmetry operations defined in Table 3.3.

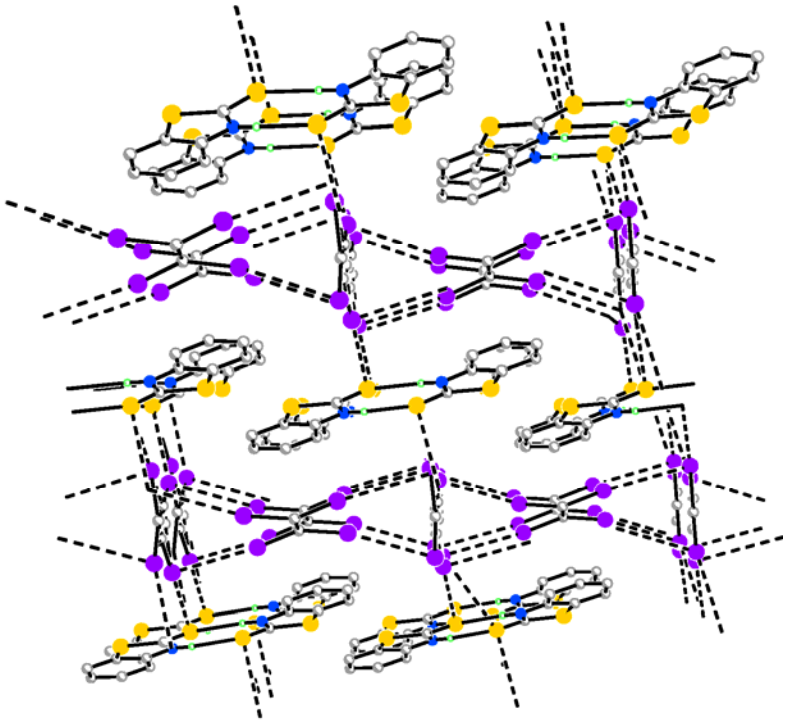

Figure 3.17. Crystal packing of MBZTH • TIE, viewed down the *a* axis.

Table 3.5. Selected Distances (Å) and Angles (º) for CH_3I complexes.

Distances	
MBZTH	
C=S	1.66(2)
C-I	2.117(19),
	2.134(19),
	2.178(15)
S•••I	3.337(5),
	3.451(5)[a]
S•••N	3.283(17) [b]
Angles	
C=S•••I	99.3(7) [a],
	110.9(7)
C-I•••S	168.5(5) [a],
	170.9(5)
C-S•••N	103.9(7)[b],
C-N•••S	112.1(11)[b],
	129.5(13) [b]

[a] Atoms listed with a lower case letter were generated by the following symmetry operators: (a) 1-x, -y, 1-z, (b) 1-x, 1-y, -z.

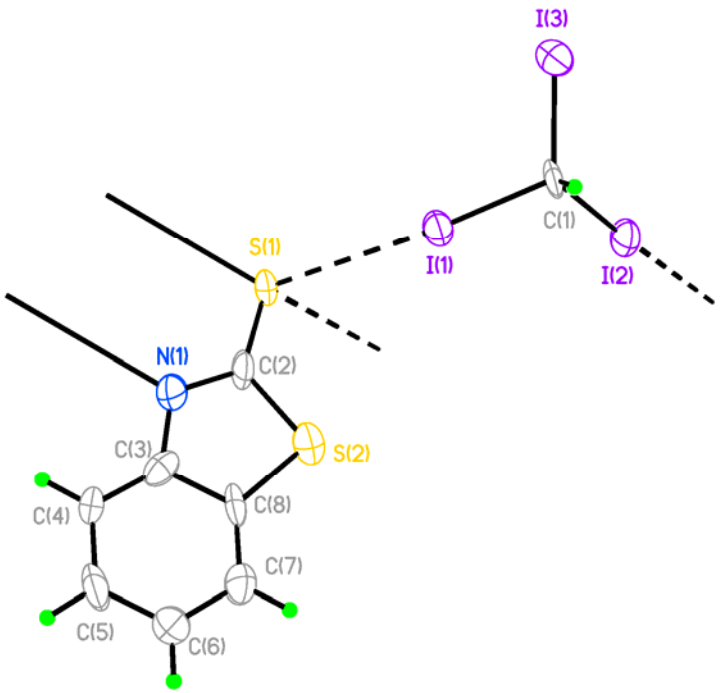

Figure 3.18. Thermal ellipsoid plot of MBZTH • CH_3I (50% probability). The atoms with letter suffixes were generated by symmetry operations defined in Table 3.4.

between donor molecules. Halogen bonded adducts and hydrogen bonded dimers form infinite ribbons. The packing diagram (figure 3.19) reveals that these ribbons are linked together through H•••I hydrogen bonding (~3.37 Å).

Conclusion

The results acquired in this study show that mercaptobenzimidazole, mercaptobenzoxazole, and mercaptobenzthiazole form halogen bonded complexes with various organoiodines. Reported complexes of these benzimidazoles are mainly confined to diiodine complexes which exhibit either molecular or ionic adducts,[1,2,3] in this study it was shown that organoiodines display a variety of bonding motifs such as adducts and chains. Also, it is important to note that the use of organoiodines allowed donor molecules to form the common N-H•••S dimer, however this characteristic is absent in diiodine complexes because iodine inhibits the formation of this hydrogen bonded dimer.

A comparison of S•••I contact distances between diiodine complexes, complexes of MMI and the complexes reported here are listed in table 3.6. The S•••I distances are significantly shorter than the complexes reported here, which is expected due to the greater polarizability of diiodine compared to organoiodines.[15]

The complex of MMI •1,4-F_4DIB resulted in two S•••I interactions compared to one observed for the 1,4-F_4DIB complexes reported here. However, our complexes have shorter S•••I distances than those of the MMI complex. The difference in length is

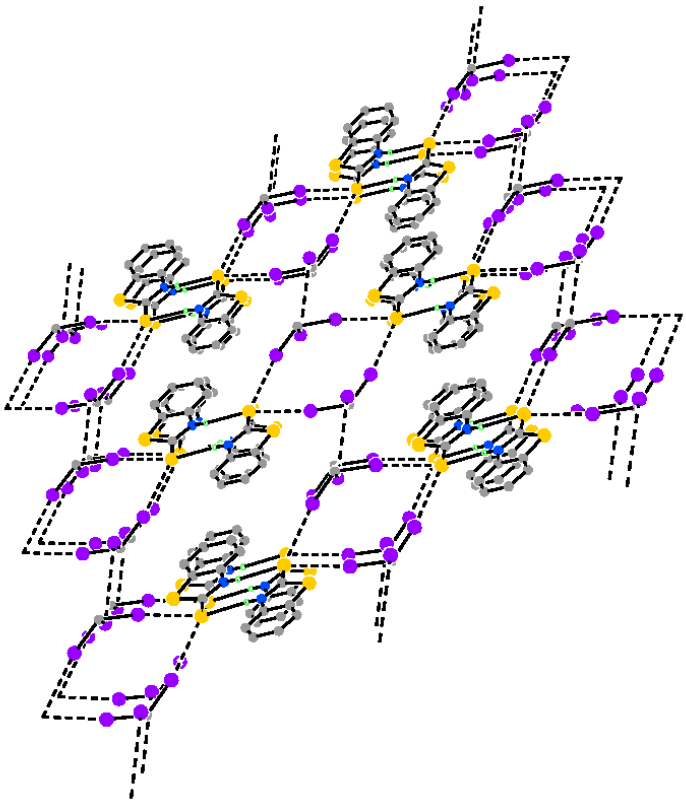

Figure 3.19. Crystal packing of MBZTH • CH_3I, viewed down the *a* axis.

Table 3.6. Comparison of S•••I Distances (Å) for reported diiodine complexes and organoiodine complexes reported here.

Donor ↓	Acceptor →	I_2	1,4-F_4DIB	1,2-F_4DIB	TIE	CHI_3
MBZIM		2.670(4)[a], 2.571(6)[b]	3.301(2)	3.309(2)	3.296(3), 3.368(8), 3.371(8), 3.528(3), 3.599(3)	
MMBZIM			3.2696(9)			
MBZOX		2.874(2)[c]	3.241(2)	3.294(3)		
MBZTH		2.728(6)[b], 2.587(5)[b]	3.3086(18)		3.281(7), 3.295(3)	3.337(5), 3.451(5)
MMI[d]			3.314(1), 3.342(1)	3.291(1), 3.843(1)	3.246(2), 3.302(2)	

[a] ref[2], [b] ref[1], [c] ref [3], [d] ref [9]

probably due to the number of interactions at the sulfur atom and other subtle effects such as solvent effects.

The MMI • 1,2-F_4DIB complex and the complexes reported here consist of one strong S•••I interaction. It appears that for 1,2-F_4DIB complexes, the phenyl ring does not play as an important role as with 1,4-F_4DIB complexes due to the similarities in S•••I bond distances. In addition to this, the absence of the hydrogen bonded ribbons in the MBZOX • 1,2-F_4DIB complex has minute effect on the strength of the halogen bond. The TIE complexes revealed that there was little difference in the halogen bond distances between the two suggesting that again the hydrogen bond ribbons play a minor role in affecting halogen bond strength. In contrast to the 1,4-F_4DIB complexes, the reported S•••I contact for the MMI • TIE complex was the shortest halogen contact compared to the TIE complexes reported here. It may suggest that for this acceptor having an electron donating group close to the donor atom resulted in a slightly stronger interaction than having the electron density spread out over a phenyl ring. Another unique observation of the MBZIM • TIE complex is that there are five unique halogen contacts with the donor atom.

However, further studies are needed to understand what affects the halogen bond strength. These studies will include replacing the methyl group on MMI with a more electron donating group to determine if a stronger halogen interaction is observed. Also, investigate how the addition of electron donating and withdrawing groups attached to the phenyl ring affect the halogen bond strength.

References

1. Daga, V.; Hadjikakou, S. K.; Hadjiliadis, N.; Kubicki, M.; dos Santos, J H. Z.; Butler, I. S. *Eur. J. Inorg. Chem.* **2002**, 1718.

2. Corban, G. J.; Hadjikakou, S.K.; Hadjiliadis, N.; Kubicki, M.; Tiekink, E.R.T.; Butler, I.S.; Drougas, E.; Kosmas, A.M. *Inorg. Chem.* **2005**, *44*, 8617.

3. Cristiani, F.; Devillanova, F. A.; Isaia, F.; Lippolls, V.; Verani, G.; Demartin, F. *Polyhedron* **1995**, *14*, 2937.

4. Antoniadis, C. D.; Corban, G. J.; Hadjikakou, S. K.; Hadjiliadis, N.; Kubicki, M.; Warner, S.; Butler, I.S. *Eur. J. Inorg. Chem.* **2003**, 1635.

5. Aragoni, M. C.; Arca, M., Demartin, F.; Devillanova, F. A.; Garau, A.; Isaia, F.; Lippolis, V.; Verani, G. *J. Am. Chem. Soc.* **2002**, *124*, 4538.

6. (a) Morris, D. R.; Hager, L. P *J. Biol. Chem.* **1966**, *241*, 3582. (b) Taurog, A. *Endocrinology* (Ed.: L. DeGroot),Academic Press, Inc. London, **1979**, *1*, 331.

7. (a) Berry, M. J.; Kieffer, J. D.; Harney, J. W.; Larsen, P. R. *J. Biol. Chem.* **1991**, *266*, 14155. (b) du Mont, W. W.; Mugesh, G.; Wismach, C.; Jones, P. G. *Angew. Chem. Int. Ed.* **2001**, *40*, 2486.

8. Esseffar, M.; Bouab, W.; Lamsabhi, A.; Abboud, J. L. M.; Notario, R.; Yanez, M. *J. Am. Chem. Soc.* **2000**, *122*, 2300.

9. P. D. Boyle, J. Christie, T. Dyer, S. M. Godfrey, I. R. Howson, C. McArthur, B. Omar, R. G. Pritchard, G.R. Williams, *J. Chem. Soc., Dalton Trans.* **2000**, 3106.

10. F. Bigoli, P. Deplano, A. Ienco, C. Mealli, M. L. Mercuri, M. A. Pellinghelli, G. Pintus, G. Saba, E. F. Trogu, *Inorg. Chem.* **1999**, *38*, 4626.

11. Boyle, P. D.; Godfrey, S. M. *Coord. Chem. Rev.* **2001**, *223*, 265.

12. (a) Deplano, P.; Ferraro, J. R.; Mercuri, M. L.; Trogu, E. F. *Coord. Chem. Rev.* **1999**, *188*, 71. (b) Aragoni, M. C.; Arca, M.; Devillanova, F. A.; Garau, A.; Isaia, F.; Lippolis, V.; Verani, G. *Coord.Chem. Re*v. **1999**, *184*, 271.

13. Jay, J. I.; Padgett, C. W.; Walsh, R. D. B.; Hanks, T.W.; Pennington, W.T. *Cryst. Growth & Des.* **2001**, *1*, 501.

14. Hunter, C.A.; Sanders, J.K.M. *J. Am. Chem. Soc.* **1990**, *112*, 5525.

15. Hanks, T. W.; Metrangolo, P.; Resnati, G.; Walsh, R. B.; Pennington, W. T. *Cryst. Growth & Des.* **2001**, *1*, 165.

CHAPTER FOUR

SOLVATED STRUCTURES OF DIPHENYLDITHIOGLYCOURIL

Introduction

Since 1877, glycouril and its derivatives have been extensively investigated.[1] They play an important role as building blocks in supramolecular chemistry[2,3,4] and are utilized in other areas such as polymer cross linkage, explosives and combinatorial chemistry.[5]

Due to their widespread interest, a variety of crystal structures have been reported for a number of their derivatives. One derivative of glycouril that is of interest to us is diphenylglycouril. Hydrogen bonding motifs observed in this crystal structure have not been reported in previously documented structures of glycouril derivatives. The only reported solvated structure of diphenylglycouril is with pyridine and where the solvent's role was to fill the voids between the hydrogen bonded ribbons.[6] One characteristic of diphenylglyocuril is the distortion observed at the bridgehead dihedral (χ) and the dihedral between ipso carbons on the phenyl rings in diphenylglycouril (τ) (figure 4.1). It has been suggested that the distortion is a result maximizing the distance between bridgehead phenyl groups. While glycouril and derivatives have been extensively studied, their sulfur analogues have received very little attention. One example is diphenyldithioglycouril, which has only been investigated to determine how reaction mechanics differ between sulfur compounds and their oxygen analogues.[7] Additional interest in this class of compounds are due to their potential for chelation which will be discussed in Chapter V.

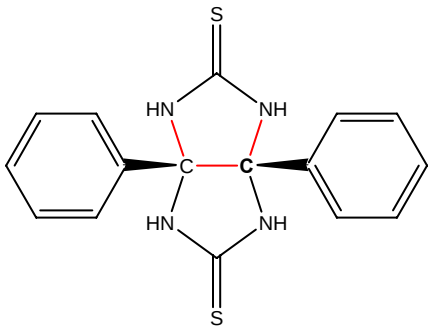

Bridgehead torsional angle (red)

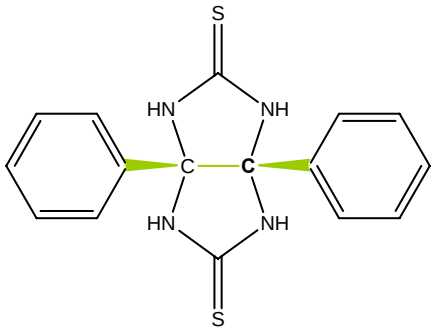

Ipso carbons of phenyl ring
torsional angle (green)

Figure 4.1. Description of torsional angles.

Herein is reported the structural and thermal characterization of diphenyldithioglycouril (DPDTGU) with various hydrogen bonding solvents that include pyridine (PYR), tetrahydrafuran (THF), and dimethylformamide (DMF).

DPDTGU and Solvated Structures

Selected distances and angles for DPDTGU and the three solvates are given in Table 4.1. The crystal packing of these structures are controlled by the formation of hydrogen bonded ribbons and hydrogen bonding with the solvent. These interactions include N-H•••S, N-H•••N, N-H•••O hydrogen bonding.

Crystal Structure of DPDTGU

The asymmetric unit of this structure (figure 4.2) contains one molecule which is situated on two two fold rotations. Extended hydrogen bonded chains link molecules of DPDTGU and run parallel to one another. These extended chains form extended hydrogen bonded ribbons (figure 4.3). The crystal packing of DPDTGU (figure 4.4) reveals separate hydrophilic (hydrogen-bonding) and hydrophobic (phenyl rings) regions. No distortion was observed for the χ and τ angles (table 4.1).

Crystal Structures of DPDTGU • $(PYR)_2$ and DPDTGU • $(THF)_2$

The structures of DPDTGU•PYR and DPDTGU•THF (figure 4.5) have similar unit cells and crystal lattice packing. The asymmetric unit of these two solvates is composed of a half molecule of DPDTGU and one solvent molecule, situated on two fold rotation axes at (½ , y , ¾) and (0, y, -¼) for PYR and THF solvates, respectively.

Table 4.1. Selected Distances (Å) and Angles (º) for DPDTGU and solvates. The DPDTGU/ solvent ratio was 1:2 for all solvates.

Distances							
DPDTGU		PYR		THF		DMF	
S•••N	3.373(8)[a]	S•••N	3.3541(18)[a]	S•••N	3.389(3)[a]	S•••N	3.288(3)[b], 3.342(2)[a]
		N•••N	2.891(3)	N•••O	2.858(19), 2.85(2)	N•••O	2.789(3)[c], 2.811(3)[d]
Angles							
DPDTGU		PYR		THF		DMF	
C=S•••N	108.69(15)[a]	C=S•••N	107.05(8)[a]	C=S•••N	108.36(13)[a]	C=S•••N	92.35(11)[b], 93.48(11)[a]
C-N•••S	120.0(7)[b], 124.9(6)[b]	C-N•••S	118.86(12)[a], 127.14(13)[a]	C-N•••S	120.2(2)[a], 124.6(2)[a]	C-N•••S	121.59(16)[b], 122.00(17)[a], 123.12(17)[b], 124.73(17)[a]
		C-N•••N	116.3(2), 119.15(13)[b], 125.01(15), 125.1(3)	C-N•••O	117.0(5), 118.1(5), 124.3(5), 128.5(5),	C=O•••N	116.8(2)[e], 129.3(2)[f]
				C-O•••N	117.1(11), 117.3(11), 121.6(9), 127.9(13)	C-N•••O	115.18(17)[c], 120.82(19)[d], 124.58(17)[d], 128.38(18)[c]
Torsional Angles							
DPDTGU		PYR		THF		DMF	
χ	0.0	-3.27(16)		0.1(3)		-15.2(3)	
τ	0.0	-5.9(4)		2.2(6)		-17.2(3)	

[a] Atoms listed with a lower case letter were generated by the following symmetry operators: For DPDTGU: (a) 1-x, ½ +y, -z, (b) 1-x, -y, -z. For DPDTGU • PYR: (a) –x+1, -y, -z+2, (b) –x+1, y, -z+3/2. For DPDTGU • THF: (a) 1-x, -y, -z, (b) 1-x, y, -½-z. For DPDTGU • DMF: (a) x+½, -y–½, -z, (b) x–½,-y–½, -z, (c) –x-(5/2), -y-1, z-½, (d) –x-3, y-½, -z-½, (e) –x+7/2, -y-1, z+½, (f) –x-3, y+½, -z-½.

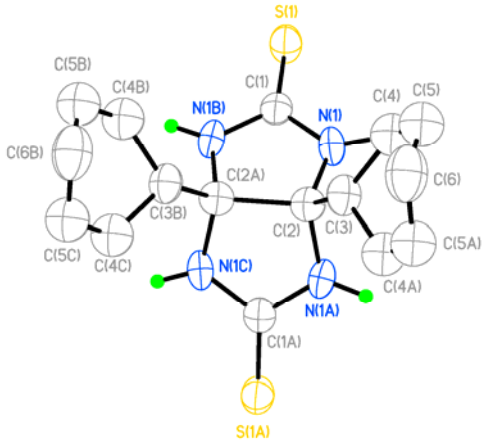

Figure 4.2. Thermal ellipsoid plot of DPDTGU, at 50% probability. Atoms listed with a upper case letter were generated by the following symmetry operators: (a) ½ -x, y, z, (b) x, ½ -y, z, (c) ½ -x, ½ - y, z.

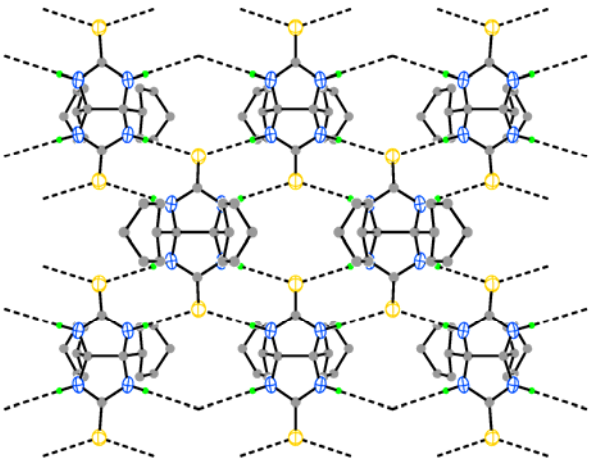

Figure 4.3 Layer of hydrogen bonded ribbons for DPDTGU.

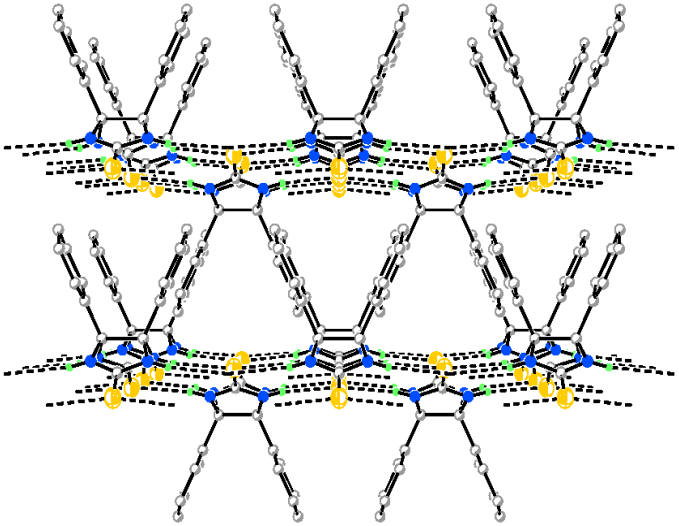

Figure 4.4 Packing diagram of DPDTGU.

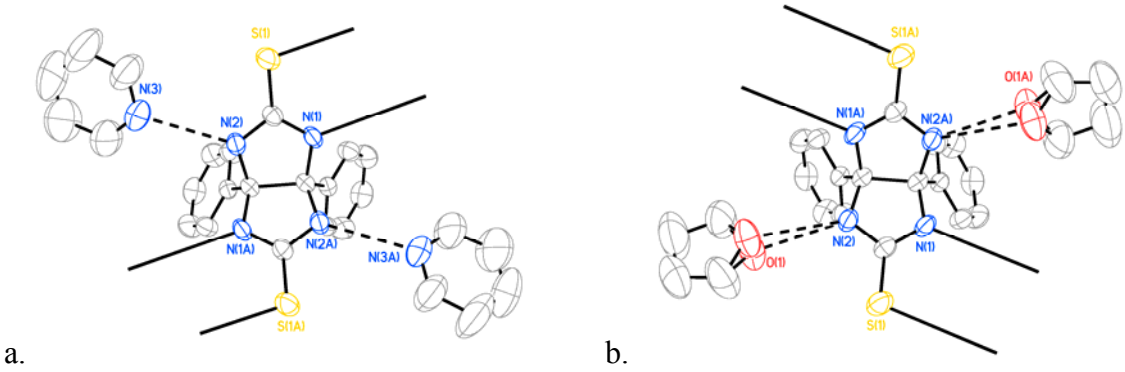

a. b.

Figure 4.5. Thermal Ellipsoid plots for a) PYR and b) THF solvates at 50% probablity. The atoms with letter suffixes were generated by the following symmetry operations: For PYR: (a) 1-x, y, 1.5-z. For THF: (b) 1-x, y, -0.5-z

These solvates exhibit N-H•••S dimerization which is common among derivatives of thiourea. Extended hydrogen bonded ribbons (figures 4.6 for PYR, figure 4.7 for THF and figure 4.8 is an overlap) link DPDTGU molecules together. Solvent molecules protrude out from these ribbons which are linked through hydrogen bonding with the amide hydrogen that is not involved with the hydrogen bonded ribbon. This behavior is in marked contrast to diphenylglycouril pyridine solvate where the solvent did not hydrogen bond with diphenylglycouril. A view of the crystal lattice packing down the *b* axis reveals layers of alternating rows of DPDTGU and solvent molecules (figures 4.9 for PYR solvate, figures 4.10 for the THF solvate). The solvent molecules fill the voids between the hydrogen bonded ribbons. The distortion for these two solvates is listed in table 4.1. The PYR solvate exhibited some distortion in the χ and τ angles however there was little distortion observed for the THF solvate.

Crystal Structure of DPDTGU•$(DMF)_2$

Molecules of DPDTGU and DMF are situated on general positions (figure 4.11). Similar to the other two solvates, the common N-H•••S ribbon is observed which link DPDTGU molecules. In addition to the hydrogen bonded ribbon, there is the formation of a 1/2 (DPDTGU/ solvent) adduct between DPDTGU and solvent molecules. Another similarity is the packing (figures 4.12) which show segregated regions of DPDTGU and solvent molecules. In contrast to the previous two structures, the solvent molecules hydrogen bond on the same side of DPDTGU and hydrogen bonding is also observed between solvent molecules. Another difference is that this solvate exhibits the most distortion.

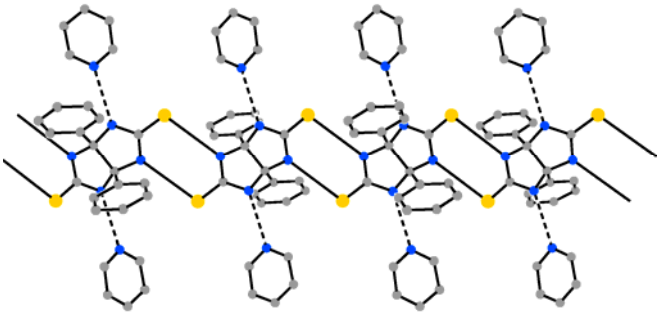

Figure 4.6. Hydrogen bonding ribbon for the PYR solvate.

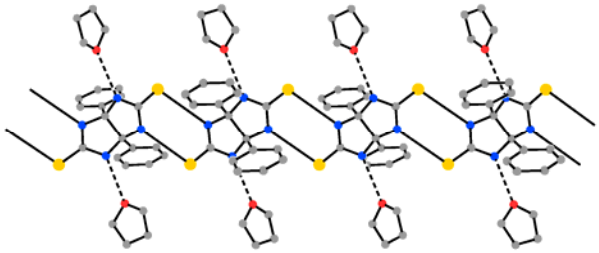

Figure 4.7. Hydrogen bonding ribbon for the THF solvate.

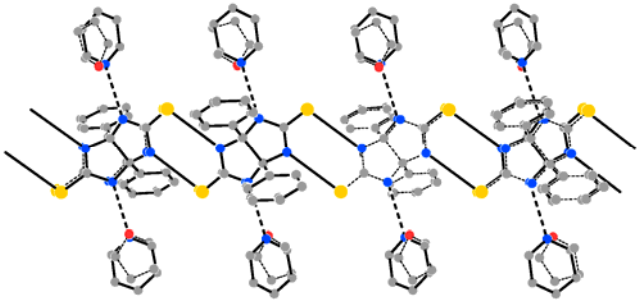

Figure 4.8. Overlap of the crystal lattice packing of PYR solvate (solid line) and THF solvate (dash), viewed down the *b* axis.

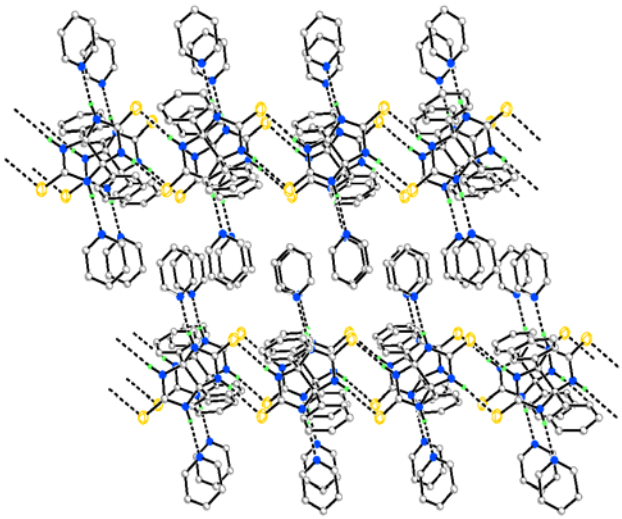

Figure 4.9. A view of the packing down the *b* axis of the PYR solvate.

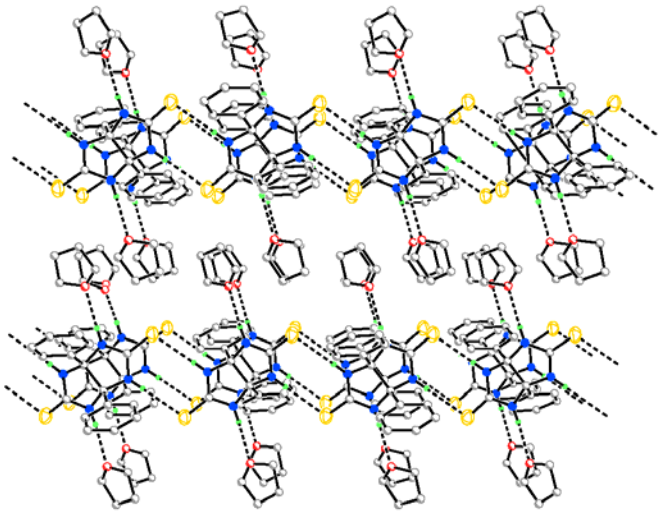

Figure 4.10. A view of the packing down the *b* axis of the THF solvate.

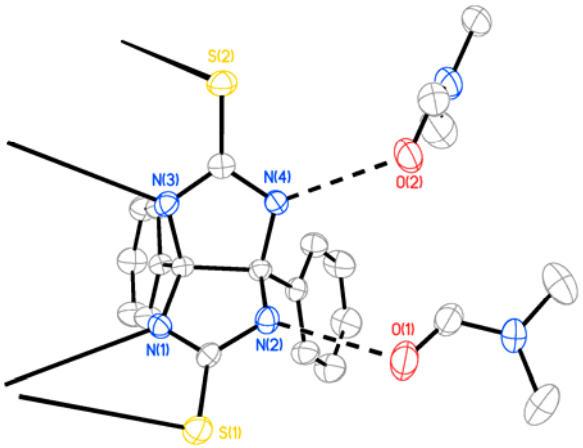

Figure 4.11. Thermal ellipsoid plot for DMF solvate at 50 % probability.

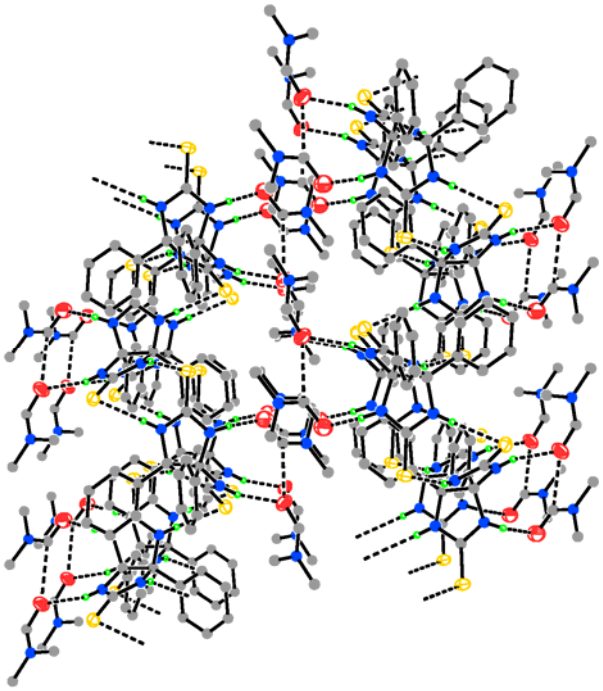

Figure 4.12. A view of the packing down the *b* axis of the DMF solvate.

Thermal and X-ray diffraction Analysis

The PYR solvate decomposes cleanly in two thermal events (figure 4.13) and endotherm at 146ºC represents the lost solvent from the crystal lattice. The first thermal event has an onset temperature at 102ºC relates to loss of bound solvent while the second event with an onset at 291ºC related to the loss of DPDTGU. Using X-ray powder diffraction analysis, it was shown that upon heating the solvate (figure 4.14), it converted back to the unsolvated form of DPDTGU.

Similar to the pyridine solvate, the decomposition of the THF solvate is also straightforward (figure 4.15). There are two endotherms at 89ºC and 102ºC which represent the loss of solvent from the crystal structure. Two endotherms were observed due to the disordered solvent molecules in the crystal lattice. The first thermal event with an onset temperature at 44 ºC was identified as the loss of bound solvent from the structure. A second thermal event with an onset at 272 ºC corresponds to the loss of DPDTGU.

Similar to the previous two solvates, the DMF solvate decomposes in two thermal events (figure 4.16). A broad endotherm at 158ºC (onset at 75ºC) relates to the loss of bound solvent from the crystal lattice, however unlike the other solvates, this endotherm occurred close to the boiling point of pure DMF. The second thermal event with an onset at 266 ºC corresponds to the loss of DPDTGU.

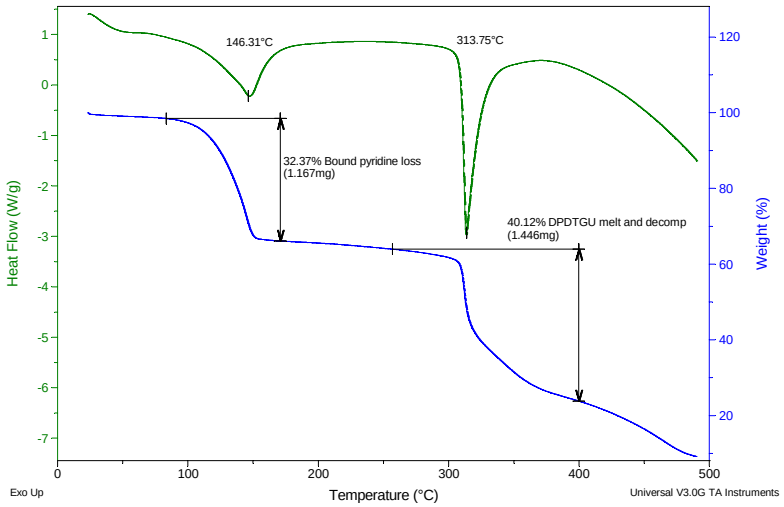

Figure 4.13. Thermal plot of PYR solvate.

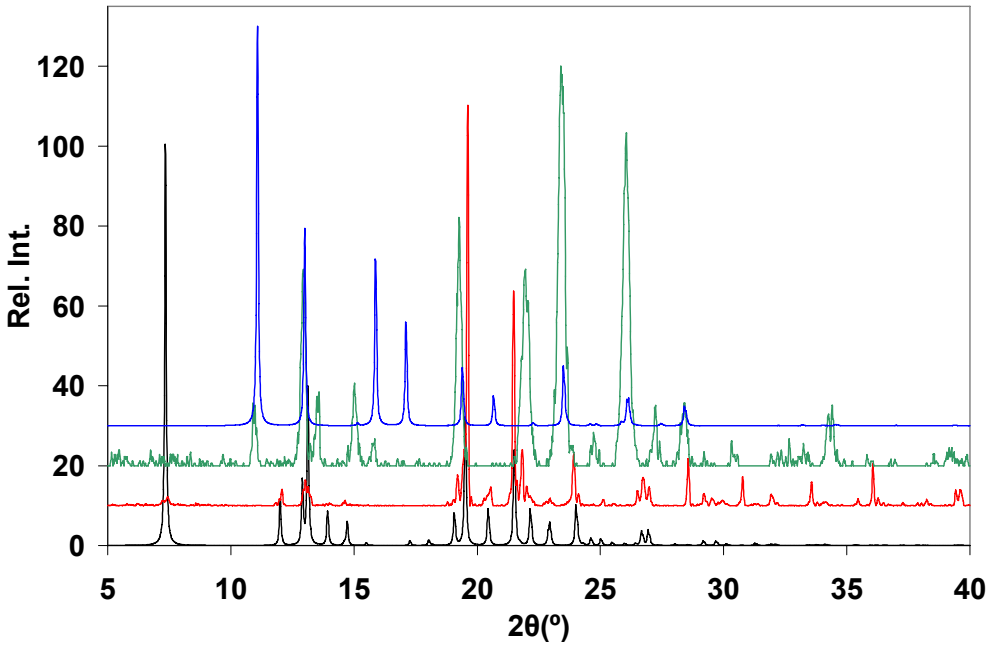

Figure 4.14. X-ray powder pattern comparison of DPDTGU • PYR: black is calculated pattern of DPDTGU • PYR, red is experimental pattern prior to heating, green is experimental pattern after heating, and blue is the calculated pattern of DPDTGU. All patterns were calculated from POWD 12.

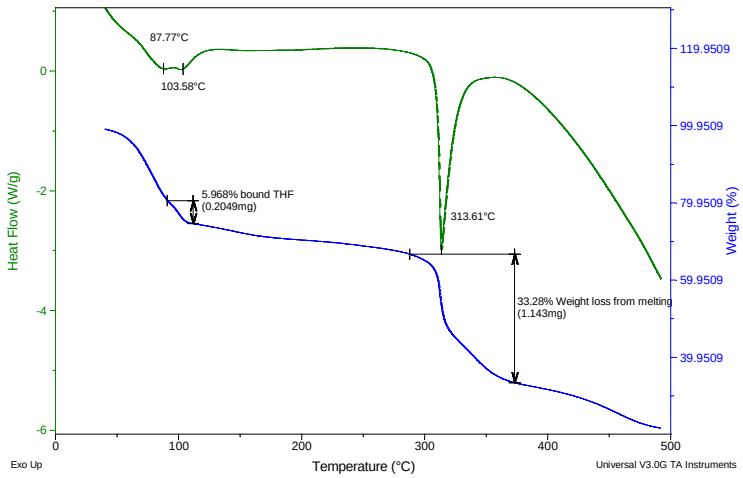

Figure 4.15. Thermal plot of THF solvate.

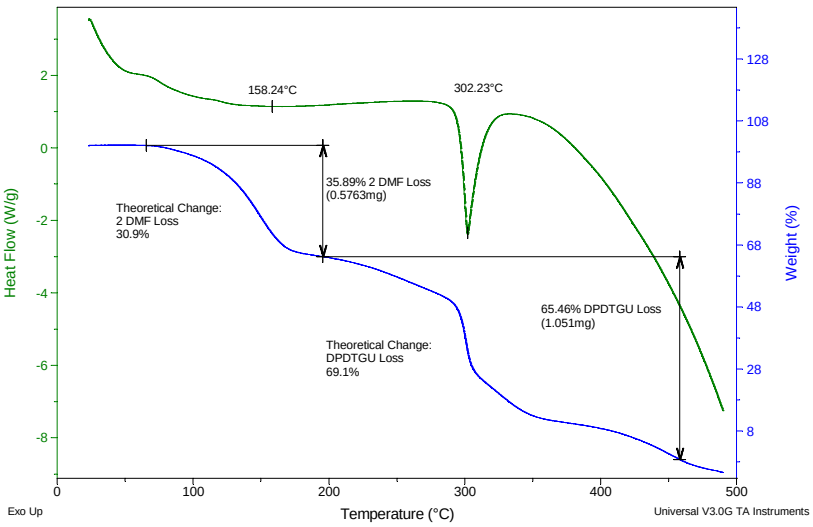

Figure 4.16. Thermal plot of DMF solvate.

Conclusion

It has been shown that DPDTGU forms solvated structures with various hydrogen bonding solvents. Unsolvated DPDTGU forms two infinite hydrogen bonded ribbons for each DPDTGU molecule. The PYR and THF solvates exhibited similar packing diagrams and unit cells. In both these solvates, the solvent hydrogen bonds opposite to one another. Extended hydrogen bonded ribbons were observed in both structures and the voids in formed by these ribbons are filled with solvent molecules. Like the other two solvates, hydrogen bonded ribbons are the major motif observed in the DMF solvate. Hydrogen bonding was also observed between solvent molecules which may have facilitated the hydrogen bonding on the same side of DPDTGU. Similar to the diphenylglycouril pyridine solvate, twisting was observed for the bridgehead carbons in these solvated structures as well. The DMF solvate exhibited the most twisting for the χ and τ dihedral angles. X-ray powder diffraction analysis of the PYR solvate revealed once the bound solvent was removed, DPDTGU transforms back to the crystal lattice of the unsolvated form. Further work is under way at investigating diphenylglycouril in solvents such as THF, Acetone, and DMF to determine the type of role solvent plays in the structure.

References

1. Schiff, H. *Justus Liebigs Ann. Chem.*, **1877**, *189*, 157.

2. (a) Branda, N.; Grotzfeld, R.M. ; Valdes, C. ; Rebek, J. *J. Am. Chem. Soc.* **1995**, *117*, 85; (b) O'Leary, B. M. ; Sazabo, T. ; Svenstrap, N.; Schalley, C. A. ; Lutzen, A.; Schafer, M.; Rebek, J. *J. Am. Chem. Soc.* **2001**, *123*, 11519; (c) Tokunaga, Y. ; Rebek, J. *J. Am. Chem. Soc.* **1998**, *120*, 66.

3. (a) Rowan, A. E. ; Elemans, J. A. A. W.; Nolte, R. J. M. *Acc. Chem. Res.* **1999**, *32*, 995; (b) Niele, F. G. M.; Nolte, R. J. M. *J. Am. Chem.* Soc. **1988**, *110*, 172; (c) Sijbesma, R. P. ; Kentgens, A. P. M.; Nolte, R. J. M. *J. Org. Chem.* **1991**, *56*, 3199; (d) Gieling, G. T. W. ; Svheeren, H. W. ; Israel, R.; Nolte, R. J. M. *Chem. Commun.* **1996**, 241; (e) Smeets, J. W. H. ; Sijbesma, R. P.; Dalen, L. V. ; Spek, A. L.; Smeets, W. J. J.; Nolte, R. J. M. *J. Org. Chem.* **1989**, *54*, 3710; (f) Schenning, A. P. H. J. ; Bruin, B. D.; Rowan, A. E.; Kooijman, H. ; Spek, A. L.; Nolte, R. J. M. *Angew. Chem. Int. Ed.* **1995**, *34*, 2132; (g) Elemans, J. A. A. W.; Claase, M. B.; Aarts, P. P. M. ; Rowan, A. E.; Schenning, A. P. H. J.; Nolte, R. J. M. *J. Org. Chem.* **1999**, *64*, 7009.

4. (a) Witt, D.; Lagona, J.; Isaacs, L. *Org. Lett.* **2000**, *3*, 3221; (b) Witt, D.; Lagona, J.; Damkaci, F.; Fettinger, J.C.; Isaacs, L. *Org. Lett.* **2000**, *2*, 755; (c) Chakraborty, A.; Wu, A.; Witt, D.; Lagona, J.; Fettinger, J.C.; Isaacs, L. *J. Am. Chem. Soc.* **2002**, *124*, 8297; (d) Chakraborty, A.; Wu, A.; Witt, D.; Lagona, J.; Damkaci, F.; Ofori, A.M. Chiles, J.K.; Fettinger, J.C.; Isaacs, L. *J. Org. Chem.* **2002**, *67*, 5817; (e) Witt, D.; Isaac, L. *Angew. Chem. Int. Ed.* **2002**, *41*, 1905.

5. (a) Jacobs, W.; Foster, D.; Sansur, S.; Lees, R.G. *Prog. Org. Coat.* **1996**, *29*, 127; (b) Parekh, G.G. US Patent 4,105,708, **1978**; (c) Wang, A.; Bassett, D. US Patent 4,310,450, **1982**; (d)Yinon, J.; Bulusu, S.; Axenrod, T.; Yazdekhasti, H. *Org. Mass Spectrom.* **1994**, *29*, 625; (e) Boileau, J.; Carail, M.; Wimmer, E.; Gallo, R.; Pierrot, M. *Propell. Explos. Pyrotech*. **1985**, *10*, 118; (f) Krause, A.; Aumueller, A.; Korona, E.; Trauth, H. US Patent 5,670,613, **1997**; (g) Karcher, S.; Kornmuller, A.; Jekel, M. *Water Sci. Technol.* **1999**, *40*, 425; (h) Pryor, K.E.; Rebek, J. *Org. Lett.* **1999**, *1*, 39.

6. Moon, K; Chen, W.; Ren, T.; Kaifer, A.E. *Cryst. Eng. Comm.* **2003**, *5*, 451.

7. Broan, C.J.; Butler, A.R. *J. Chem. Soc., Perkin Trans. II* **1989**, 731.

CHAPTER FIVE

HALOGEN BONDED COMPLEXES OF DPDTGU AND ITS DERIVATIVES

Introduction

Dithioglycouril derivatives are ideal for crystal engineering via donor – acceptor complexes due to their ability to form stronger interactions than their oxygen counterparts. Oxygen electron donors form strong hydrogen bonds but are far poorer as a effective electron donors for halogen bonding.[1] This interaction, commonly referred to as "halogen bonding", is the donation of electrons from an electron donor (such as dithioglycouril) to the σ* antibonding orbital of an electron acceptor (tetraiodoethylene or 1,2-diiodotetrafluorobenzene).

Of particular interest is developing systems that involve chelated halogen bonds. Chelation is the ability of a molecule (such as a chalcogen donor) to bind in more than one location to another molecule, in this case an organoiodine. Due to these additional interactions a chelated halogen bond may provide a more robust synthon for crystal design. They might also better facilitate solution studies, which could lead to a better understanding of halogen bonding in biological.

Chelated complexes must be specifically engineered to match the bite angle of the donor with the acceptor sites of the organoiodine. The bite angle is the L-M-L angle formed when a multi dentate ligand binds to a metal (see figure 5.1).[2]

Chelation in metal complexes is well known, but little attention has been given to this phenomenon in halogen bonded complexes. The only reported complex of a chelated

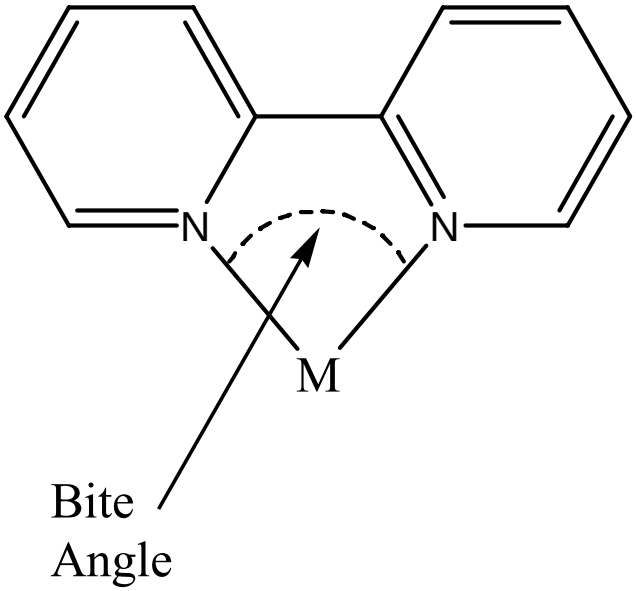

Figure 5.1. L-M-L bite angle.

halogen bonded interaction is that of tert-2-pyridyl pyrazine (Tppz) with tetraiodoethylene (TIE), figure 5.2.[2]

Herein is reported the structural analysis of DPDTGU with tetraiodoethylene (TIE) and 1,2 -diiodotetrafluorobenzene (1,2-F_4DIB). A complex of 1,4-Dimethyl-2,5-bis-methylsulfanyl-3a,6a-diphenyl-1,3a,4,6a-tetrahydro-imidazo[4,5-d]imidazole (1,4 DMbMSDPGU) with 1,4- diiodotetrafluorobenzene (1,4-F_4DIB) and a hydrogen triiodide salt of 1,6-Dimethyl-2,5-bis-methylsulfanyl-3a,6a-diphenyl-1,3a,6,6a-tetrahydro-imidazo[4,5-d]imidazole (1,6 DMbMSDPGU) will also be discussed (figure 5.3).

Halogen Bonded Complexes

Selected distances and angles for the four complexes are given in Table 5.1 and 5.2. Crystal packing of these complexes is controlled by noncovalent interactions including S•••I, N•••I, and I•••I contacts. N-H•••S Hydrogen bonding is also observed in the 1,2-F_4DIB complex.

DPDTGU • TIE• $(THF)_3$ • H_2O

The asymmetric unit contains one donor and acceptor molecule, each situated on general positions (figure 5.4). There are four unique S•••I contacts with an average distance of 3.324(14) Å. Orthogonal geometry is observed at the sulfur atom and linear geometry is present at the iodine atom (average C=S•••I and C-I•••S angles are 94(5) and 171(4)º). Two of the halogen contacts form a chelated halogen bonding interaction between DPDTGU and TIE, and the other two link adducts into layers (figure 5.5). The common N-H•••S ribbon observed in crystal structures containing the thiourea moiety is

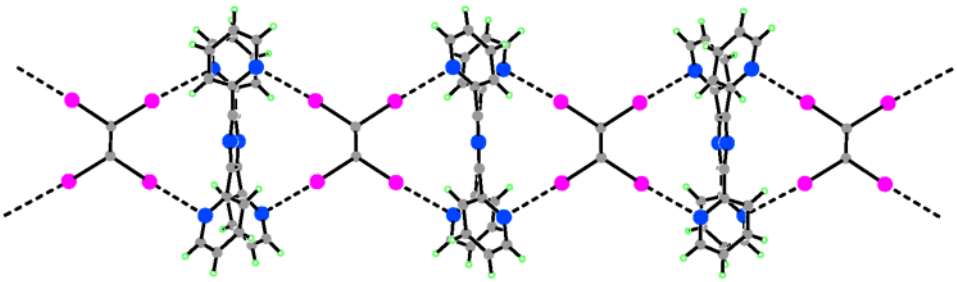

Figure 5.2. Tppz • TIE complex.

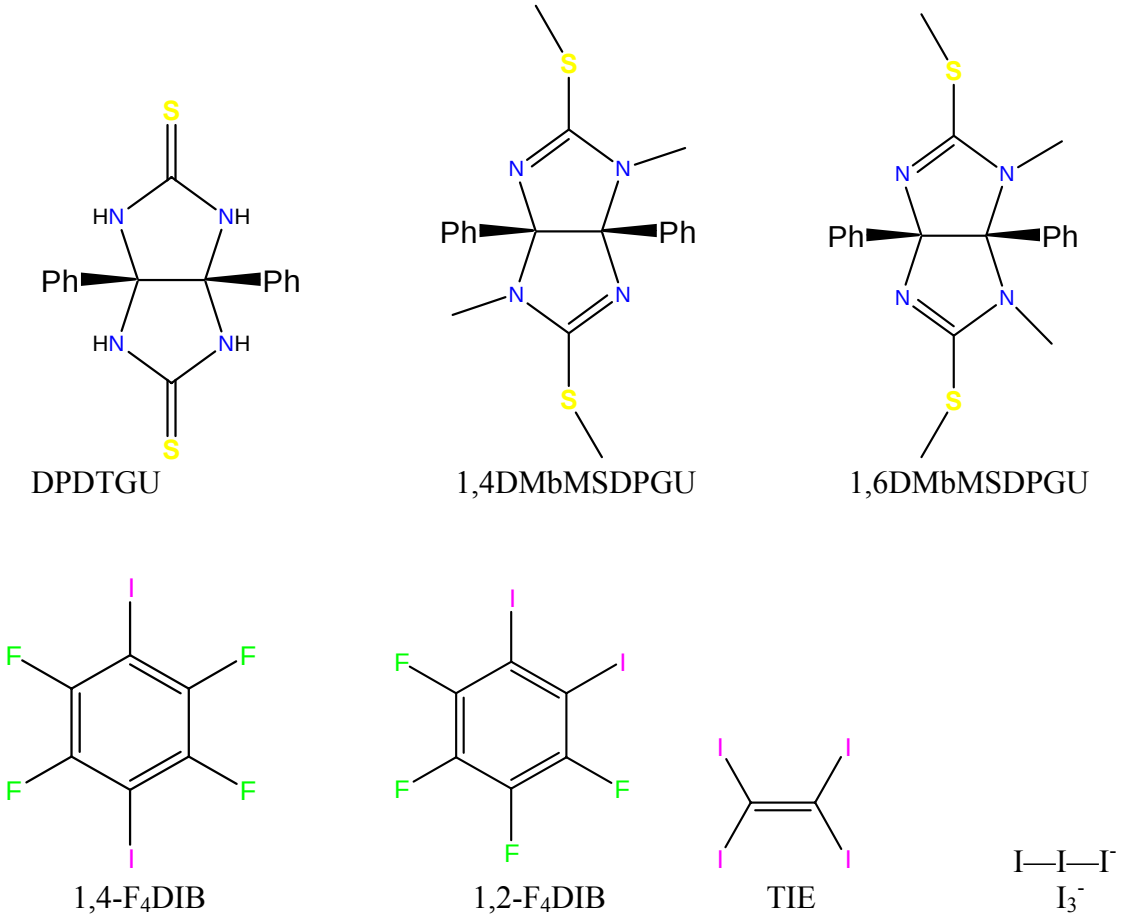

Figure 5.3. Structures of donors and acceptors

Table 5.1. Selected Distances (Å) and Angles (º) for DPDTGU complexes.

	TIE		1,2-F_4DIB
	Distances		
S•••I	3.307(3), 3.316(3)[b], 3.331(3)[a], 3.337(3)	S•••I	3.273(7), 3.388(7)[a]
O•••N	2.817(13), 2.826(14), 2.867[c], 2.871(14)	S•••N	3.40(2)(b)
		N•••O	2.90(4)
	Angles		
	TIE		1,2-F_4DIB
C=S•••I	89.9(3)[a],90.7(3) 93.9(3), 100.6(3)[b]	C=S•••I	86.6(7)[a], 91.4(8)
C-I•••S	165.9(3), 170.6(3)[e], 173.5(3), 174.2(3)[d]	C-I•••S	169.5(8)[c], 170.9(6)
C-O•••N	112.5(9), 123.6(10), 133.5(13)[c],117.6(11)[c], 123.2(12), 135.5(14)	C=S•••N	110.1(8)[b]
C-N•••O	119.5(7)[f], 124.6(6)[f], 125.5(7), 118.2(6), 131.5(7), 113.2(7), 135.0(7), 110.0(6)	C-N•••S	123.1(14)[b], 122.2(14)[b]
		C-N•••O	132.0(19)[d], 114.0(17)[d]

[a] Atoms listed with a lower case letter were generated by the following symmetry operators: For TIE: (a) –x, 1-y, 1-z, (b) 1–x, 1-y, 1-z, (c) 1-x, ½ + y, ½ - z, (d) -1-x, 1-y, -z, (e) –x, 1-y, -z, (f) 1-x, -½ +y, ½ - z. For 1,2-F_4DIB : (a) x, 1-y, z - ½ , (b)1-x, 1-y, 1-z, (c) x, 1-y, ½ +z, (d) 1-x, y, ½ -z

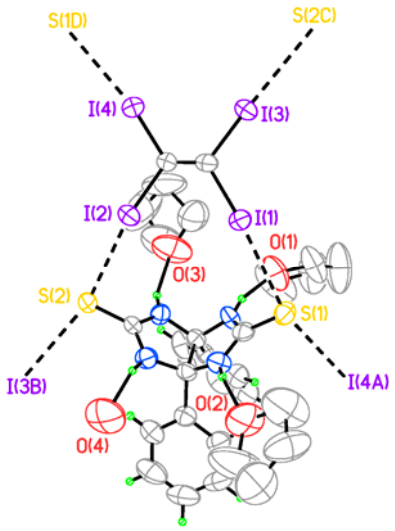

Figure 5.4. Thermal ellipsoid plot (50% probability) for DPDTGU • TIE • $(THF)_3$ • H_2O. Atoms listed with a capital letter were generated by the following symmetry operators: (a) x, ½ - y, ½ + z (b) 1+x, ½ - y, ½ + z (c) x-1, ½ - y, -½ + z (d) x, ½ - y, -½ + z .

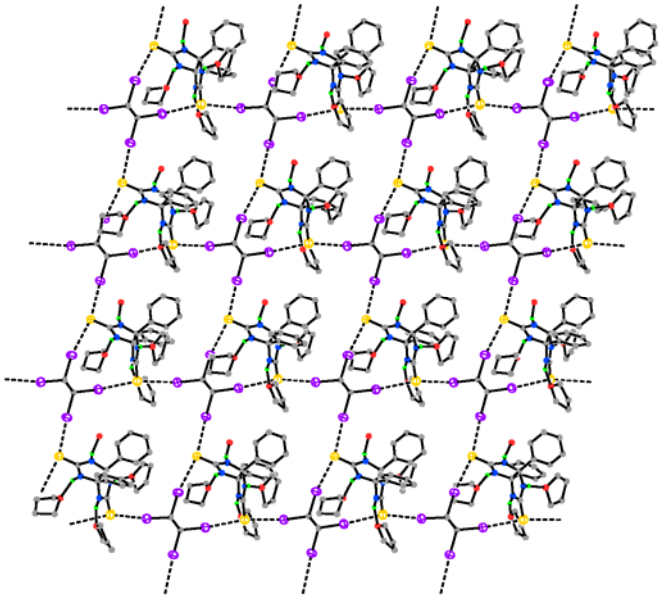

Figure 5.5a. Layered complex of DPDTGU • TIE • $(THF)_3$ • H_2O : view normal to one layer

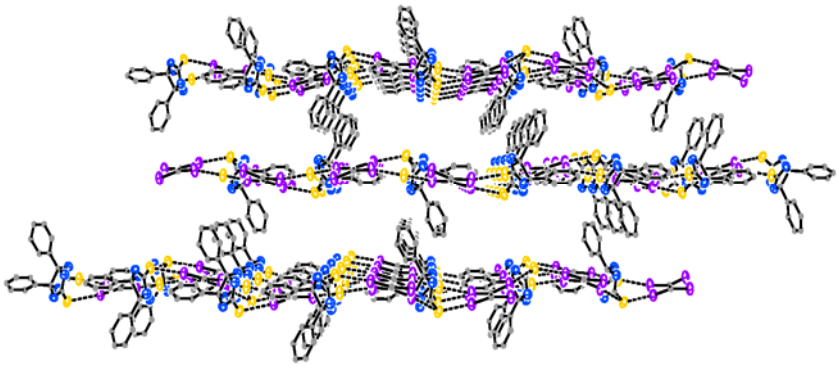

Figure 5.5b. Layered complex of DPDTGU • TIE • $(THF)_3$ • H_2O : stacked layers, solvent is not displayed

not observed here, as the donor hydrogen bonds with three THF molecules and a water molecule, situated on general positions.

DPDTGU • 1,2-F_4DIB • $(H_2O)_2$

The unit cell is composed of a donor and acceptor molecule that are situated on a two-fold rotational axis (½ , y, ¾) and a general position, respectively (figure 5.6). Similar to the previous complex, two S•••I interactions (average distance of 3.33(8) Å) were observed for each sulfur atom and displays orthogonal geometry (average C=S•••I angle of 89(3)º). The structural motifs present are extended halogen bonded chains and out of the plane of these chains the common N-H•••S ribbon occurs. In addition to these ribbons, DPDTGU also hydrogen bonds with additional water molecules. The packing of this complex shows that the crystal lattice is segregated into hydrophilic and hydrophobic regions (figure 5.7). Unfortunately chelation was not observed for this complex, which was probably due to the slightly wider bite angle (87º compared to 42º for the TIE complex) required for 1,2-F_4DIB. Even though chelation was not observed, this complex illustrates the important aspect that hydrogen and halogen bonding are complementary not competing interactions with these donors.

Products of Tetramethyldiphenylglycouril (TMDPDTGU) Synthesis

Methylation of DPDTGU was attempted using a synthesis developed by Moon, Chen, Ren, and Kaifer (Figure 5.8).[3] The only modification to this synthesis was using the reactant DPDTGU instead of DPGU. The NaH is added first to a solution of DPDTGU to deprotonate the amide protons. During this step, two tautomers are formed

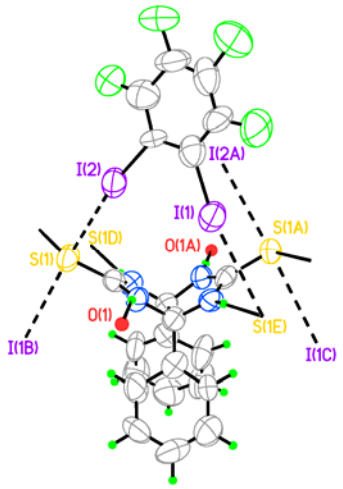

Figure 5.6. Thermal ellipsoid plot (50% probability) of DPDTGU • 1,2-F_4DIB • $(H_2O)_2$. Atoms listed with a capital letter were generated by the following symmetry operators: (a) 1 – x, y, 3/2 – z (b) x, 1 - y , -½ + z (c) 1 – x , 1 – y, 2 – z (d) 1 – x , 1 – y, 1 – z (e) x, 1 – y, ½ + z.

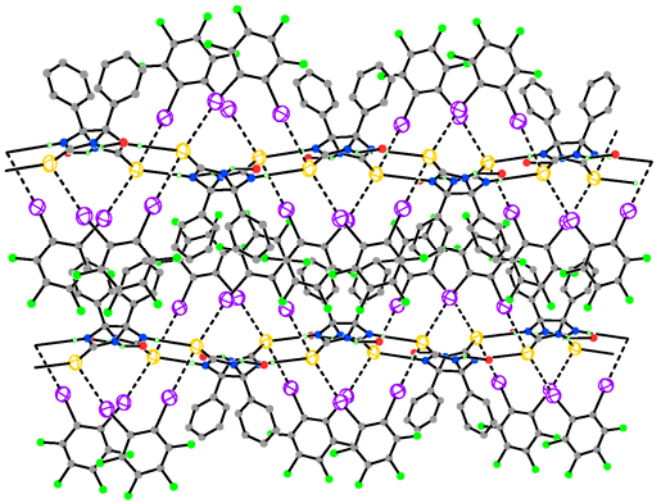

Figure 5.7. Packing of DPDTGU • 1,2-F_4DIB • $(H_2O)_2$ complex, view down the *a* axis

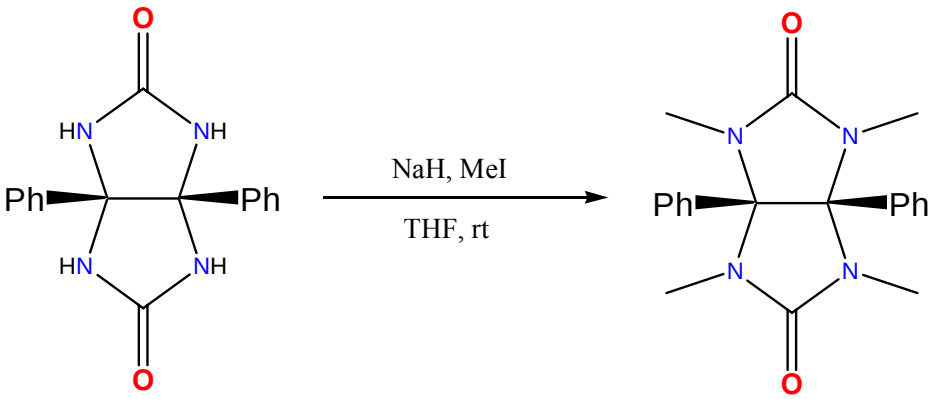

Figure 5.8. Proposed synthesis of TMDPGU[3]

(figure 5.9), since S^- is a better base and nucleophile than N^-, tautomer (b) has a greater probability of being formed. Since this tautomer is mostly likely to occur, the resulting product was actually a mixture of two products 1,4 DMbMSDPGU and 1,6 DMbMSDPGU.

1,4 DMbMSDPGU • 1,4-F_4DIB

The asymmetric unit contains one donor and acceptor molecule lying on general positions (figure 5.10). Two unique N•••I contacts (average distance of 3.15(2) Å) link donor and acceptor molecules. The average C-N•••I angles are 113(2) and 138(5)º and the C-N-C angle is 105.7(3)º, the sum of these angles is approximately 360º which identifies the nitrogen atom as sp^2 hybridized and has trigonal planar geometry. Linear geometry is observed at the iodine atom (C-I•••N angle of 173.04(15)º). The halogen contacts lead to the formation of extended chains that propagate throughout the crystal lattice (figure 5.11). Another unique aspect of this complex, is that N•••I halogen contacts are preferred over S•••I even though the sulfur atom is a softer base than the nitrogen atom. Also the relative strength of a thione ($R_2C=E$) is greater than a thioethers (R_2E), however the nature of the R group also has influence on the strength of the interaction.[5]

1,6 DMbMSDPGU • $(2I_3 \bullet I_2)^{-2}$

The unit cell is composed of one donor and acceptor (I_3^-) situated on a mirror plane at x, 0, y (figure 5.12). A unique aspect of this structure is that it is a protonated salt. This salt also forms one unique S•••I contact (3.8710(13) Å) and it chelates with I_3^-. Orthogonal geometry occurs at the sulfur atom (C-S•••I angle of 84(17)º) and linear

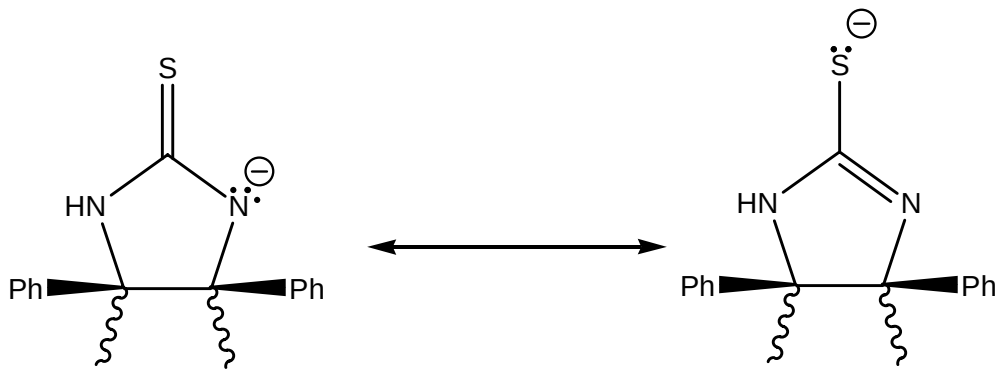

(a) (b)

Figure 5.9. Tautomers formed in the synthesis of TMDPDTGU.

Table 5.2. Selected Distances (Å) and Angles (º) for 1,4 DMbMSDPGU and 1,6 DMbMSDPGU complexes

	1,4-F_4DIB		$(2I_3 \bullet I_2)^{-2}$
Distances			
N•••I	3.135(3)[a], 3.170(3)	S•••I	3.8710(13)
		I•••I	3.4260(14)
Angles			
	1,4-F_4DIB		$(2I_3 \bullet I_2)^{-2}$
C- N•••I	111.4(2), 141.6(3), 134.8(3)[a],114.4(2)[a]	C-S•••I	71.88(12), 96.8(3)
C- I•••N	173.04(14), 173.04(15)[b]	I-I•••S	72.41(2), 172.82(2)
		I-I•••I	89.886(19), 178.018(18)[a]

[a] Atoms listed with a lower case letter were generated by the following symmetry operators: For $(2I_3 \bullet I_2)^{-2}$: (a) –x, y, 1-z. For 1,4-F_4DIB: (a) x-1, y-1, z-1 (b) 1+x, 1+y, 1+z.

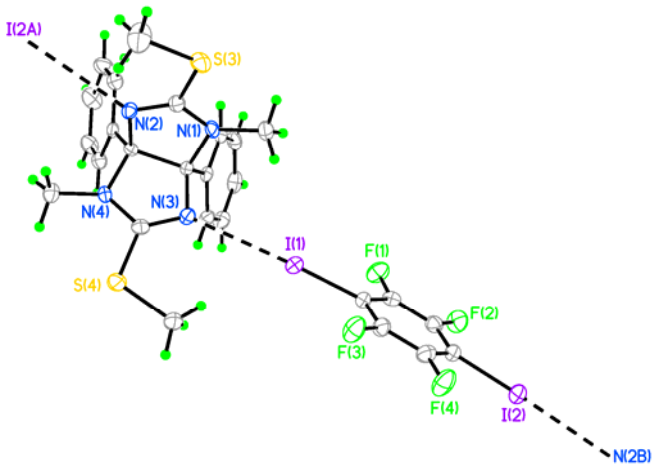

Figure 5.10. Thermal ellipsoid plot (50% probability) of 1,4 DMbMSDPGU • 1,4-F_4DIB. Atoms listed with a capital letter were generated by the following symmetry operators: (a) x-1, y-1, z-1 (b) 1+x, 1+y, 1+z.

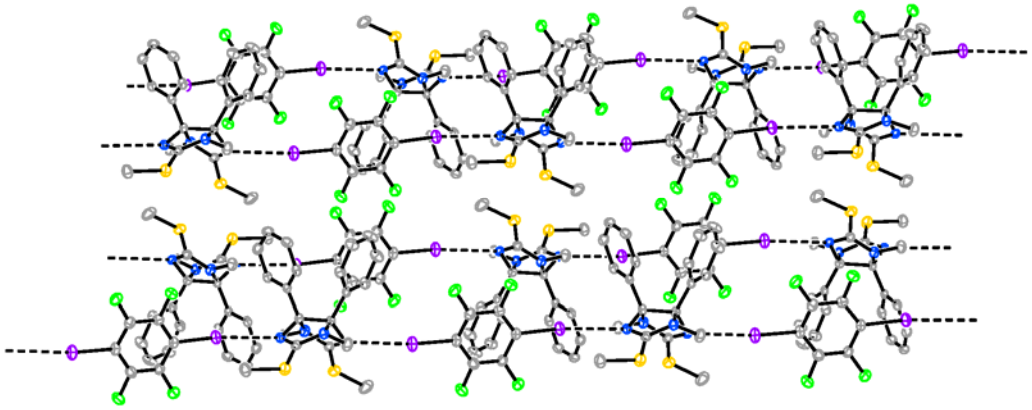

Figure 5.11. Packing of 1,4 DMbMSDPGU • 1,4-F_4DIB. Hydrogen atoms not shown for clarity.

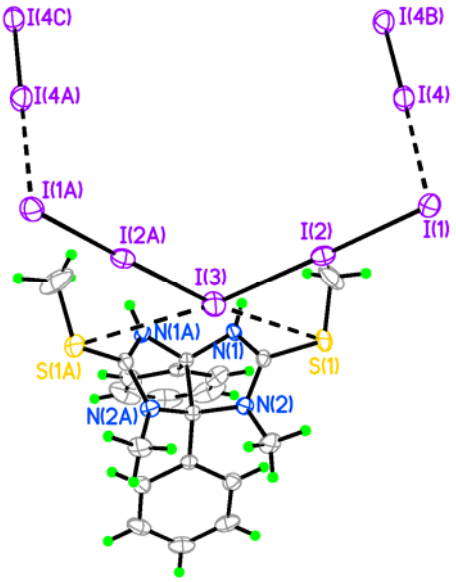

Figure 5.12. Thermal ellipsoid plot (50% probability) of 1,6DMbMSDPGU • $(2I_3 \bullet I_2)^{-2}$. Atoms listed with a capital letter were generated by the following symmetry operators: (a) x, –y, –z (b) –x, y, -1 – z (c) –x, -y, -1-z.

geometry is observed at the iodine atom (I-I-I^-•••S angle of 172.82(2)º) involved in the chelated halogen bond. The donor is crystallographically disorderd with the proton having 50% probability of being located on either nitrogen atom. This disordered proton allows for formation 1/1 hydrogen bonded (N-H^+•••N) adducts. A 2/2 bridging amphoteric adduct is the major motif present. A fourteen member polyiodide dianion ring is formed within the amphoteric bridging adduct. The bridging iodine molecule, which behaves as a Lewis acid, lies on a two fold rotation axis at 0, y, ½. (figure 5.13).

Conclusion

It has been shown that DPDTGU is an ideal candidate for halogen bonding with organoiodines. DPDTGU does chelate with TIE though the phenomena was not observed with 1,2-F_4DIB presumably due to the wider bite angle for this acceptor. Current attempts to synthesize tetramethyl diphenyldithioglycouril (TMDPDTGU) have been met with little success but have resulted in two unique by products: 1,4 DMbMSDPGU and 1,6 DMbMSDPGU. These two byproducts also halogen bond with 1,4-F_4DIB and triiodide anion, respectively. Future attempts to synthesize TMDPDTGU will include protection of the thione prior to the methylation. Also, diphenyldiselenoglycouril is of interest because the larger selenium atom can be ideal to chelate with acceptors with a slightly wider bite angle than TIE such as 1,2-F_4DIB. The overall objective of this project is to eventually synthesize a tetrathione which may behave as a bridging bidentate ligand.

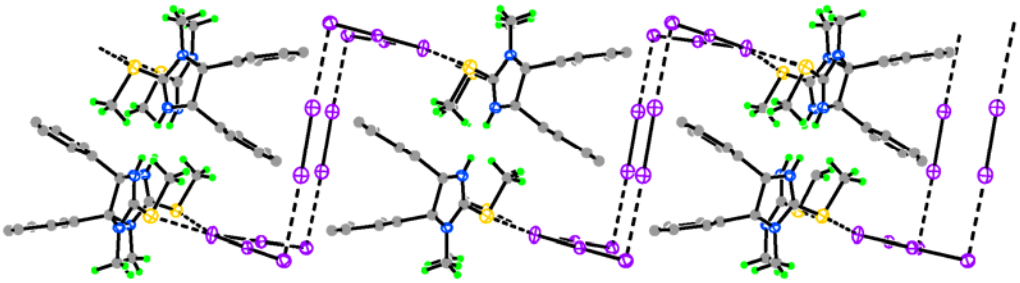

Figure 5.13. Packing of 1,6 DMbMSDPGU • $(2I_3 \bullet I_2)^{-2}$.

References

1. (a) Corradi, E.; Meille. S. V.; Messina, M. T.; Metrangolog, P.;Resnati, G. *Angew. Chem. Int. Ed. Engl.* **2000**, *39*, 1782. (b) Pearson, R. *Am. Chem. Soc*. **1963**, *85*, 3533.

2. Padgett, C.W.; Walsh, R.D.; Drake, G.W.; Hanks, T.W.; Pennington, W.T. *Cryst.* Growth & Des. **2005**, 5, 745.

3. Toreki, R; " Organometallic HyperTextBook" www.ilpi.com/organomet/coordnum.html (02/23/08)

4. Moon, K; Chen, W.; Ren, T.; Kaifer, A.E. *Cryst. Eng. Comm.* **2003**, *5*, 451.

5. Boyle, P.D.; Godfrey, S.M. *Coord. Chem. Rev.* **2001**, *223*, 265.

CHAPTER SIX

CRYSTAL STRUCTURES ELUCIDATED FROM X-RAY POWDER DIFFRACTION DATA WITHOUT PRIOR INDEXING

Introduction

This chapter is part of a published paper ("*Crystal structures elucidated from X-ray powder diffraction data without prior indexing*", Padgett, C.W.; Arman, H.D.; Pennington, W.T. *Cryst. Growth and Des.* **2007**, *7*, 367.) Recent technological advances in single crystal X-ray diffraction analysis, particularly with regard to improvements in computer speed and the advent of reliable area detectors such as imaging plates and charge coupled devices (CCDs),[1] have greatly reduced the time needed for structure determination. These detectors can also allow the use of slightly smaller crystals than for a scintillation detector, but the generation of data-quality single crystals is still the limiting obstacle for this method in many cases. While these same technologies have also led to improvements in powder X-ray diffraction analysis, structure elucidation from X-ray powder data is still far behind single crystal methods. The slower progress in powder methods has primarily resulted from a lack of algorithms and of computer speed sufficient for fitting complex crystal structures to their powder patterns. Only recently have computers become capable of solving such complicated problems in a reasonable time. Despite these obstacles, the relative ease of obtaining microcrystalline powders provides a major advantage over single crystal techniques.

In principle, powder diffraction data contains the same information as single crystal diffraction data, but with the three-dimensional diffraction data compressed into one dimension due to the fact that the powder diffraction measurement is averaged over

all possible crystal orientations. As a consequence, powder diffraction patterns contain substantial overlap of peaks. This causes severe difficulties in extracting reliable intensities of individual diffraction maxima, drastically reducing the probability of a successful structure determination. However, recent progress in overcoming these problems has been made, and some successes have been reported. [2,3,4,5,6,7,8,9,10]

Most methods follow a three-step process. First, the powder pattern is indexed to determine unit cell parameters and possible crystal systems. Algorithms for indexing powder patterns, like ITO,[11] TREOR90,[12] and DICVOL91[13] have been developed that have little trouble determining unit cell parameters from high quality X-ray data, for all but the lower symmetry space-groups. Second, global optimization techniques such as Monte Carlo,[14] simulated annealing,[15] or genetic algorithms[16] are used to find a structure in optimal agreement with the experimental powder diffraction pattern. Finally, once the crystal structure is approximately known, Rietveld refinement methods[17] are used to fit a model consisting of the unit cell dimensions, atomic coordinates, and thermal displacement parameters to the experimental data.

Organic compounds often form molecular crystals with relatively large unit cells and low symmetry space groups. Large unit cells result in a compressed diffraction pattern with significant peak overlap. Low symmetry space groups compound the problem as the number of unique diffraction peaks increases. Light atoms, commonly found in organic crystals, generally have weaker scattering power that can result in poorly diffracting crystals, further complicating the analysis. In addition to these problems which are typically encountered with organic molecular crystals, a more

general one is preferred orientation, which results from anisotropic crystal habits, and leads to overrepresentation of some diffracting vectors and under-representation or absence of others. Coupling all these problems dramatically increases the difficulty of solving organic crystal structures from powder diffraction data, as weak overlapping diffraction peaks with inaccurate intensities are difficult, if not impossible to index.
In order to overcome these problems, a new method was introduced for simultaneous cell determination and pattern indexing and structure elucidation implemented in a Windows™ based parallel program, *OCEANA* (*O*rganic *C*rystal structure *E*lucidation *A*pplying a *N*on-indexed *A*pproach). Results from tests of the method on several organic compounds with known crystal structures are presented to demonstrate the effectiveness of the technique, and the successful analysis of one compound with a previously unknown structure is reported.

Computational Methodology

In *OCEANA*, a genetic algorithm (GA) is used to locate the global minimum, i.e. the trial structure which possesses the best figure of merit (Figure 6.1). With the purpose of providing the GA with manageable sized regions to search, *OCEANA* performs a grid search over six user-defined unit cell parameter ranges in a given space group and if the calculated density associated with a grid point is within an acceptable range for the material being studied, the parameters are passed to a GA.[18] The GA can adjust the unit cell parameters to obtain a better fit, but only within the associated grid step, thus ensuring that the density is maintained within the user defined range and that no unit cell

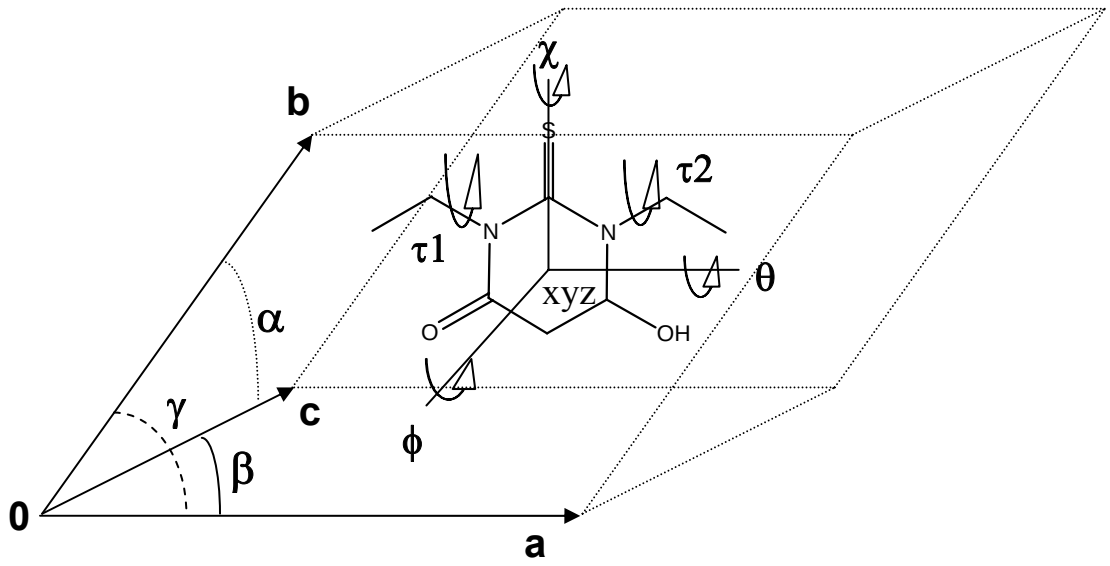

Figure 6.1. Example gene {*a, b, c, α, β, γ,* x, y, x, ϕ, θ, χ, τ1, τ2, …, τn) where (*a, b, c, α, β, γ,*) correspond to the unit cell parameters, (x, y, z, ϕ, θ, χ) represent position and orientation of molecule and (τ1, τ2, …, τn) are used for internal degrees of freedom.

parameter deviates far from the current grid point. For example, if the current grid point has a unit cell dimension, a, equal to 5 Å and a step size of 0.5 Å, then the GA can adopt values of a within the range 4.75 Å to 5.25 Å. Likewise, a unit cell angle, β, of 97º with a step size of 1º could adopt values ranging from 96.5 to 97.5º. The GA generates a random population of a user-specified number of genes (N). Each gene in this population consists of at least twelve bases, six representing the cell parameters {a, b, c, α, β, γ} and six representing the position and orientation {x, y, z, θ, ϕ, χ} of the molecule in the unit cell (Figure 6.2), and represents a possible crystal structure for the material. Additional bases can be included to accommodate internal degrees of freedom for the molecule, such as unhindered rotation about bonds. Once the genes have been created, they are ranked by a user-defined combination of the fit of the calculated to observed powder pattern in terms of the residual, R_{wp}, and the potential packing energy of the material, E_{ij}. Where w_i is a weighting factor related to the experimental error at point i, Y_{Expi} is the ith point from the experimental spectrum and Y_{Cali} is the ith point from the calculated structure. The potential packing energy is calculated from a Buckingham potential modified to include charge (equation 2) using the atom-atom potential method.[19] The (Exp-6-1) Buckingham equation[20] is shown below

$$E_{ij} = Ae^{-Br_{ij}} - \frac{C}{r^6} + \frac{q_i q_j}{r} \qquad (2)$$

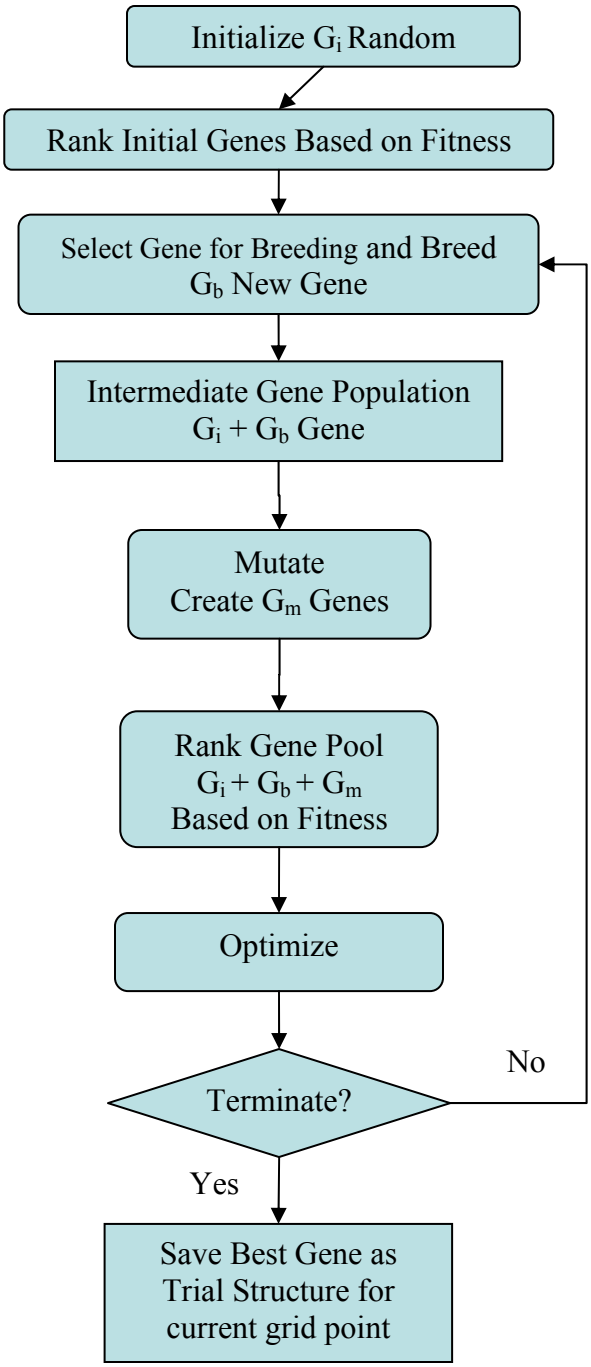

Figure 6.2. Flow chart of the genetic algorithm used in Crystal-GA.

Where A, B, C are parameters derived from experimental quantities such as sublimation energy, known crystal structures and spectroscopy for each atomic species[21]. The q's are atomic charges and are currently not used in the energy calculation. In this study, genes were ranked based on a ninety percent/ten percent weighting of R_{wp} and energy, respectively. After the initial genes have been ranked, they undergo natural selection, using either a tournament or roulette wheel method, with single point or multipoint crossover breeding.[22] A small percentage of the resulting gene pool is randomly mutated to add diversity to the gene pool and to prevent convergence to a local minimum, but copies of all genes are kept to prevent a high mutation rate from destroying good genes. Finally the full set of genes consisting of parents, offspring, and mutants are optimized using a simplex optimization algorithm,[23] thus effecting Lamarckian evolution.[24] The optimized genes are then evaluated and ranked. Genes which fall outside the initial constraints as a result of breeding or mutation are removed, and the N best of those that remain are kept as parents for the next iteration. Upon convergence or after a user-specified number of iterations, the GA stops and selects the best gene to be the trial structure model for that grid point. The best trial structures from all the grid points are saved as potential starting points for Rietveld refinement.[17,25]

The *OCEANA* software assumes known molecular connectivity and permits flexible molecules via user-specified dihedral degrees of freedom. *OCEANA* also allows the use of electrostatics via user-specified charges. Although the software does not require prior cell indexing, a space group must be specified for each run. For unknown compounds, only the most common space-groups can feasibly be tested. A reasonable

range of unit cell values based on approximate molecular dimensions must also be defined to reduce the computing time required. Any crystallographic information that can be obtained prior to analysis significantly reduces the computational burden and increases the probability of determining the correct structure. Incomplete single crystal data can give space-group and unit cell information. Other techniques such as examination of crystal morphology, optical goniometry, and etch tests can provide evidence about the point group symmetry of the bulk crystal, allowing the assignment of crystal class.[26] Second harmonic generation can determine if a structure is centrosymmetric,[27] solid state NMR can offer additional information on the symmetry of the structure,[28] and other methods can determine the presence and direction of a polar axis in a crystal.[29] The density of a compound can be used along with the unit cell values to determine the number of formula units in the unit cell.[28]

Experimental

The test compounds, benzene (BNZ; CCDC Refcode[30] : BENZEN[31]), naphthalene (NAPHTH; CCDC Refcode: NAPHTA11[32]), benzoquinone (BNZQ; CCDC Refcode: BNZQUI [33]), thiosemicarbazide (TSCRBZ; CCDC Refcode: TSCRBZ01[34]), 1,3-diethyl-2-thiobarbituric acid (DETBA; CCDC Refcode: DETSBR01[35]), 1,4-diiodobenzene (DIBENZ; CCDC Refcode: ZZZPRO06[36]), decafluoro-biphenylacetylene (PFDPAY; CCDC Refcode: PFDPAY[37]) and the previously unreported compound, bis(5-quinoline)diacetylene (5QDA), figure 6.3, were tested in the seven space groups most

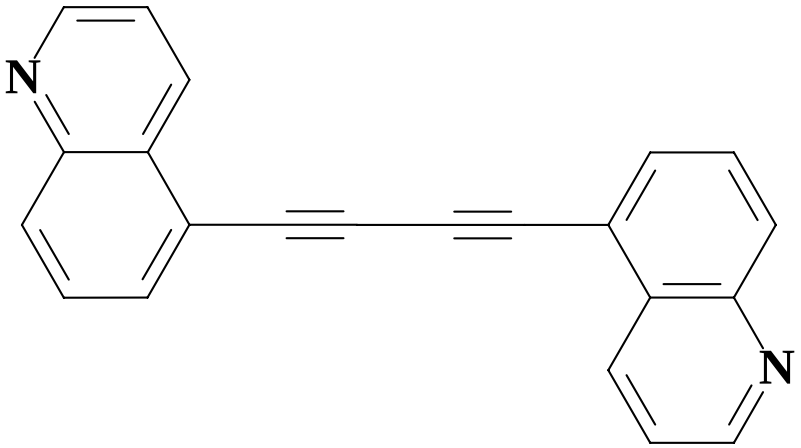

Figure 6.3. Structure of bis(5-quinoline)diacetylene (5QDA).

commonly observed for small organic molecules (*P-1, $P2_1$, C2, $P2_1/c$, C2/c, $P2_12_12_1$, and Pbca*).[38] The density ranges for all test compounds were set around their observed densities (BNZ: 1.24-1.34, TSCRBZ: 1.42-1.52, BNZQ: 1.23-1.43, NAPHTH: 1.11-1.24, DETBA: 1.32-1.42, DIBENZ : 2.75-2.95, PFDPAY: 1.85-1.95 g/cm^3) which were obtained from the Cambridge Structural Database.[39] The density range for 5QDA (1.28-1.42 g/ml) was determined by observing its buoyancy in a series of standard density solutions. The X-ray powder patterns for NAPHTH, BNZQ, DETBA, and 5QDA were collected at 293±2 K on a Scintag 2000 XDS θ/θ diffractometer (Cu Kα radiation; $\lambda_{\alpha 1}$ = 1.546029, $\lambda_{\alpha 2}$ = 1.544451 Å). Step scans of 0.01º were made over a 2θ range of 5-80º for 7.5-10.5 seconds per step. The test patterns for the known structures of BNZ, TSCRBZ, DIB, and PFDPAY were calculated using POWD12,[40] and all were elucidated to a similar degree of accuracy.

All data refinement was carried out using GSAS.[27] Low-angle data was omitted from the powder patterns during refinement to minimize the effects of surface roughness and incomplete interception of the beam at these angles. Lattice parameters and scale factors were refined for all compounds including the unknown. The peak profiles were described using a pseudo-Voight function and preferred orientation was expressed using a March-Dollase model, for all compounds under investigation. Hydrogen atoms were omitted for all compounds. Thermal motion was modeled with common isotropic displacement coefficient except for BNZQ, where the oxygen atoms were refined using common anisotropic parameters. Crystal data, Rietveld refined parameters, and final refinement values for R_{wp}, R_p, and $R(F^2)$ of all compounds are listed in Table 6.1, and of

5QDA are listed in Table 6.2. Calculations were performed on a cluster of Intel machines ranging from 500 Mhz to 2 Ghz (using a master-slave MPIconfiguration), all running under the Windows™ operating system and MPICH-NT.[41] Input molecules were drawn and minimized in Titan (using DFT with the LACVP* basis set),[42] then imported to *OCEANA*. Buckingham atom-atom potential parameters were obtained from the literature.[21]

Elucidated Structures

The structures of BNZ, NAPHTH, BNZQ, TSCRBZ, DETBA, DIBENZ, and PFDPAY were solved to verify the effectiveness of the program and methodology. 5QDA, a previously unknown structure, was also determined from its X-ray powder pattern by *OCEANA*. Figure 6.4 shows the overlay of the Rietveld refined structure from *OCEANA* and the known structure from the Cambridge Crystallographic Database[30] and a comparison of the calculated and observed powder patterns. *OCEANA* requires that structures in which the molecule possesses crystallographic symmetry (i.e. Z'<1), be accessed through a subgroup of the space group obtained by disregarding those symmetry elements upon which the molecule is situated, resulting in a model with one whole molecule in the asymmetric unit. This is the case for all of the reported compounds except DETBA, TSCRBZ and PFDPAY. It should be noted that the analysis of DETBA starting from the Titan-optimized rigid structure was not successful, due to ~20º discrepancy in rotation of each exocyclic ethyl group about its N-C bond. However, when two internal degrees of freedom were included to allow for these rotations, the structure was successfully determined. Of particular interest were NAPHTH, BNZQ, and DETBA

Table 6.1. Crystallographic data for reported and calculated structures of the test compounds.

	BNZ	NAPHT	BNZQ	TSCRBZ	DETBA
Space Group	$P2_1/c$ (No. 14)	$P2_1/c$ (No. 14)	$P2_1/c$ (No. 14)	$P\text{-}1$(No. 2)	$P2_12_12_1$ (No. 19)
a (Å)[a]	5.417(5)/ 5.4171	8.658(10)/ 8.6869(9)	5.767[b]/ 5.799(3)	6.008(5)/ 6.0080	4.8749(1)/ 4.89208(17)
b (Å) [a]	5.376(19)/ 5.3762	6.003(10)/ 6.0123(6)	6.795[b]/ 6.816(3)	7.311(6)/ 7.311	21.0787(4)/ 21.1393(11)
c (Å) [a]	7.352(7)/ 7.3517	8.235(5)/ 8.2938(8)	7.055[b]/ 7.081(3)	4.925(5)/ 4.9250	9.4437(2)/ 9.4672(5)
α(º) [a]	90	90	90	103.01(5)/ 103.0091	90
β (º) [a]	110.00(8)/ 110.0028	122.92(8)/ 122.597(3)	101.47[b]/ 101.598(4)	96.27(4)/ 96.2693	90
γ(º) [a]	90	90	90	77.21(4)/ 77.2105	90
Z	2	2	2	2	4
Atomic Displ., range (Å)	0.015-0.025	0.019-0.100	0.083-0.165	0.020-0.083	0.072-0.366
Atomic Displ., average (Å)	0.019(5)	0.05(3)	0.11(3)	0.05(3)	0.13(8)
# observations	[d]	5999	4499	[d]	6299
# variables		10	14		13
R_{wp}		0.1628	0.1730		0.1568
R_p		0.1218	0.1349		0.1181
$R(F^2)$		0.1911	0.1712		0.3381
2θ range(º)		20-80	15-60		17-80
# Rigid Body Atoms		10	8		13
Preferred Orientation plane		(*2 0 0*)	(*1 0 -2*)		(*1 3 0*)
Bkg. function		3-term n!/Q^{2n} Power series	6-term cosine		4-term cosine
Profile Param.[c]		G*U*, *asym*, *shft*, *stec*[1]	G*U*, GW, L*Y*, *stec*[1], *shft*		G*U*, L*Y*,*LX*

[a] Observed/Calculated values. [b] Esd's not reported.
[c] G*U* = Gaussian *U* ; GW = Gaussian W; L*Y* = Cauchy *Y* ; LX = Cauchy *X*; 1: unique axis (111). [d] No Rietveld Refinement performed.

Table 6.2. Crystallographic data for reported and calculated structures of the test compounds. (cont.)

	DIB	PFDPAY
Space Group	*Pbca* (No. 61)	*Pbca* (No. 61)
a (Å)[a]	16.977(3)/16.9777	9.59(1)/ 9.5899
b (Å) [a]	7.335(1)/7.3349	9.59(1)/ 9.5900
c (Å) [a]	6.160(1)/6.1594	27.34(2)/ 27.3400
α(º) [a]	90	90
β (º) [a]	90	90
γ(º) [a]	90	90
Z	4	8
Atomic Displ., range (Å)	0.059- 0.304	0.182 – 0.024
Atomic Displ., average (Å)	0.18	0.09(4)
# observations	b	b
# variables		
R_{wp}		
R_p		
$R(F^2)$		
2θ range(º)		
# Rigid Body		
Atoms		
Preferred Orientation plane		
Bkg. function		
Profile Param.[c]		

[a] Observed/Calculated values. [b] No

Table 6.3. Crystallographic and Rietveld data for 5QDA .

	5QDA
Space Group	$P2_1/n$ (No. 14)
Z	4
a (Å)	3.8402(4)
b (Å)	29.128(6)
c (Å)	6.7762(12)
β (º)	88.735(8)
# observations	4299
# variables	14
R_{wp}	0.1204
R_p	0.0912
$R(F^2)$	0.1510
2θ range(º)	17-60
# Rigid Body Atoms	12
Preferred Orientation plane	(*1 1 -1*)
Bkg. function	3-term $n!/Q^{2n}$ Power series
Profile Param.	G*U*, L*Y*, *asym*, *stec*[1]

* G*U* = Gaussian *U* ; L*Y* = Cauchy *Y*; 1: unique axis (111).

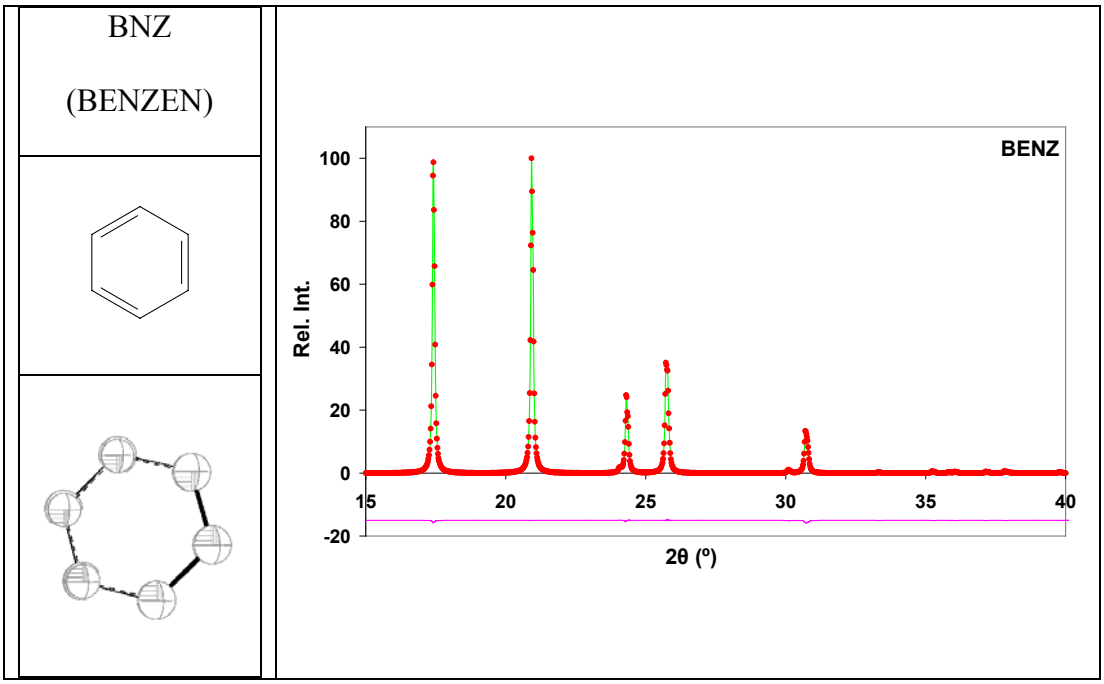

a) Benzene

NAPHTH (NAPHTA11) 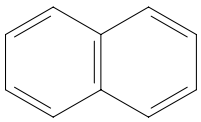 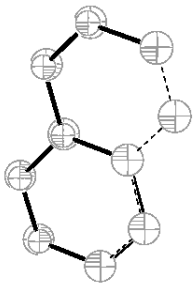	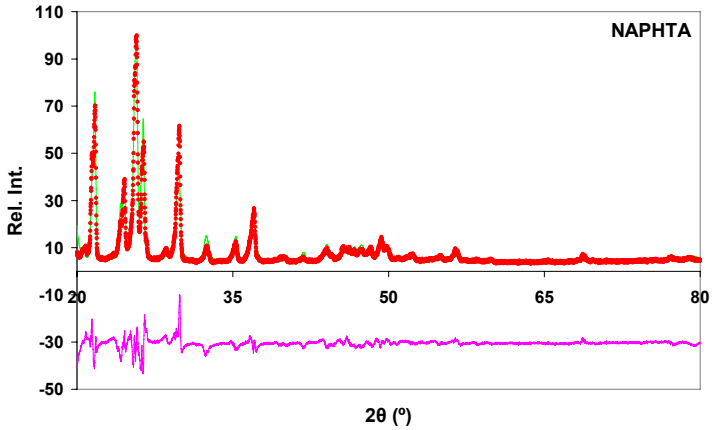

b) Naphthalene

BNZQ (BNZQUI) 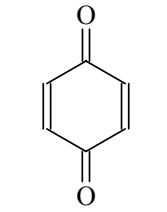 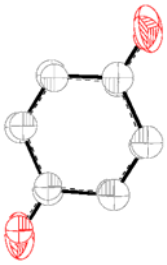	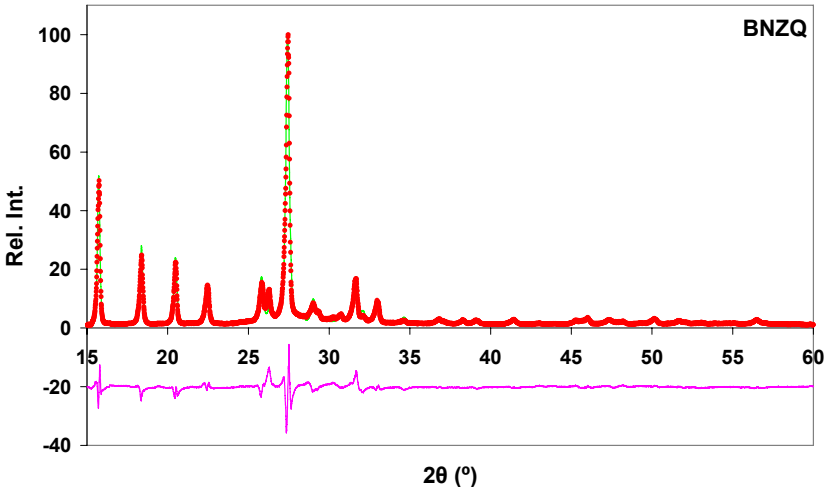

c) Benzoquinone

TSCRBZ (TSCRBZ01)	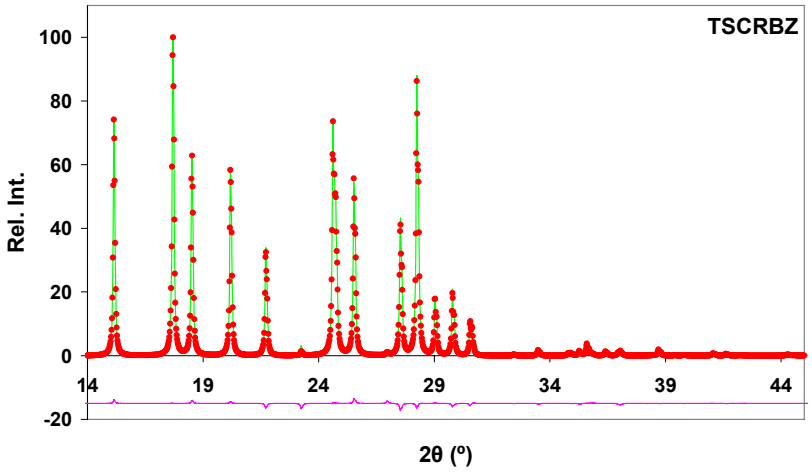
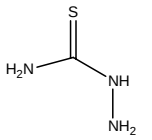	
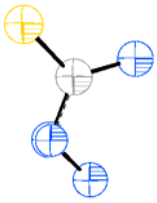	

d) Thiosemicarbazide

DETBA (DETSBR01)	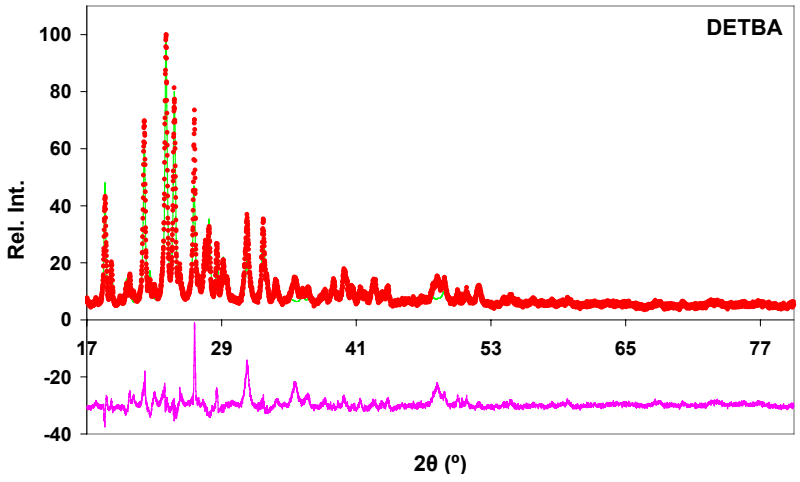
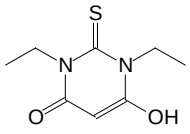	
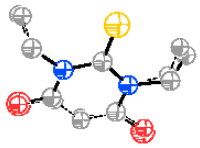	

e) 1,3-diethyl-2-thiobarbituric acid

DIBENZ (ZZZPRO01)	
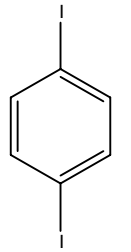	
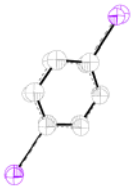	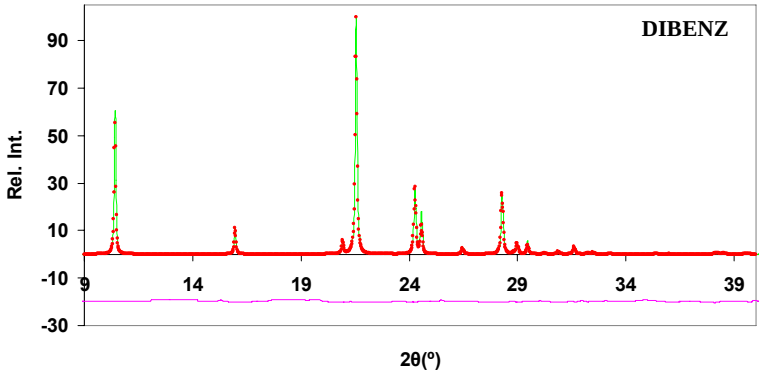

f) 1,4-diiodobenzene

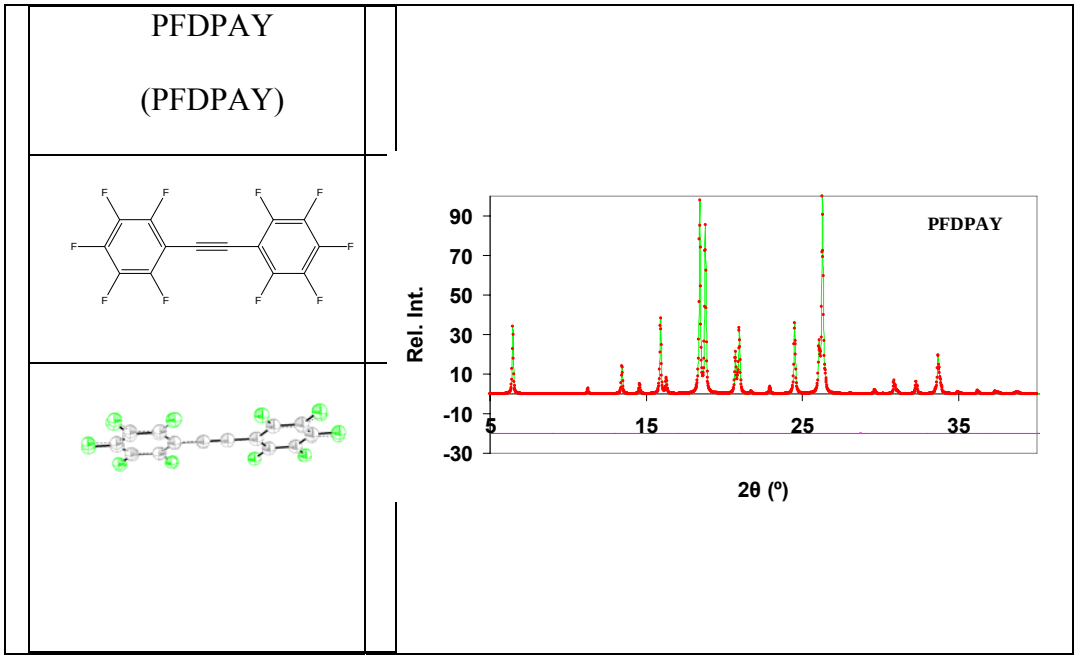

g) decafluoro-biphenylacetylene

Figure 6.4. Structure overlays and Observed, calculated and difference patterns for the test compounds: a) Benzene, b) Naphthalene, c) Benzoquinone, d) Thiosemicarbazide, e) 1,3-diethyl-2-thiobarbituric acid, f) 1,4-diiodobenzene, g) decafluoro-biphenylacetylene. Solid structures represent the best model from Rietveld refinement and dashed structures are from the Cambridge Structural Database. For the powder patterns, the observed data is shown as points and the calculated pattern as a line. The difference curve is plotted at the bottom of the graph on the same scale as the others.

as the powder patterns collected for these compounds could not be indexed by any of three commonly used indexing programs, ITO, [11] TREOR,[12] and DICVOL91.[13] *OCEANA* simultaneously determined the unit cell parameters and the correct structures for all of these compounds from their powder patterns.

An important characteristic of bis(aryl)diacetylenes, such as 5QDA, is their ability to undergo photoinduced topopolymerization so long as the molecules pack within empirically determined criteria.[43,44,45] The resulting polymers are highly conjugated, deeply colored, and display interesting optical and nonlinear optical properties.[44] Depending on the packing of the molecules, topopolymerization can produce an all-*trans* or all-*cis* polymer.[46] Upon exposure to UV light 5QDA does appear to polymerize, so determination of its crystal structure is very important. However, numerous attempts to grow crystals of 5QDA suitable for single crystal work have been unsuccessful, leading us to elucidate its structure from powder diffraction data. Comparison of the observed and calculated diffraction patterns for 5QDA is shown in Figure 6.5. The planar 5QDA molecules (maximum displacement from the mean plane is 0.073(4) Å) stack in a columnar array along the *a* axis (see Figure 6.6), with a stacking angle of 103º and a separation of 3.8Å, and should produce an all-*cis* polymer upon irradiation.

Conclusion

OCEANA has been used to successfully determine structures from X-ray powder diffraction data without prior indexing of the pattern. Similar programs require the data to be indexed first in order to obtain unit cell parameters, before structure elucidation can begin. *OCEANA* determines unit cell parameters, indexes the powder pattern and solves

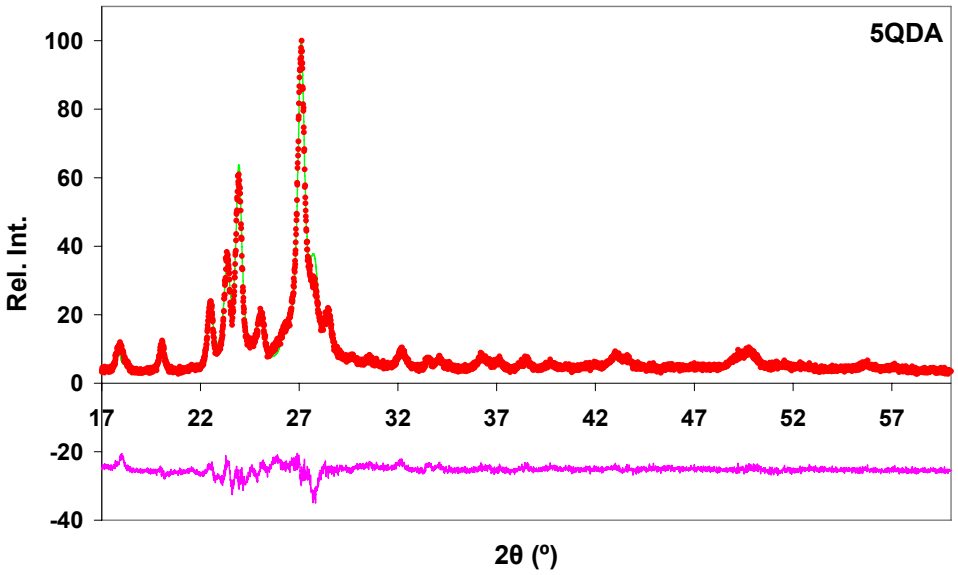

Figure 6.5. Observed, calculated and difference patterns for bis(5-quinoline)diacetylene. The red points represent observed data points and the green line represents the calculated pattern. The difference curve (purple) is plotted on the same scale as the others.

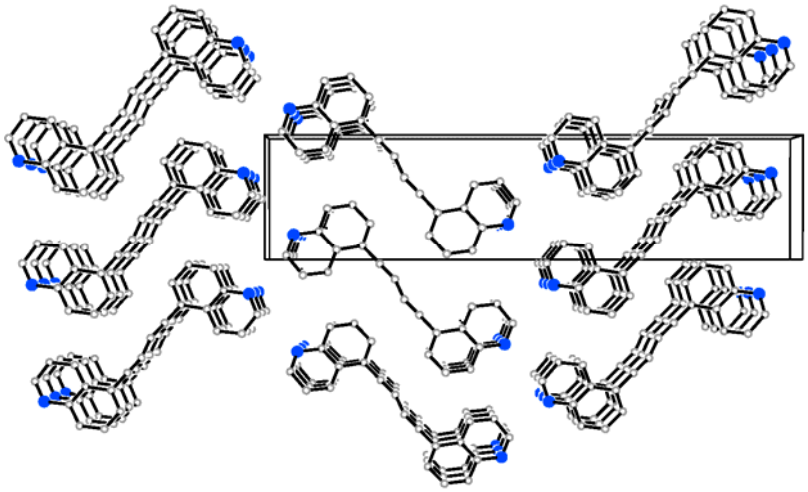

Figure 6.6. View of the crystal packing down the ***a*** axis for 5QDA.

the crystal structure simultaneously. These operations admittedly come at a large computational price, but *OCEANA* does provide a viable option when traditional attempts at indexing fail. Any information about space-group and unit cell parameters which can be input to the program will, however, facilitate the speed and ease with which *OCEANA* can find a correct solution. It should also be noted that all of the experimental X-ray patterns used in this study were collected on a conventional laboratory system. That *OCEANA* successfully determined these structures despite the poor quality data available, provides further evidence of its power. These problems, of course could be overcome by collection of high resolution data at a synchrotron facility, which should yield even more impressive results.[47]

References

1. Tate, M. W.; Eikenberry, E. F.; Barna, S. L.; Wall, M. E.; Lowrance, J. L.; Gruner, S.M. *J. Appl. Crystallogr.* **1995**, 28, 196.

2. David, W. I. F. *J. Appl. Crystallogr.* **1987**, *20*, 316.

3. David, W. I. F. *Nature.* **1990**, *346*, 731.

4. David, W. I. F. *J. Appl. Crystallogr*. **1999,** *32*, 654.

5. Sayre, D. *Acta Crystallogr*. **1952**, *5*, 60.

6. Eastermann, M. A.; McCusker, L.B.; Baerlocher, Ch. *J. Appl. Crystallogr*. **1992**, *32*, 1169.

7. Eastermann, M. A.; Gramlich, V. *J. Appl. Crystallogr*. **1993**, *26*, 396.

8. Jansen, J.; Peschar, R.; Schenk, H. *J. Appl. Crystallogr*. **1992**, *25*, 237.

9. Cascarano, G.; Giacovazzo, C.; Giuagliardi, A.; Steadman, A. *Acta Crystallogr. A*. **1991**, *47*, 480.

10. Bricogne, G. *Acta Crystallogr. A*. **1991**, *47*, 803.

11. Visser, J. W. J Appl. Crystallogr. **1969**, *2*, 89.

12. Werner, P. E.; Eriksson, L.; Westdahl, M. *J. Appl. Crystallogr.* **1985**, *18*, 367.

13. Boultif, A.; Louer, D. *J. Appl. Crystallogr*. **1991**, *24*, 987.

14. Harris, K. D. M.; Tremayne, M.; Lightfoot, P.; Bruce, P. G. *J. Am. Chem. Soc.* **1994**, *116*, 3543.

15. Engel, G. E.; Wilke, S.; König, O.; Harris, K. M. D.; Leusen, F. J. J. *J. Appl. Crystallogr*. **1999**, *32*, 1169.

16. Harris, K. D. M.; Johnston, R. L.; Kariuki, B. K. *Acta Crystallogr*. **1998**, *A54*, 632.

17. Rietveld, H. M. *J. Appl. Cryst*. **1969**, *2*, 65.

18. *OCEANA* has direct access to triclinic, monoclinic, and orthorhombic space-groups with one molecule in the asymmetric unit and access to ones with Z' < 1 through their subgroups.

19. Pertsin, A. J.; Kitaigorodsky, K. I. In *The Atom-Atom Potential Method. Applications to Organic Molecular Solids*; Springer-Verlag: 1987.

20. Buckingham, R.A. *Proc. R. Soc. London, Ser. A* **1938**, 168, 264-283.

21. Filippini, G.; Gavezzotti, A. *Acta Crystallogr*. **1993**, *B49*, 868-880.

22. Bauer, R.J., Jr. In *Genetic Algorithms and Investment Strategies*; John Wiley and Sons, Inc.: New York, 1994.

23. Press, W.H.; Flannery, B.P.; Teukolsky, S.A.; Vetterling, W.T. In *Numerical Recipes: The Art of Scientific Computing*; Cambridge University Press: New York, 1986, pp 289.

24. Solomon, E.P.; Berg, L.R.; Martin, D.W. In *Biology*; Saunders College Publishing: New York, 1999, 5th ed., pp 371.

25. Larson, A.C.; Von Dreele, R.B. *Report No. LA-UR-86-748*; Los Alamos Lab: 1987.

26. Bloss, F.D. In *Crystallography and Crystal Chemistry, An Introduction*; Holt, Rinhart and Winston, Inc.: New York, 1971; 135.

27. Dougherty, J.P.; Kurtz, S.K. *J. Appl. Crystallogr*. **1976**, *9*, 145.

28. David, W.I.F.; Shankland, K.; etc. In *Structure Determination from Powder Diffraction Data*; Oxford University Press: New York, 2002; 308.

29. Curtin, D.Y.; Paul, I.C. *Chem. Rev*. **1981**, *81*, 525.

30. Allen, F.H. *Acta Crystallogr.* **2002**, *B58*, 380.

31. a) Bacon, G.E.; Curry, N.A.; Wilson, S.A. *Proc. R. Soc. London, Ser.A*. **1964**, *279*, 98. b) For the $P2_12_12_1$ polymorph of benzene (BENZEN04, not shown): Fourme, R.; Andre, D.; Renaud, M. *Acta Crystallogr*. **1971**, *27*, 1275.

32. Trotter, J. *Acta Crystallogr*. **1960**, *13*, 86.

33. Cruickshank, D. W. J. *Acta Crystallogr*. **1957**, *10*, 504.

34. Hansen, F.; Hazell, R. G. *Acta Chem. Scand*. **1959**, *23*, 1359.

35. Bideau, J. P.; Bravic, G.; Filhol, A. *Acta Crystallogr.* **1977**, *B33*, 3847.

36. Boese, R.; Miebach, T. *Private Communication*, **1996**, CSD320041.

37. Williams, D.E.; Houpt, D.J., *Acta Cryst*, B42, **1986**, 286.

38. Mighell, A. D.; Himes, V. L.; Rogers, J. R. *Acta Crystallogr*. **1983**, *A39*, 737.

39. Harris, K.D.M. *Cryst. Growth & Des.* **2003**, *3*, 887.

40. Smith, D.K.; Nichols, M.C.; Zolensky, M.E. In *POWD12, A Fortran IV Program for Calculating X-ray Powder Diffraction Patterns*; Department of Geosciences, The Pennsylvania State University: University Park, PA., 1983.

41. Gropp, W.; Lusk, E.; Doss, N. *Parallel Computing*. **1996**, *22*, 789.

42. Titan; Wavefunction, Inc., 18401 Von Karman Ave., Suite 370, Irvine, CA 92912.

43. Baughman, R. H.; Yee, K. C. *J. Poly. Sci.: Macromol. Rev*. **1978**, *13*, 248.

44. Bloor, D.; Chance, R. R.; Eds. In *Polydiacetylenes*; Martinus Nijhoff: Boston, 1985.

45. Likhatchev,D.; Alexandrova, L.; Salcedo, R.; Ogawa, T. *Polym. Bull.* **1995**, *34*, 149.

46. Coates, G.W.; Dunn, A.R.; Henling, L.M.; Dougherty, D.A.; Grubbs, R.H. *Angew. Chem. Int. Ed. Engl.* **1997**, *36*, 248.

47. The poor resolution and inability of most conventional laboratory X-ray powder diffractometers to accurately determine peak positions across the full range of scattering angles is well-known. (See: Shirley, R. *NBS Spec. Publ.* **1980**, *567*, 361; Smith, G.; Kahara, E. *J. Appl. Crystallogr.* **1975**, *8*, 681.

CHAPTER 7

EXPERIMENTAL

X-ray Crystallographic Studies

Verification of sample purity and identity was performed by X-ray powder diffraction analysis. X-ray powder patterns of single crystal results, calculated by the program POWD12,[1] were compared to diffraction patterns obtained from bulk reaction products. A Scintag XDS/2000 theta-theta diffractometer with Cu $K\alpha_1$ radiation (λ = 1.54060 Å) and an intrinsic germanium solid-state detection system at room temperature (295 ± 1 K) were used to collect powder diffraction data. Pertinent crystallographic information from single-crystal examination is given in Table 2.3. All measurements were performed using a Rigaku AFC8S diffractometer with graphite-monochromated Mo Kα radiation (λ = 0.71073 Å) and a Mercury CCD detector at 163 ± 1 K.

Thermal Analysis

Differential scanning calorimetry (DSC) and thermal gravimetric analysis (TGA) were carried out using TA Instruments SDT-2960 simultaneous DSC-TGA instrument. Clean alumina sample pans (90 μL volume) were tared on the microbalance arms prior to use. Sample masses ranged from 5 - 6 mg. The sample and reference were heated from 25 to 600 °C at a rate of 10 °C/min. Measurements of temperature and heat flow data were recorded in one second intervals and data analysis was performed using the *TA Universal Analysis* software package.[3] Thermal events were characterized according to the positions of endotherms and exotherms in relation to mass loss. Mass loss and onset calculations were performed by standard methods.

Single Crystal Analysis

Contact distances are measured between an electron donor and an electron acceptor to determine if a halogen interaction is present. An interaction is present if the measured contact distance is less than the sum of van der Waal radii (table 7.1)[5] of the two atoms of interest. For example, one halogen bonding contact distance was reported, for the crystal structure of MBZIM and 1,4-F_4DIB, with a distance 3.301(2) Å.. Since the reported distance is less than the sum of the van der Waal radii for sulfur and iodine atoms (3.78 Å) then an interaction is present. The shorter the contact distance results in a stronger the interaction.

Materials and Methods

Reagents were purchased from either Aldrich Chemical Company or ACROS Organics and were used as received unless otherwise stated. Thiourea and benzyl were purchased from Eastman and Baker & Adamson, respectively and were used as received. Solvents were acquired from commercial sources. Carbon and hydrogen elemental analyses were performed by Atlantic Microlabs in Norcross, GA.

Synthesis of Halogen Bonded Complexes

Complexes were synthesized using slow evaporation or vapor diffusion crystallization techniques. The solvent evaporation technique involves dissolving stoichiometric ratios of donor and acceptor in a solvent and allowing the mixture to slowly evaporate. Solvents used include methylene chloride, chloroform, hexane, and acetone. A good solvent is one where donor and acceptor are moderately soluble in. Vapor diffusion involves dissolving the donor and acceptor in a solvent, and then sealing

Table 7.1. List of van der Waals radii for selected atoms. Radii are reported in angstroms (Å).

Atom	Radius
C	1.70
N	1.55
O	1.52
P	1.80
S	1.80
Se	1.90
F	1.47
Cl	1.75
Br	1.85
I	1.98

the container in a second container containing a solvent in which both acceptor and donor are not soluble. The second solvent must be miscible with the first and also the more volatile of the two. The object is for the more volatile solvent to vaporize and mix in with the primary solvent to transform it in to an insoluble mixture forcing the components to crystallize out of solution. Also prevents crust of microcrystals from forming as the solvent level drops. One such solvent system is methylene chloride/pentane. Methylene chloride is used to dissolve the donor and acceptor while pentane is the more volatile solvent that diffuses into the methylene chloride.

References

1. Smith, D.K.; Nichols, M.C.; Zolensky, M.E. In *POWD12, A Fortran IV Program for Calculating X-ray Powder Diffraction Patterns*; Department of Geosciences, The Pennsylvania State University: University Park, PA., 1983.

2. Jacobson, R. A. REQABS, subroutine of Crystal Clear, Rigaku/MSC, The Woodlands, TX, 1999.

3. *Universal Analysis* for Windows 95/98, Version 3.6C, Build 3.6.0.17, TA

4. Broan, C.J.; Butler, A.R. *J. CHEM. SOC. PERKIN TRANS. II* **1989**, 731-740.

5. (a) Winter, M. "*Vander der Waals Radius*" www.webelements.com/webelements/scholar/properties/definitions/van-der-waals-radius (04/30/08) (b) Bondi, A. *J. Phys. Chem.***1964**, *68*, 441. (c) Pauling, L. *The Nature of the Chemical Bond*, Cornell University Press, USA, **1945**. (d) Huheey, J.E.; Keiter, E.A.; Keiter, R.L. *Inorganic Chemistry : Principles of Structure and Reactivity*, 4th ed., HarperCollins, New York, USA, **1993**. (e) Porterfield, W.W. "*Inorganic chemistry, a unified approach*" Addison Wesley Publishing Co., Reading Massachusetts, USA, **1984**. (f) James, A.M.; Lord, M.P. "*Macmillan's Chemical and Physical Data*" Macmillan, London, UK, **1992**.

APPENDICES

Appendix A

X-ray Powder Diffraction Data

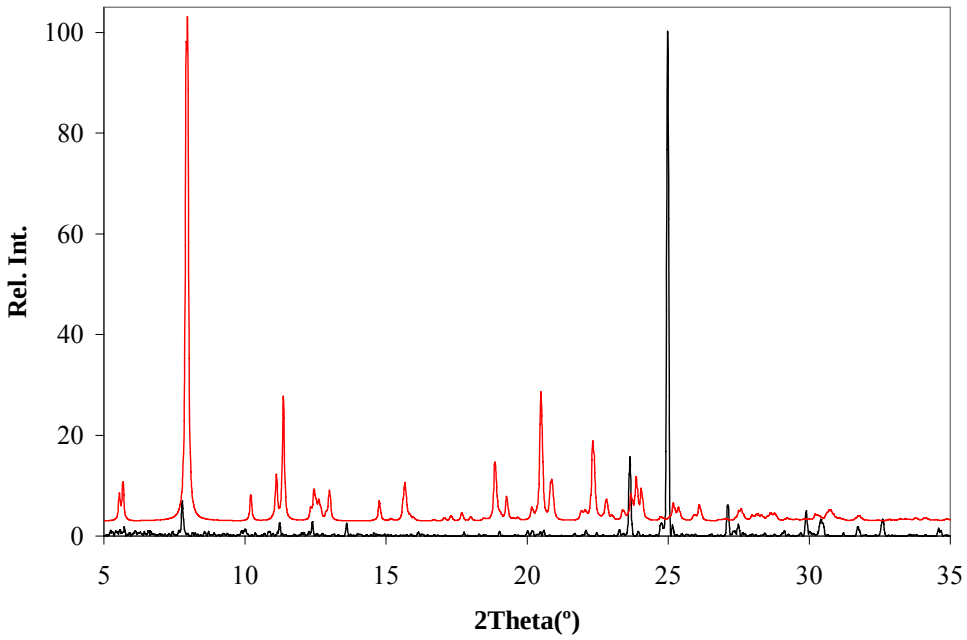

Figure A-1: X-ray powder pattern comparison of TPhPSe • TIE complex. The experimental powder pattern is plotted in black and the pattern calculated from POWD12 is plotted in red.

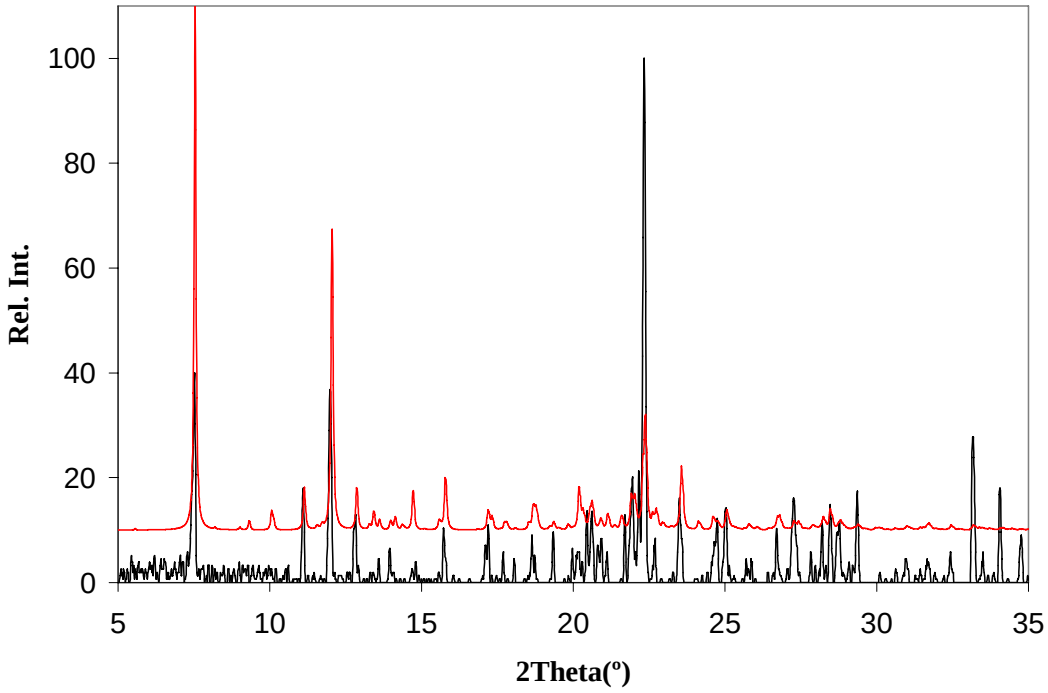

Figure A-2: X-ray powder pattern comparison of TPhPSe • 1,4-F_4DIB complex. The experimental powder pattern is plotted in black and the pattern calculated from POWD12 is plotted in red.

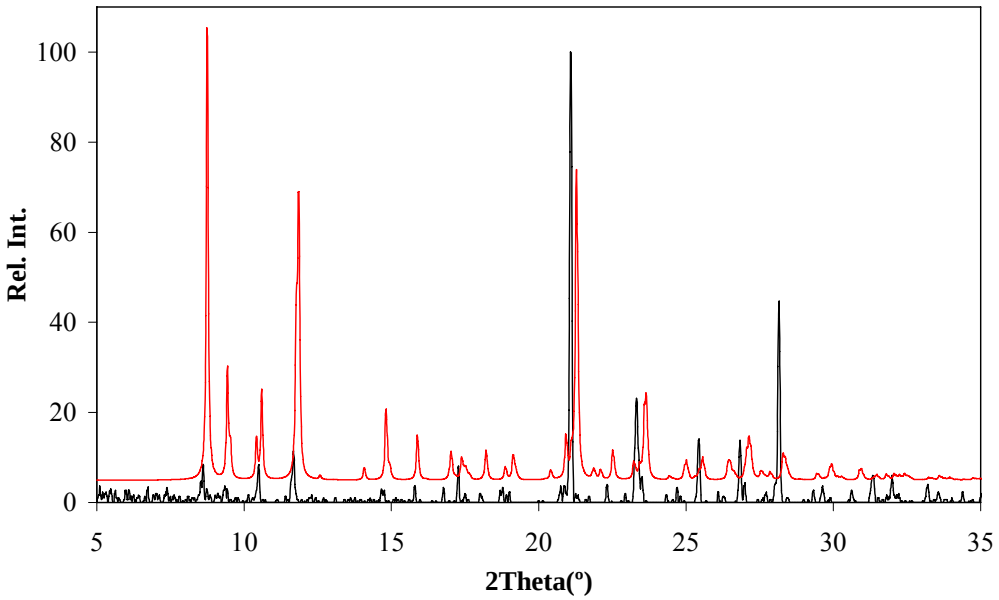

Figure A-3: X-ray powder pattern comparison of TPhPSe • 1,4-F_4DIB complex. The experimental powder pattern is plotted in black and the pattern calculated from POWD12 is plotted in red.

Appendix B

Crystallographic Data For Reported Complexes

Table B-1: Crystallographic Data for Ph_3PSe complexes

	TIE	1,4-F_4DIB	1,2-F_4DIB
formula	$C_{78}H_{60}P_4Se_4I_{12}$	$C_{48}H_{30}F_8I_4P_2Se_2$	$C_{24}H_{15}F_4I_2PSe$
M_w	2959.78	1486.22	743.09
CCDC#	660560	660406	660559
Crystal system	Monoclinic	Monoclinic	Monoclinic
Space group	$P2_1/n$	$P2_1/c$	$P2_1/n$
a/Å	22.196(2)	9.6878(16)	11.1579(18)
b/Å	9.4096(11)	23.464(4)	12.5788(21)
c/Å	22.360(3)	22.214(4)	16.975(3)
α(°)			
β(°)	91.266(5)	103.584(4)	90.669(6)
γ(°)			
V/Å^3	4668.9(9)	4908.4612(0)	2382.2871(0)
Z	2	4	4
D_c/g cm^{-3}	2.105	2.014	2.072
μ/mm^{-1}	5.645	4.157	4.277
Transmission coeff.	0.5006 – 1.000	0.6279 -1.000	0.8311 -1.000
No. data measured	40,963	46,344	22,251
No. data unique(R_{merge})	9465 (0.079)	9983(0.1167)	4835(0.0828)
No. obsd data ($I > 2\sigma(I)$)	8280	5441	3647
R_1[a]	0.0775(0.0895)	0.0516(0.0572)	0.0546(0.0865)
wR_2[b]	0.1665(0.1719)	0.1184(0.1225)	0.0841(0.0937)

[a] $R_1 = \Sigma||F_0| - |F_c||/\Sigma|F_0|$ for observed data ($I > 2\sigma(I)$); number in parentheses is for all data. [b] $wR_2 = \{\Sigma[w(F_0^2 - F_c^2)^2]/\Sigma[w(F_0^2)^2]\}^{1/2}$ for observed data ($I > 2\sigma(I)$); number in parentheses is for all data.

Table B-2: Crystal Data for 1,4-F_4DIB complexes with benzimidazoles

	MBZIM	MMBZIM	MBZOX	MBZTH
formula	$S_1N_2I_2F_4C_{13}H_6$	$S_2N_4O_2I_2F_4C_{22}H_{20}$	$S_2N_2O_2I_2F_4C_{20}H_{10}$	$S_4N_2I_2F_4C_{20}H_{10}$
M_w	552.06	766.35	704.22	736.34
Crystal system	monoclinic	triclinic	monoclinic	monoclinic
Space group	*P2₁/c*	*P-1*	*C2/c*	*P2₁/n*
a/Å	5.646(1)	4.945(1)	31.00(1)	5.841(2)
b/Å	33.359(5)	11.519(3)	4.324(2)	15.969(5)
c/Å	8.526(2)	11.990(4)	19.118(8)	13.675(4)
α(º)		106.672(7)		
β(º)	92.185(5)	98.150(6)	113.578(9)	93.673(8)
γ(º)		92.716(7)		
V/Å^3	1604.7(5)	644.9(3)	2349.8(9)	1174.6(5)
Z	2	1	2	2
D_c/g cm^{-3}	2.285	1.973	1.991	2.082
μ/mm^{-1}	4.086	2.658	2.906	3.077
Transmission coeff.	0.4204 – 1.000	0.6695 – 1.000	0.7030 – 1.000	0.6719 – 1.000
No. data measured	12167	6090	10376	11016
No. data unique(R_{merge})	3096(0.0578)	2563(0.0165)	2398(0.0762)	2379(0.0430)
No. obsd data ($I > 2\sigma(I)$)	2772	2467	2015	2055
R_1[a]	0.0575 (0.0642)	0.0221 (0.0234)	0.0691 (0.0871)	0.0461 (0.0565)
wR_2[b]	0.1335 (0.1375)	0.0479 (0.0486)	0.1216 (0.1284)	0.0947 (0.0996)

[a] $R_1 = \Sigma||F_0| - |F_c||/\Sigma|F_0|$ for observed data ($I > 2\sigma(I)$); number in parentheses is for all data. [b] $wR_2 = \{\Sigma[w(F_0^2 - F_c^2)^2]/\Sigma[w(F_0^2)^2]\}^{1/2}$ for observed data ($I > 2\sigma(I)$); number in parentheses is for all data.

Table B-3: Crystal Data for 1,2-F_4DIB complexes with benzimidazoles

	MBZIM	MBZOX
formula	$S_1N_2I_2F_4C_{13}H_6$	$S_1N_1O_1I_2F_4C_{13}H_5$
M_w	552.06	553.04
Crystal system	triclinic	monoclinic
Space group	*P-1*	*P2$_1$/n*
a/Å	8.2368(14)	13.744(7)
b/Å	8.5594(15)	4.465(2)
c/Å	12.643(3)	25.211(13)
α(°)	88.742(17)	
β(°)	85.274(16)	95.967(19)
γ(°)	66.509(10)	
V/Å^3	814.6(3)	1538.8896(0)
Z	1	2
D_c/g cm^{-3}	2.251	2.387
μ/mm^{-1}	4.024	4.264
Transmission coeff.	0.7540 – 1.000	0.5923 – 1.000
No. data measured	7873	11163
No. data unique(R_{merge})	3288(0.0648)	2880(0.0963)
No. obsd data ($I > 2\sigma(I)$)	1938	1901
R_1[a]	0.0516(0.1053)	0.0618(0.1099)
wR_2[b]	0.0772(0.0884)	0.1034(0.1178)

[a] $R_1 = \Sigma||F_0| - |F_c||/\Sigma|F_0|$ for observed data ($I > 2\sigma(I)$); number in parentheses is for all data. [b] $wR_2 = \{\Sigma[w(F_0^2 - F_c^2)^2]/\Sigma[w(F_0^2)^2]\}^{1/2}$ for observed data ($I > 2\sigma(I)$); number in parentheses is for all data.

Table B-4: Crystal Data for TIE complexes with benzimidazoles

	MBZIM	MBZTH
formula	$S_1N_2I_4C_9H_6$	$S_2N_1I_4C_9H_5$
M_w	681.82	698.86
Crystal system	monoclinic	triclinic
Space group	*P2₁/c*	*P-1*
a/Å	8.4352(17)	7.4346(11)
b/Å	15.280(3)	10.8583(11)
c/Å	11.824(2)	11.2236(13)
α(°)		66.47(3)
β(°)	90.073(12)	70.71(3)
γ(°)		70.68(3)
V/Å^3	1524.0(5)	763.0384(0)
Z	4	2
D_c/g cm^{-3}	2.972	3.042
μ/mm^{-1}	8.294	8.416
Transmission coeff.	0.4697 – 1.000	0.5836 – 1.000
No. data measured	14255	7068
No. data unique(R_{merge})	3093(0.0305)	2953(0.0397)
No. obsd data ($I > 2\sigma(I)$)	2803	2479
R_1[a]	0.0490(0.0532)	0.0398(0.0532)
wR_2[b]	0.1105(0.1127)	0.0783(0.0826)

[a] $R_1 = \Sigma||F_0| - |F_c||/\Sigma|F_0|$ for observed data ($I > 2\sigma(I)$); number in parentheses is for all data. [b] $wR_2 = \{\Sigma[w(F_0^2 - F_c^2)^2]/\Sigma[w(F_0^2)^2]\}^{1/2}$ for observed data ($I > 2\sigma(I)$); number in parentheses is for all data.

Table B-5: Crystal Data for MBZTH • IODOFR complex

	MBZTH
formula	$S_2N_1I_3C_8H_6$
M_w	560.71
Crystal system	triclinic
Space group	*P-1*
a/Å	7.1312(14)
b/Å	7.4596(15)
c/Å	13.299(3)
α(º)	74.85(2)
β(º)	86.74(3)
γ(º)	82.29(2)
V/Å^3	676.6(2)
Z	2
D_c/g cm^{-3}	2.753
μ/mm^{-1}	7.203
Transmission coeff.	0.5835 – 1.000
No. data measured	5801
No. data unique(R_{merge})	2346(0.0642)
No. obsd data ($I > 2\sigma(I)$)	1835
R_1[a]	0.0805(0.1003)
wR_2[b]	0.1647(0.1706)

[a] $R_1 = \Sigma||F_0| - |F_c||/\Sigma|F_0|$ for observed data ($I > 2\sigma(I)$); number in parentheses is for all data. [b] $wR_2 = \{\Sigma[w(F_0^2 - F_c^2)^2]/\Sigma[w(F_0^2)^2]\}^{1/2}$ for observed data ($I > 2\sigma(I)$); number in parentheses is for all data.

Table B-6: Crystal Data of DPDTGU Solvates

	PYR	THF	DMF
formula	$S_2N_6C_{26}H_{24}$	$S_2O_2N_4C_{24}H_{30}$	$S_2O_2N_6C_{22}H_{28}$
M_w	484.64	470.65	472.63
CSDC#	661113	661114	661112
Crystal system	Monoclinic	Monoclinic	Orthorhombic
Space group	*C2/c*	*C2/c*	$P2_12_12_1$
a/Å	26.235(6)	25.167(7)	9.306(2)
b/Å	7.7485(16)	7.7949(16)	11.662(3)
c/Å	13.859(3)	14.074(4)	22.4456(5)
α(°)			
β(°)	113.418(5)	116.864(8)	
γ(°)			
V/Å^3	2576.5(10)	2463.03(10)	2436.0(10)
Z	4	4	4
D_c/g cm^{-3}	1.249	1.269	1.286
μ/mm^{-1}	0.232	0.244	0.249
Transmission coeff.	0.7710- 1.000	0.5122 –1.000	0.9058 – 1.000
No. data measured	11682	10377	23367
No. data unique(R_{merge})	2536 (0.0503)	2210(0.0931)	4951 (0.0479)
No. obsd data ($I > 2\sigma(I)$)	1998	1416	4593
R_1[a]	0.0515(0.0715)	0.0684(0.1125)	0.0509 (0.0562)
wR_2[b]	0.0928(0.0998)	0.1205(0.1342)	0.1008 (0.1047)

[a] $R_1 = \Sigma||F_0| - |F_c||/\Sigma|F_0|$ for observed data ($I > 2\sigma(I)$); number in parentheses is for all data. [b] $wR_2 = \{\Sigma[w(F_0^2 - F_c^2)^2]/\Sigma[w(F_0^2)^2]\}^{1/2}$ for observed data ($I > 2\sigma(I)$); number in parentheses is for all data.

Table B-7: Crystal Data of DPDTGU complexes

	TIE	1,2-F_4DIB
formula	$C_{30}H_{40}I_4N_4O_4S_2$	$C_{28}H_{18}F_8I_4N_4O_2S_2$
M_w	1091.87	1165.69
CSDC#	N/A	N/A
Crystal system	monoclinic	monoclinic
Space group	*P2₁/c*	*C2/c*
a/Å	14.150(2)	15.752(4)
b/Å	16.939(3)	21.905(4)
c/Å	22.470(3)	14.229(4)
α(°)		
β(°)	127.710(6)	108.37(1)
γ(°)		
V/Å^3	4260.8(12)	4659(2)
Z	4	
D_c/g cm^{-3}	1.662	1.657
μ/mm^{-1}	3.055	2.882
Transmission coeff.	0.0436-1.00	0.3783-1.00
No. data measured	38363	19499
No. data unique(R_{merge})	8048(0.0796)	4056(0.2603)
No. obsd data ($I > 2\sigma(I)$)	6320	2943
R_1[a]	0.0747(0.0979)	0.1597(0.1997)
wR_2[b]	0.1424(0.1516)	0.3192(0.3448)

[a] $R_1 = \Sigma||F_0| - |F_c||/\Sigma|F_0|$ for observed data ($I > 2\sigma(I)$); number in parentheses is for all data. [b] $wR_2 = \{\Sigma[w(F_0^2 - F_c^2)^2]/\Sigma[w(F_0^2)^2]\}^{1/2}$ for observed data ($I > 2\sigma(I)$); number in parentheses is for all data.

Table B-8: Crystal Data of 1,4 DMbMSDPGU and 1,6 DMbMSDPGU complexes

	1,4 DMbMSDPGU • 1,4-F_4DIB	1,6 DMbMSDPGU • $(2I_3•I_2)^{-2}$.
formula	$C_{26}H_{22}F_4I_2N_4S_2$	$C_{20}H_{23}I_7N_4S_2$
M_w	784.40	1270.88
CSDC#	N/A	N/A
Crystal system	triclinic	monoclinic
Space group	*P-1*	*C2/m*
a/Å	9.987(2)	13.4656(18)
b/Å	11.076(2)	19.3883(18)
c/Å	13.638(3)	13.714(2)
α(º)	97.051(5)	
β(º)	108.990(5)	116.120(4)
γ(º)	96.598(4)	
V/Å^3	1396.3(5)	3214.7(7)
Z	2	4
D_c/g cm^{-3}	1.866	2.630
μ/mm^{-1}	2.452	6.905
Transmission coeff.	0.00	0.8280-1.00
No. data measured	13899	16407
No. data unique(R_{merge})	5627(0.0212)	3370(0.0192)
No. obsd data ($I > 2\sigma(I)$)	4738	3150
R_1[a]	0.0385(0.0476)	0.0251(0.0274)
wR_2[b]	0.0723(0.0778)	0.0521(0.0533)

[a] $R_1 = \Sigma||F_0| - |F_c||/\Sigma|F_0|$ for observed data ($I > 2\sigma(I)$); number in parentheses is for all data. [b] $wR_2 = \{\Sigma[w(F_0^2 - F_c^2)^2]/\Sigma[w(F_0^2)^2]\}^{1/2}$ for observed data ($I > 2\sigma(I)$); number in parentheses is for all data.

Appendix C

Halogen bonded complexes of chalcogen donors

Table C-1: List of halogen bonded complexes of Chalcogen donors

Acceptors → / Donors ↓	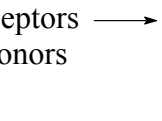 C_2I_4	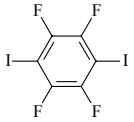 $C_6F_4I_2$	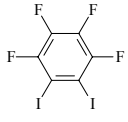 $C_6F_4I_2$	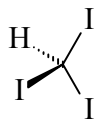 CHI_3	I_2
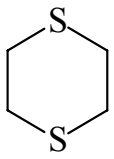 $C_4H_8S_2$	**Cd4090** $C_4H_8S_2$ / C_2I_4	**Cd1764** $C_4H_8S_2$ / $(C_6F_4I_2)_2$		**Known**[1] $C_4H_8S_2$ / CHI_3	**Known**[2] $C_4H_8S_2$ / $(I_2)_2$ **Cd6235** $C_4H_8S_2$ / $(I_2)_2$
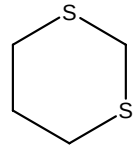 $C_4H_8S_2$					**Cd6211** $C_4H_8S_2$ / $(I_2)_2$
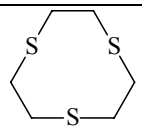 $C_6H_{12}S_3$	**Cd2011** $(C_6H_{12}S_3)_2$ / $(C_2I_4)_3$	**Cd1777** $C_6H_{12}S_3$ / $C_6F_4I_2$		**Cd2063** $C_6H_{12}S_3$ / $(CHI_3)_3$	
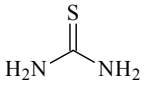 CH_4N_2S		**Cd1963** CH_4N_2S / $C_6F_4I_2$			
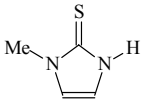 $C_4H_6N_2S$	**Cd0260**[3] $C_4H_6N_2S$ / C_2I_4	**Cd0243**[3] $C_4H_6N_2S$ / $C_6F_4I_2$	**Cd0323**[3] $C_4H_6N_2S$ / $C_6F_4I_2$		
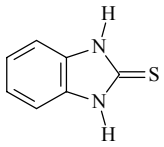 $C_7H_6N_2S$	**Cd3019** $C_7H_6N_2S$ / C_2I_4	**Cd1825** $C_7H_6N_2S$ / $C_6F_4I_2$	**Cd2102** $C_7H_6N_2S$ / $C_6F_4I_2$		**Known**[4] **Cd5288** $(C_7H_6N_2S)_2$ / $(I_2)_3$ /$(H_2O)_2$

Table C-2: List of halogen bonded complexes of Chalcogen donors (cont.)

Acceptors → Donors ↓	New polymorph of donor	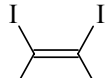 C_2I_4	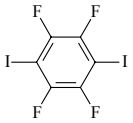 $C_6F_4I_2$	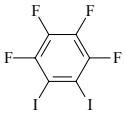 $C_6F_4I_2$	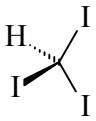 CHI_3
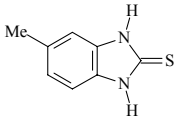 $C_8H_8N_2S$			**Cd3018** $(C_8H_8N_2S)_2$ / $C_6F_4I_2$ / $(H_2O)_2$		
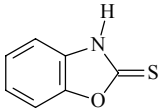 C_7H_5NOS	**Cd2025**		**Cd1990** $(C_7H_5NOS)_2$ / $C_6F_4I_2$	**Cd5396** C_7H_5NOS / $C_6F_4I_2$	
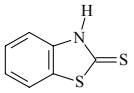 $C_7H_5NS_2$		**Cd5073** $C_7H_5NS_2$ / C_2I_4	**Cd1950** $(C_7H_5NS_2)_2$ / $C_6F_4I_2$		**Cd5378** $(C_7H_5NS_2)_2$ / CHI_3
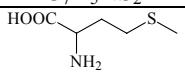 $C_5H_{11}NO_2S$			**Cd5194** $(C_5H_{11}NO_2S)_2$ / $C_6F_4I_2$		
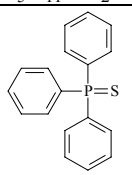 $C_{18}H_{15}PS$			**Cd5353** $C_{18}H_{15}PS$ / $C_6F_4I_2$		
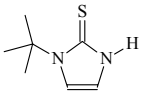 $C_7H_{12}N_2S$	**Cd1898**	**Cd1992** $(C_7H_{12}N_2S)_2$ / C_2I_4	**Cd1952** $C_7H_{12}N_2S$ / $C_6F_4I_2$		
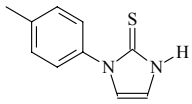 $C_{10}H_{10}N_2S$	**Cd1919**				
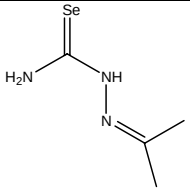 $C_4H_9N_3Se$	**Cd5253**			**Cd5193** $C_4H_9N_3Se$ / $C_6F_4I_2$	

Table C-3: List of halogen bonded complexes of Chalcogen donors (cont.)

Acceptors → Donors ↓	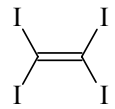 C_2I_4	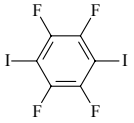 $C_6F_4I_2$	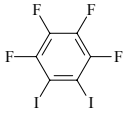 $C_6F_4I_2$	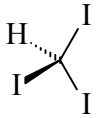 CHI_3
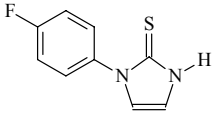 $C_9H_7N_2FS$		**Cd1883** $(C_9H_7N_2FS)_2$ / $C_6F_4I_2$		
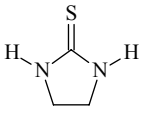 $C_3H_6N_2S$	**Cd5104** $(C_3H_6N_2S)_3$ / $(C_2I_4)_2$	**Cd1880** $C_3H_6N_2S$ / $C_6F_4I_2$		**Cd3017** $C_3H_6N_2S$ / CHI_3
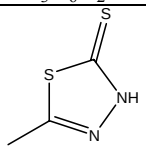 $C_3H_4N_2S_2$		**Cd5431** $C_3H_4N_2S_2$ / $(C_6F_4I_2)_2$		
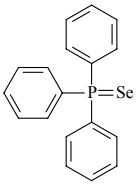 $C_{18}H_{15}PSe$	**Cd4061** $(C_{18}H_{15}PSe)_4$ / $(C_2I_4)_3$	**Cd2065** $C_{18}H_{15}PSe$ / $C_6F_4I_2$	**Cd3076** $C_{18}H_{15}PSe$ / $C_6F_4I_2$	
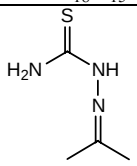 $C_4N_3SH_9$ MW= 131.14	**Cd5289** $(C_4H_9N_3S)_2$ / C_2I_4	**Cd4062** $C_4H_9N_3S$ / $C_6F_4I_2$	**Cd1991** $C_4H_9N_3S$ / $(C_6F_4I_2)_2$ **Cd3049** $C_4H_9N_3S$ / $C_6F_4I_2$	
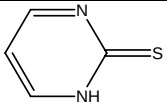 $C_4H_4N_2S$		**Cd5113** $(C_4H_4N_2S)_2$ / $C_6F_4I_2$		
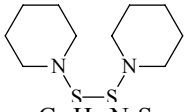 $C_{11}H_{22}N_2S_2$		**Cd5588** $C_{11}H_{22}N_2S_2$ / $C_6F_4I_2$		

Table C-4: List of halogen bonded complexes of Chalcogen donors (cont.)

Acceptors → Donors ↓	New polymorph of donor	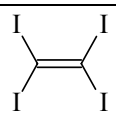 C_2I_4	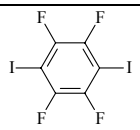 $C_6F_4I_2$	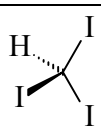 CHI_3	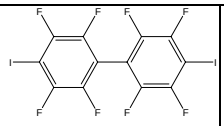 $C_{12}F_8I_2$	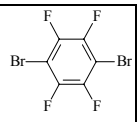 $C_6F_4Br_2$
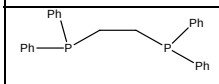 $C_{26}H_{24}P_2$			**Cd6212** $C_{26}H_{24}P_2$ /$(C_6F_4I_2)_3$ **Cd6490** $C_{26}H_{24}P_2$ / $C_6F_4I_2$	**Cd6314** $C_{26}H_{24}P_2$ /CHI_3 **Cd6503** $C_{26}H_{24}P_2$ / $(CHI_3)_4$ / $(I^-)_2$ (ionic)		
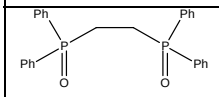 $C_{26}H_{24}P_2O_2$			**Cd6020** $C_{26}H_{24}P_2O_2$ / $C_6F_4I_2$			**Cd6236** $C_{26}H_{24}P_2O_2$ / $C_6F_4Br_2$ (no XB)
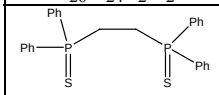 $C_{26}H_{24}P_2S_2$		**Cd6021** $C_{26}H_{24}P_2S_2$ / C_2I_4			**Cd6315** $C_{26}H_{24}P_2S_2$ / $C_{12}F_8I_2$	
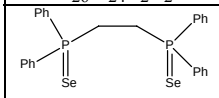 $C_{26}H_{24}P_2Se_2$	**Cd6176**	**Cd6175** $C_{26}H_{24}P_2Se_2$ / C_2I_4				
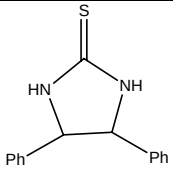 $C_{15}H_{14}N_2S$	**Cd5800**					
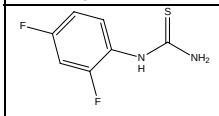 $C_7H_6F_2N_2S$	**Cd5937**					
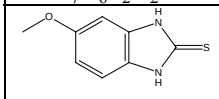 $C_8H_8N_2OS$	**Cd5920**					

Table C-5: List of halogen bonded complexes of Chalcogen donors (cont.)

Acceptors → Donors ↓	New polymorph of donor	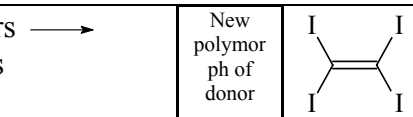 C_2I_4	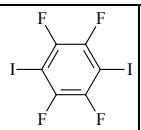 $C_6F_4I_2$	I_2	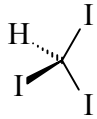 CHI_3	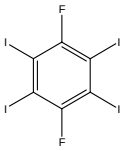 $C_6I_4F_2$
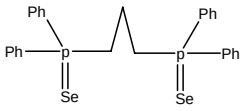 $C_{27}H_{26}P_2Se_2$	**Cd6057**	**Cd6139** $C_{27}H_{26}P_2Se_2$ / C_2I_4				
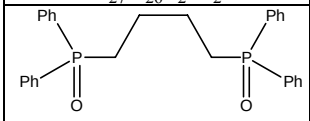 $C_{28}H_{28}P_2O_2$			**Cd6150** $C_{28}H_{28}P_2O_2$ / $C_6F_4I_2$			
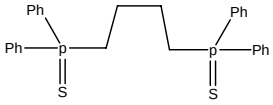 $C_{28}H_{28}P_2S_2$	**Cd6014** **Cd6012**					**Cd6232** $C_{28}H_{28}P_2S_2$ / $C_6I_4F_2$
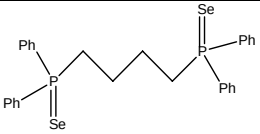 $C_{28}H_{28}P_2Se_2$		**Cd6284** $C_{28}H_{28}P_2Se_2$ / C_2I_4				
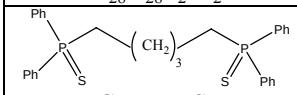 $C_{29}H_{30}P_2S_2$		**Cd6192** $C_{29}H_{30}P_2S_2$ / C_2I_4				
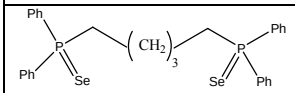 $C_{29}H_{30}P_2Se_2$	**Cd6191**					
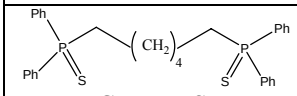 $C_{30}H_{32}P_2S_2$	**Cd6153**			**Cd6286** $C_{30}H_{32}P_2S_2$ / $(I_2)_2$		
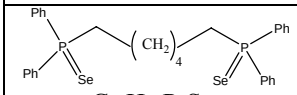 $C_{30}H_{32}P_2Se_2$					**Cd6313** $C_{30}H_{32}P_2Se_2$ / $(CHI_3)_2$	

Table C-6: List of halogen bonded complexes of Chalcogen donors (cont.)

Acceptors → Donors ↓	New polymorph of donor	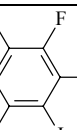 C_2I_4	$C_6F_4I_2$	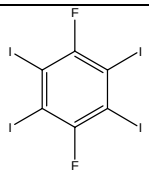 $C_6I_4F_2$
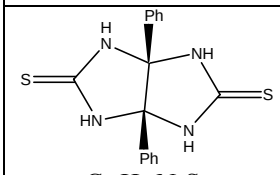 $C_{16}H_{14}N_4S_2$	(THF) **Cd5680** (PYR) **Cd5283a** (unsolvate) **Cd5833** (DMF) **Cd5972**	**Cd5724** $C_{16}H_{14}N_4S_2$ / $C_6F_4I_2$	**Cd5726** $C_{16}H_{14}N_4S_2$ / $(C_6F_4I_2)_2$	
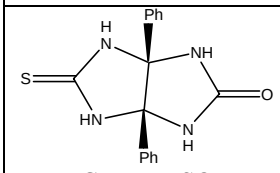 $C_{16}H_{14}N_4SO$	**CD5600**			
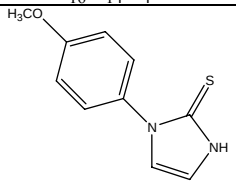 $C_{10}H_{10}N_2S_1O_1$	**Cd5479a**			
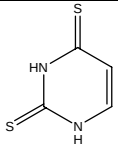 $C_4H_4N_2S_2$	**Cd5432**			
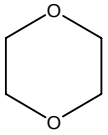 $C_4H_8O_2$				**Cd6149** $C_4H_8O_2$ / $C_6I_2F_4$
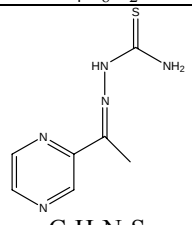 $C_7H_9N_5S$	**Cd5725**			

References

1. Bjorvatten, T.; Hassel, O. " *Acta Chem. Scand.* **1961**, *15*, 1429.
P2₁/m, a = 6.56(3), b = 21.06(11), c = 4.47(2) Å, β = 104.4(5)º, V = 598 Å^3

2. Chao, G.Y.; McCullough, J.D. *Acta Cryst.* **1960**, *13*, 727.
P2₁/c, a = 6.838(6), 6.393(6), c = 16.775 (10) Å, β = 114.5(3)º, V = 667 Å^3

3. Jay, J.I.; Padgett, C.W.; Walsh, R.D.B.; Hanks, T.W.; Pennington, W.T. *Cryst. Growth & Des.* **2001**, *1*, 501.
mmim·TIE: *C*2/*c*, *a* = 20.1789(12), *b* = 10.7824(10), *c* = 14.5072(2) Å, *β* = 118.767(1)°, *V* = 2766.9(3) Å^3
mmim·*p*-F_4DIB: *C*2/*c*, *a* = 26.915(3), *b* = 7.9216(6), *c* = 14.2630(4) Å, *β* = 105.618(1)°, *V* = 2928.7(4) Å^3
mmim·*o*-F_4DIB: P-1, *a* = 7.4987(7), *b* = 8.1906(12), *c* = 11.6512(12) Å, α = 83.245(4)°, β = 84.695(3)°, γ = 86.135(3)°, *V* = 706.35(14) Å^3

4. Daga, V.; Hadjikakou, S.K.; Hadjiliadis, N.; Kubicki, M.; dos Santos, J.H.Z.; Butler, I.S. *Eur. J. Inorg. Chem.* **2002**, 1718.
(mercaptobenzimidazole·I_2)$_2$·I_2·2H_2O: *P2₁/c*, a = 13.4828(14), b = 4.6704(4), c = 21.267(2) Å, β = 101.029(8)º, V = 1376.3(2)Å^3
mercaptobenzothiazole·I_2: *P2₁2₁2₁*, a = 4.189(1), b = 9.770(3), c = 27.704(8) Å, V = 1133.8(5)Å^3
(mercaptobenzothiazole·I_2)·I_2: *P2₁/n*, a = 8.357(2), b = 17.829(4), c = 9.603(2) Å, β = 94.39(3)º, V = 1426.6(6)Å^3

Appendix D

Halogen bonded complexes of nitrogen heterocycles

Table D-1: List of halogen bonded complexes of nitrogen heterocycles

Acceptors → Donors ↓	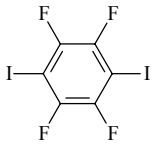 $C_6F_4I_2$	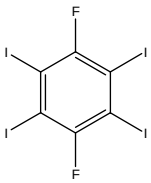 $C_6I_4F_2$	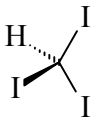 CHI_3	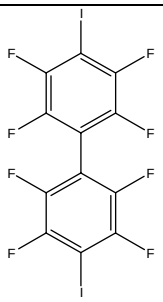 $C_{12}F_8I_2$
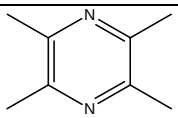 $C_8H_{12}N_2$		**Cd6375** $C_8H_{12}N_2$ / $C_6I_4F_2$		**Cd6348** $C_8H_{12}N_2$ / $C_{12}F_8I_2$
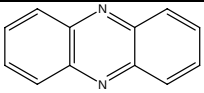 $C_{12}H_8N_2$		**Cd6350** $C_{12}H_8N_2$ / $C_6I_4F_2$		**Cd6400** $C_{12}H_8N_2$ / $C_{12}F_8I_2$
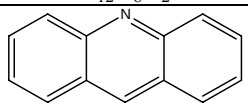 $C_{13}H_9N$				**Cd6349** $C_{13}H_9N$ / $C_{12}F_8I_2$
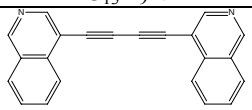 $C_{22}H_{12}N_2$				**Cd6351** $C_{22}H_{12}N_2$ / $C_{12}F_8I_2$
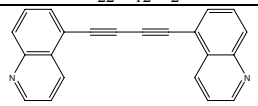 $C_{22}H_{12}N_2$	**Cd5244** $C_{22}H_{12}N_2$ / $C_6F_4I_2$		**Cd5298** $C_{22}H_{12}N_2$ / $(CHI_3)_2$	**Cd6464** $C_{22}H_{12}N_2$ / $C_{12}F_8I_2$
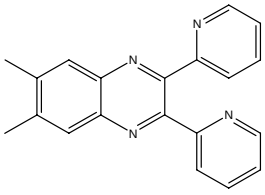 $C_{20}H_{16}N_4$	**Cd6480** $(C_{20}H_{16}N_4)_2$ / $(C_6F_4I_2)_3$			
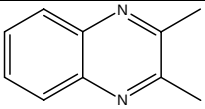 $C_{10}H_{10}N_2$	**Cd6463** $C_{10}H_{10}N_2$ / $C_6F_4I_2$			

Table D-2: List of halogen bonded complexes of nitrogen heterocycles (cont)

Acceptors → Donors ↓	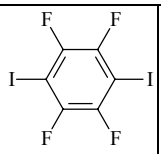 $C_6F_4I_2$	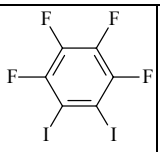 $C_6F_4I_2$	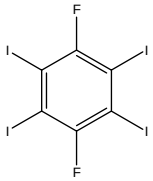 $C_6I_4F_2$	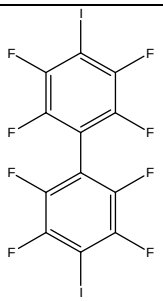 $C_{12}F_8I_2$
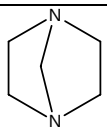 $C_5H_{10}N_2$		**Cd6386** $C_5H_{10}N_2$ / $C_6F_4I_2$	**Cd6479** $C_5H_{10}N_2$ / $(C_6I_4F_2)_2$	**Cd6491** $C_5H_{10}N_2$ / $C_{12}F_8I_2$
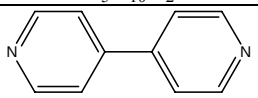 $C_{10}H_8N_2$				**Cd6385** $C_{10}H_8N_2$ / $C_{12}F_8I_2$
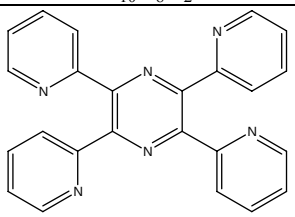 $C_{24}H_{16}N_6$	**Cd5974** $C_{24}H_{16}N_6$ / $C_6F_4I_2$			**Cd6618** $C_{24}H_{16}N_6$ / $(C_{12}F_8I_2)_2$